



pennsylvania

DEPARTMENT OF TRANSPORTATION

Bridge Waterproofing Details – Phase 2

FINAL REPORT

June 12, 2017

By Qiang Yu
University of Pittsburgh

COMMONWEALTH OF PENNSYLVANIA
DEPARTMENT OF TRANSPORTATION

CONTRACT # 4400011482
WORK ORDER # PIT 05



1. Report No. FHWA-PA-2017-002-PIT WO 5		2. Government Accession No.		3. Recipient's Catalog No.	
4. Title and Subtitle Bridge Waterproofing Details - Phase 2				5. Report Date 06/12/2017	
				6. Performing Organization Code	
7. Author(s) Qiang Yu				8. Performing Organization Report No.	
9. Performing Organization Name and Address University of Pittsburgh 3700 O'Hara Street Pittsburgh, PA 15261				10. Work Unit No. (TRAVIS)	
				11. Contract or Grant No. 4400011482, PIT WO 5	
12. Sponsoring Agency Name and Address The Pennsylvania Department of Transportation Bureau of Planning and Research Commonwealth Keystone Building 400 North Street, 6 th Floor Harrisburg, PA 17120-0064				13. Type of Report and Period Covered Final Report 4/13/2015 – 06/12/2017	
				14. Sponsoring Agency Code	
15. Supplementary Notes Ronald D. Schreckengost, Jr., P.E. Sr. Civil Engineer Supervisor - Transportation PA Department of Transportation District 10-0 2550 Oakland Avenue, PO Box 429 Indiana PA 15701 Phone: 724.357.7696 Fax: 724.357.5951					
16. Abstract The objective of this research is to provide the implementation roadmaps for the recommendations proposed in Phase I to enhance the capability and robustness of the current waterproofing system in District 10-0 of PennDOT. Built upon the results obtained in the numerical simulations and experimental characterizations, the research team developed the necessary implementation guidance for practice. The developed implementation roadmaps include improving the design of abutment/beam adjunction, using crystalline waterstops for construction joints and old-new concrete interfaces, building an overlap in the waterproofing membrane to mitigate the delamination risk at the location of beam seat, reinforcing elastomeric concrete to produce stronger and more durable header materials for expansion joints, and designing a sensing system to monitor the movement of expansion joints as well as to detect the water leakage.					
17. Key Words Waterproofing system, Water leakage, Abutment, Membrane delamination, Header materials, Sensing system				18. Distribution Statement No restrictions. This document is available from the National Technical Information Service, Springfield, VA 22161	
19. Security Classif. (of this report) Unclassified		20. Security Classif. (of this page) Unclassified		21. No. of Pages 118	22. Price N/A

Bridge Waterproofing Details Phase II

The contents of this report reflect the views of the author(s) who is(are) responsible for the facts and the accuracy of the data presented herein. The contents do not necessarily reflect the official views or policies of the US Department of Transportation, Federal Highway Administration, or the Commonwealth of Pennsylvania at the time of publication. This report does not constitute a standard, specification or regulation.

This work was sponsored by the Pennsylvania Department of Transportation and the U.S. Department of Transportation, Federal Highway Administration.



Bridge Waterproofing Details Phase II

TABLE OF CONTENTS

EXECUTIVE SUMMARY	1
1 OBJECTIVE OF RESEARCH	1
2 PRELIMINARY DESIGN AND EVALUATION	1
3 DESIGN AND IMPLEMENTATION	2
4 RECOMMENDATION AND IMPLEMENTATION ROADMAP	3
4.1 ENHANCED ABUTMENT/BEAM ADJUNCTION DESIGN	3
4.2 USE OF CRYSTALLINE WATERSTOP	5
4.3 MITIGATION OF THE DELAMINATION OF WATERPROOFING MEMBRANE	7
4.4 SENSORING SYSTEM	7
4.5 HEADER MATERIALS	9
5 ADJUSTMENT IN CONSTRUCTION	9
CHAPTER 1 PRELIMINARY DESIGN	10
1 INTRODUCTION	10
2 PRELIMINARY DESIGN OF ABUTMENT/BEAM ADJUNCTION	10
3 PRELIMINARY INVESTIGATION OF CRYSTALLINE WATERSTOPS	16
4 DELAMINATION MITIGATION OF WATERPROOFING MEMBRANE	20
5 EVALUATION OF HEADER MATERIALS	21
6 PRELIMINARY DESIGN OF SENSORING SYSTEM	24
7 SUMMARY	27
CHAPTER 2 DESIGN AND IMPLEMENTATION I	28
1 INTRODUCTION	28
2 DESIGN OF ABUTMENT/BEAM ADJUNCTION	28
3 IMPLEMENTATION OF CRYSTALLINE WATERSTOPS	39
4 CONSTRUCTION OF OVERLAPPED WATERPROOFING MEMBRANE	46
5 DISPLACEMENT MONITORING SYSTEM	52
4 SUMMARY	55
CHAPTER 3 DESIGN AND IMPLEMENTATION II	57
1 INTRODUCTION	57
2 EVALUATION OF HEADER MATERIALS	57
3 WATER LEAKAGE DETECTION SYSTEM	71
6 SUMMARY	79
CHAPATER 4 EXECUTABLE IMPLEMENTATION	81
1 IMPLEMENTATION ROADMAP	81
2 ADJUSTMENT IN CONSTRUCTION	86
REFERENCES	88
APPENDIX	90
1 TABLES	90
2 FIGURES	114



Bridge Waterproofing Details Phase II

Executive Summary

1 Objective of Research

Bridges are the critical components in transportation networks, which play an important role in the local and national economic growth and social development. Therefore, to ensure the functionality of bridges within their whole expected lifetime is one of the most important goals of the state Departments of Transportation, including PennDOT. To achieve this goal, a safe and robust design of waterproofing details is indispensable.

Waterproofing details constitute an important protection system to prevent the structural members in bridge substructures from water-related deterioration, which is responsible for the premature serviceability loss of the key structural members found in many bridges (Tinnea, et al., 2006). However, a comprehensive investigation carried out in the tasks of Phase I found out that some deficiencies existed in the current PennDOT practice, which were evidenced by the severe water leakage observed in some young bridges in PennDOT District 10-0.

Based on the investigations in Phase I, recommendations to improve the current waterproofing practice were proposed, which included 1) improving the design of abutment/beam adjunction; 2) using high performance waterstops; 3) mitigating the risk of membrane delamination; 4) seeking for stronger and more durable header materials; and 5) developing a monitoring system to size the gap of expansion joint as well as to detect the water leakage.

To implement these recommendations proposed in Phase I, enhanced designs, material characterizations and experimental tests need to be developed to assess their applicability in practice, optimize their performance in service, as well as ease their installation in construction. The objective of this study is to evaluate these recommendations analytically as well as experimentally. Based on the evaluations, implementation roadmaps are generated to guide the applications of these recommendations in practice.

2 Preliminary Design and Evaluation

To generate the implementation roadmaps for practice, the initial work is aimed at developing preliminary designs and the corresponding analytical and experimental methods to evaluate these designs. In this investigation, the preliminary designs and characterizations are broken down to the following five subtasks:

1. Enhanced abutment/beam adjunction design;
2. High performance waterstops;
3. Delamination mitigation of waterproofing membrane;
4. Improvement of header materials;
5. Sensing system

In the enhanced abutment/beam adjunction design, the focus is placed on eliminating (or minimizing) the joints on bridge abutments so as to simplify the adjunction geometry. Three preliminary designs were proposed to improve the capacity of waterproofing at abutment/beam adjunction. For high performance waterstops, crystalline waterstops are explored and investigated due to their unique working mechanisms, which are very different from the conventional polymer-based waterstops. To evaluate the use of crystalline waterstops, a series of tests was designed. To mitigate the membrane delamination, the investigation is focused on the membrane covering the gap at beam seat. A design containing an overlap was proposed and experiments were designed to test its effectiveness and installation efficiency. For the



Bridge Waterproofing Details Phase II

sensing system, an integrated system is probed to monitor the displacement of joints as well as detect the occurrence of water leakage. In the preliminary design, different types of sensor heads were investigated and the remote data transfer and storage were probed.

3 Design and Implementation

Based on the preliminary design and evaluation, numerical analyses and experimental tests were carried out to generate and optimize the implementation roadmaps. According to the nature of the analyses and tests, the tasks are divided into two groups, i.e., Design and Implementation I and II.

In Design and Implementation I, the enhanced designs were numerically examined to ensure that high stress level, which may lead to significant changes in steel amount and placement, was not induced by the geometry simplification. In order to comply with the current practice, four typical girders used in PennDOT were selected to study the structural responses of their abutment/beam adjunctions. In addition, for each type of girder, different skew angles and different span lengths were selected to investigate the application scope of the enhanced designs. The investigation finds that for the typical concrete girders or steel beams used in PennDOT practice, the proposed designs will not cause excessive deflection, neither abnormal stress distribution leading to significant change in reinforcement amount and placement. Therefore, the proposed designs can be designed based on AASHTO standard design process and then implemented in practice to improve the waterproofing capacity.

In Design and Implementation I, the implementation of crystalline waterstops was probed experimentally. Based on the availability and previous application results, the crystalline waterstops from two suppliers were selected for this investigation. To test the effectiveness and construction friendliness of the selected crystalline waterstops, water tank test, cyclic loading test and old-new concrete interface test were carried. The test results show that both crystalline waterstops performed well in all different test conditions. Furthermore, compared to the conventional waterstops, the installation of crystalline waterstops is more efficient and less labor intense.

In Design and Implementation I, an overlap was designed and then tested to mitigate the risk of membrane delamination. Two types of materials, i.e., fiberglass powder and dry fine sand, were selected among others and then used to generate the overlap at the gap of beam seat. Test results show that for both in-plane and out-plane shear induced by the relative movement at the gap, the overlap was able to significantly mitigate the peeling stress in the waterproofing membrane, and thus reduce the risk of delamination. The tests also indicate that if the proposed installation steps are followed, the use of fiberglass powder and dry fine sand will not bring any serious burdens in construction.

In Design and Implementation I, a displacement monitoring system was designed and fabricated to size the expansion joint. A LVDT displacement sensor head, capable of working outdoors, was selected. To record the real-time measurement, a wireless signal transmitter and receiver combo was used to read and store the signals captured by the LVDT sensor head. To build the link between the sensor head and the combo, a conditioning circuit was designed and fabricated. The tests on the displacement monitoring system show that movement of different frequencies was accurately captured and recorded.

In Design and Implementation II, three types of header materials, namely the Class AAAP concrete, elastomeric concrete and steel wire-reinforced elastomeric concrete, were comprehensively investigated. Five types of tests were designed to characterize their strength, impact resistance, wearing resistance and durability. The test results transpire that the



Bridge Waterproofing Details Phase II

reinforcement provided by steel wires improved the resistance of elastomeric concrete to the physical and chemical attacks imposed in the tests, and thus should enhance its resistance to rutting. Therefore, elastomeric concrete reinforced with steel wires may provide better performance when it is used as a header material for block-outs.

In Design and Implementation II, a water leakage detection system was designed and integrated with the displacement monitoring system. In this investigation, both electric and optical fiber sensor heads were explored. Due to its ease in fabrication, the electric sensor head was finally selected for the integrated system. A conditioning circuit, which is linked with the electric sensor head through a controller, was designed to generate analog signals. This system shares the wireless signal transmitter and receiver combo with the displacement monitoring system. Tests show that the integrated system can work well and the signals captured by both sensor heads can be successfully recorded and stored by the transmitter and receiver combo.

4 Recommendation and Implementation Roadmap

Based on the preliminary designs and the tests on their implementations, an implementation roadmap is generated for each design. Note that these roadmaps are built upon the experimental observations in the laboratory. Although conditions mimicking the real worksite environments were applied in the tests, these roadmaps may need to be further adjusted and optimized based on the performance in their real applications.

4.1 Enhanced Abutment/Beam Adjunction Design

Three designs are recommended to improve the waterproofing design at abutment/beam adjunction. Design I is shown in Fig. 1.

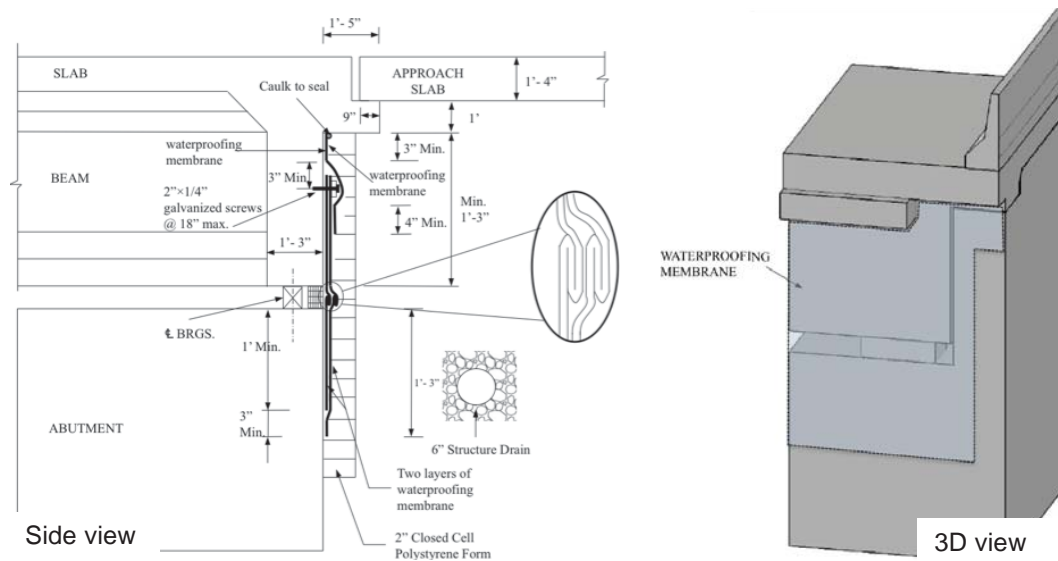


Fig. 1. Design I for abutment/beam adjunction.

The advantages of this design include:

1. An extension slab is used to move the expansion joint away from the abutment;
2. The paving notch is eliminated;



Bridge Waterproofing Details Phase II

3. The geometry of the adjunction is greatly simplified;
4. In addition to the gap at beam seat, the gaps between the abutment and cheekwalls can be fully covered by waterproofing membrane;
5. The flat surface benefits the installation of waterproofing membrane;
6. Its application scope can cover the typical beams, span lengths and skew angles in the current practice.

Design II is illustrated in Fig. 2. Compared to Design I, this design does not contain an extension slab. Instead, it uses a lip-shaped support to carry the approach slab. Thus, the position of the expansion joint is unmoved, which may lead to a higher risk of water leakage (e.g., water may directly enter the backfill through the expansion joint).

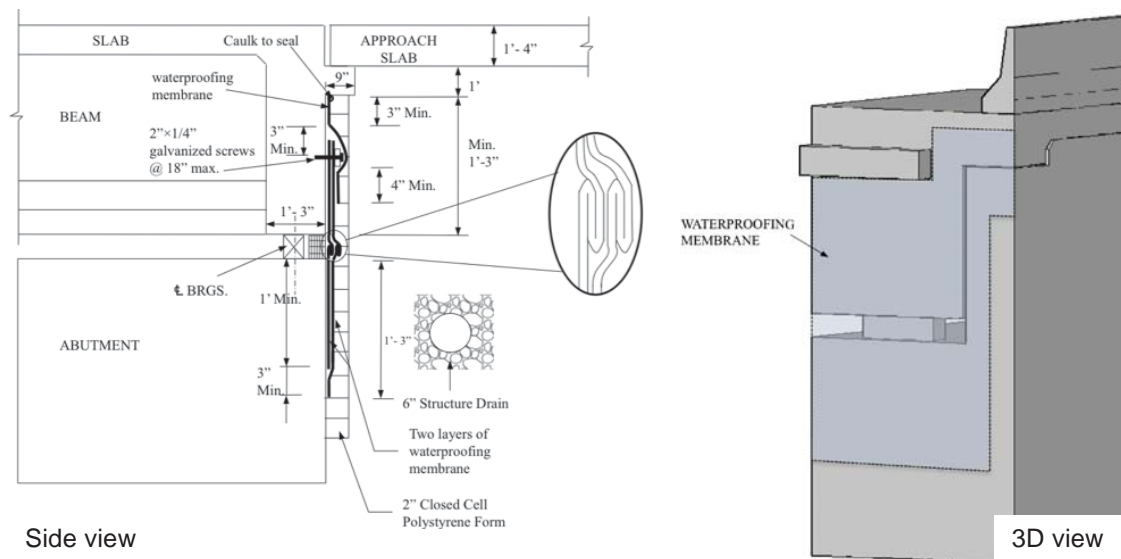


Fig. 2. Design II for abutment/beam adjunction.

However, compared to the current practice and Design I, this design has its unique advantages, which include:

1. Tensile stress in the lip support is lower than that in the extension slab of Design I;
2. Paving notch is eliminated;
3. The geometry of the adjunction is greatly simplified;
4. The open gaps at beam seat and between the abutment and cheekwalls can be fully covered by waterproofing membrane;
5. The flat surface benefits the installation of waterproofing membrane;
6. Its application scope can cover the typical beams, span lengths and skew angles in the current practice.

Design III is demonstrated in Fig. 3. Compared to Designs I and II, this design does not have an extension slab or a lip support. Thus, the expansion joint is unmoved and the paving notch is

Bridge Waterproofing Details Phase II

remained, although a step-like seat is created in the paving notch to accommodate the approach slab (Fig. 3). Due to its relatively complex geometry, this design may lead to a higher risk of water leakage than Designs I and II.

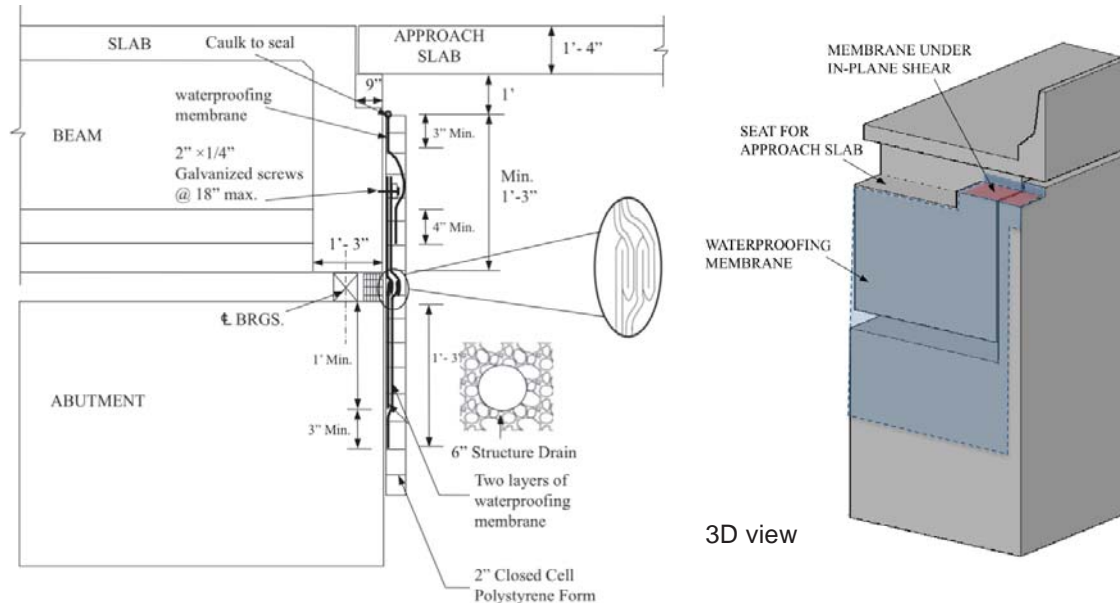


Fig. 3. Illustration of Design III for the enhanced abutment.

However, compared to the current practice and Designs I and II, this design has its own advantages, which include:

1. The simple structural form of the step-like seat leads to simple structural design;
2. All the gaps between the abutment, abutment stem and cheekwalls can be covered by the waterproofing membrane;
3. The flat surface benefits the installation of waterproofing membrane;
4. Its application scope can cover the typical beams, span lengths and skew angles in the current practice.

4.2 Use of Crystalline Waterstops

Crystalline waterstops are recommended to improve the waterproofing capacity of construction joints and old-new concrete interfaces. Anchored at their unique working mechanisms, crystalline waterstops bring advantages in installation and construction. Since they use chemical reactions to stop water ingress, their implementation roadmaps consist of 1) material preparation and 2) installation process, which are described in Table 1.

Before installation, two types of mixes usually need to be prepared. The first one is slurry-like and will be applied to the whole contact surface. The other one is paste-like and will be applied to seal the pre-formed groove. The recommended size of the pre-formed groove should be as deep as $\frac{1}{4}$ of the thickness of concrete sections but no more than 1.25 in., and as wide as twice of the depth while no more than 2 in.

Bridge Waterproofing Details Phase II

Table 1. Implementation roadmaps of Krystol and Xypex waterstops

	Krystol waterstop	Xypex waterstop
Preparation	<ol style="list-style-type: none"> 1. Prepare the slurry with a volume ratio of Krystol slurry powder to water being 3:1; 2. After mixing, stir for 1 minute to achieve a uniform slurry; 3. Prepare the grout with a ratio of Krystol grout powder to water being 4:1; 4. After mixing, stir for 1 minute to achieve a uniform paste-like product 	<ol style="list-style-type: none"> 1. Prepare the slurry treatment with a volume ratio of Xypex concentrate powder to water being 2:1; 2. After mixing, stir for 1 minute to achieve a uniform slurry; 3. Prepare the dry-pack with a ratio of concentrate powder to water being 4:1; 4. After mixing, stir for 1 minute to achieve a uniform paste-like product; 5. Prepare the Plug N pack with a ratio of pack powder to water being 3:1; 6. After mixing, stir for 1 minute to achieve a uniform paste-like product;
Installation	<ol style="list-style-type: none"> 1. Clean the concrete surface with clean water and then make the concrete surface-dry; 2. Use a brush to pave the slurry on the concrete surface to form a uniform layer about 0.04 in. thick; 3. Cure this layer for 12 to 24 hours before the casting of the next part of the joint; 4. 24 hours after the next casting, clean the pre-formed groove and then make it surface-dry; 5. Pave the groove with the slurry; 6. Wait for at least 10 minutes, then fill the groove with the grout; 7. Then use the slurry to make the surface flat; 8. Cure the treatment with light mist or wet burlap for 24 hours. 	<ol style="list-style-type: none"> 1. Clean the concrete surface with clean water and then make the concrete surface-dry; 2. Use a brush to pave the slurry on the concrete surface to form a uniform layer about 0.04 in. thick; 3. Cure this layer for 48 hours before the casting of the next part of the joint; 4. 24 hours after the next casting, clean the pre-formed groove and then make it surface-dry; 5. Pave the groove with the slurry; 6. Wait for at least 10 minutes, fill the groove with the dry-pack, and then use the Plug N pack to make the surface flat; 7. Cure the treatment with light mist or wet burlap for 24 hours.

Note that due to the inherent working mechanisms of crystalline waterstops, curing time is needed for them. This may demand for careful construction management to avoid prolonging the total construction time.



4.3 Mitigation of The Delamination of Waterproofing Membrane

The construction of an overlap is recommended to mitigate the risk of the delamination of waterproofing membrane. The main advantage of this overlap is that it accommodates the relative movement between the concrete parts without causing any peeling stress in the waterproof membrane. The key steps of its implementation roadmap include:

- Prepare fiberglass powder or dry fine sand;
- Based on the expected relative movement and gap size, determine the size of cover to be removed from the waterproofing membrane;
- With the aid of proper tools (e.g., a sharp blade and a straightedge), remove the cover of waterproofing membrane to expose its adhesive surface;
- Uniformly spread the fiberglass powder or dry fine sand on the exposed surface until it is no longer sticky;
- Peel off the rest of the cover of the membrane and start the installation as recommended in the current practice;
- Examine the bond quality between the membrane and concrete before adding the polystyrene foam layer to protect the membrane;
- Fold the overlap and then install the polystyrene foam layer to support it.

4.4 Sensing System

A sensing system is recommended to monitor the movement of the expansion joint as well as to detect the water leakage. The system is illustrated in Fig. 4.

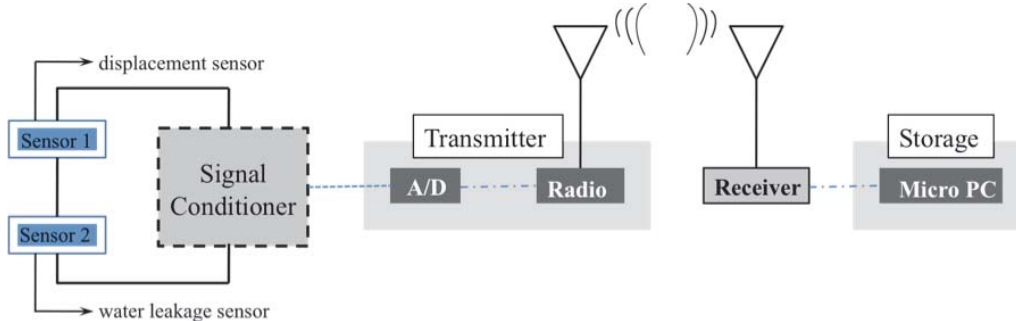


Fig. 4. Illustration of the key components in the sensing system.

The key components of this system include:

1. A LVDT displacement sensor head (e.g., LDI 119-150-A20A from OMEGA Engineering)
2. An electric cable sensor head for water leakage detection (e.g., the SeaHawk sensor cable from RLE Technology)
3. A circuit board containing two conditioning circuits, one for the LVDT and the other for the cable sensor
4. A controller (e.g., LD310 from RLE Technology), which converts the water leakage detected by the sensor head to analog signals and sends them to the circuit

Bridge Waterproofing Details Phase II

5. A wireless signal transmitter and receiver combo (e.g., V-link/WSDA from LORD Sensing)
6. Power supplies for sensor heads and wireless combo (e.g., YIX30L batteries)

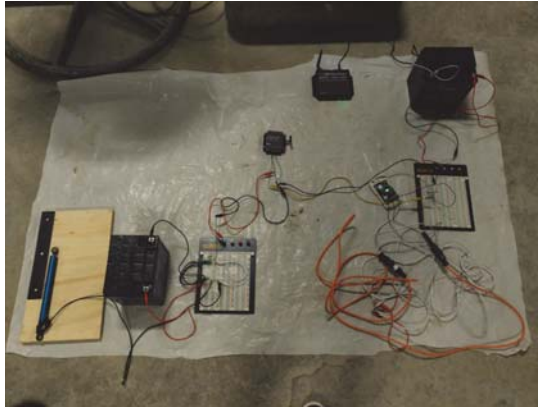


Fig. 5: The integrated sensing system fabricated.

A sensing system fabricated with these key components is shown in Fig. 5. To protect the sensing system from damages induced by animals and moisture during its outdoor use, all the key components are encased in steel boxes (Fig. 6a); in the box the parts are protected by polyurethane foam (Fig. 6b); acrylic conformal spray is sprayed on the circuit board to protect it from moisture (Fig. 6c); and vehicle wires (Fig. 6d) are used to connect all the components through the small holes on the boxes. To prevent the contact with the water on the ground, plastic seats are added on the boxes (Fig. 6a,b). Since the holes for the pass of wires are small and blocked with the polyurethane foam, there is no need to guard them with steel fence.

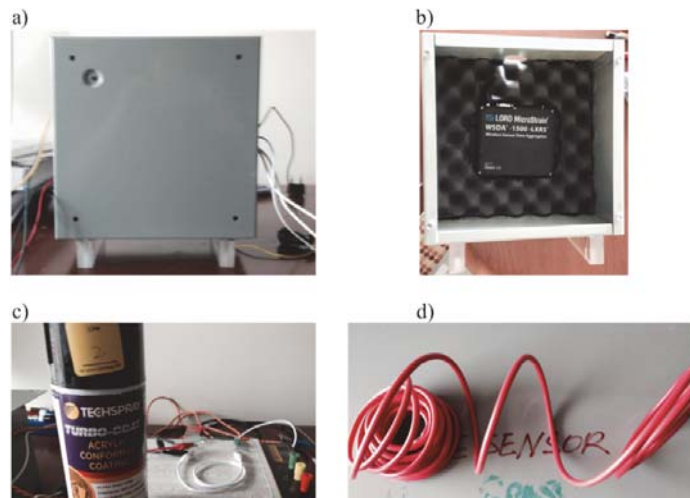


Fig. 6. a) Steel box for parts; b) polyurethane foam inside the box to protect the parts ; c) spray to protect the circuit board; and d) outdoor electric wire.

Bridge Waterproofing Details Phase II

4.5 Header Materials

Elastomeric concrete reinforced with steel wires is recommended to improve the performance of block-outs. Its implementation roadmap is described as follows:

- Use steel wires (of diameters not greater than 1/8 in.) to fabricate steel wire frames
- Place the steel wire frames in the molds based on the designed layout;
- Mix the elastomeric concrete as recommended by the supplier;
- Pour the elastomeric concrete into the molds;
- Wait until the elastomeric concrete is hardened.

Since elastomeric concrete is sticky, attention should be paid to ensure its flowability during casting to avoid segregation. It is recommended that the spacing between the steel wire frames and the spacing between the steel wires in each frame should be at least 3 times as large as the maximum aggregate size of the elastomeric concrete.

5 Adjustment in Construction

In this investigation, the implementation roadmaps are made based on the numerical analyses and experimental tests. The size scales and environmental conditions are different from the real applications in construction. Thus, certain adjustment may be needed in construction, which includes:

1. Structural design. In the enhanced designs for abutment/beam adjunction, an extension slab exists in Design I and a lip support exists in Design II. Although numerical investigation shows that these structural changes will not lead to high tensile stress, standard design following AASHTO code is needed for bridges of different spans and skew angles to determine the reinforcement ratio and placement layout. Considering that these structural regions are in the disturbed regions, the strut-and-tie method may be explored to conduct the standard structural design for the extension slab and lip support.
2. Construction management. Different from the conventional polymer-based waterstops, the implementation of crystalline waterstops requires curing. Therefore, adjustment may be needed to incorporate the implementation of crystalline waterstops into the construction management so as to avoid the increase of construction time. Besides construction scheduling, material and construction specifications would need to be developed based on an actual field placement.
3. Placement of steel wire. The block-out size is much larger than the specimens used in the experimental test. Thus, the placement of steel wire in elastomeric concrete may be more challenging in worksite than in the lab. Adjustment may be needed to improve the efficiency and construction friendliness of steel wire placement in the real construction.

Besides, adjustment on the installation and maintenance of the sensing system is also of great importance for improving its serviceability.



Chapter 1 Preliminary Design

1. Introduction

The service quality of bridges has a profound effect on the sustainable growth of the interconnected communities. Any premature loss in serviceability of a bridge will tremendously disturb the local transportation system, which eventually leads to staggering direct and indirect costs (e.g., replacement, retrofit, and traffic delay and detour). Therefore, a longer service lifetime, e.g., a design service life of 100 years, is generally expected for bridges in many state Departments of Transportation including PennDOT. To achieve this goal, a strong and robust waterproofing system is indispensable for bridges.

However, a comprehensive investigation carried out in Phase I found that deficiencies existed in the waterproofing details of the current PennDOT practice, which were evidenced by the severe water leakage and water-related deterioration observed in the abutments of five young bridges in PennDOT District 10-0. To remedy the existing inadequacy of the current practice, some conceptual recommendations were proposed in Phase I, which compassed: 1) eliminating the expansion joint or moving the expansion joint away from the abutment; 2) using high performance waterstops; 3) mitigating the risk of membrane delamination; 4) sizing the gap of expansion joint; and 5) detecting the locations of water leakage. The search for stronger and more durable header materials was also recommended to improve the performance of block-outs.

To implement these conceptual recommendations, preliminary designs of structural forms, material characterizations and experimental tests need to be developed to assess their construction applicability. The objective of this task is to develop the preliminary implementation roadmaps for these conceptual recommendations, with a specific focus on conducting preliminary designs and evaluations, which include: 1) abutment design to eliminate the expansion joint; 2) use of crystalline waterstops; 3) method to mitigate membrane delamination; 4) improvement of head materials; and 5) design of sensing and monitoring system.

Based on the preliminary implementation roadmaps provided in this task (Task I), works on optimization and finalization of these implementation roadmaps will be carried out Tasks II and III with the aid of numerical analyses and experimental testing.

2. Preliminary Design of Abutment/Beam Adjunction

The waterproofing details at abutment/beam adjunction are critical because any of their failure may create a direct leakage path for water to reach the important structural members, e.g., beams and bearings. However, due to the geometrical complexity of the junction where beams, abutment, cheekwalls and approach slab meet, the design, installation and maintenance of waterproofing details at this adjunction are challenging.

In Phase I, it was found that the best way to simplify the design and construction of waterproofing details at abutment/beam adjunction is to use integral abutment to completely eliminate the expansion joint; see Fig. 7. Similar effect can also be achieved by using semi-integral abutment. Since there is no open gap, the focus of waterproofing design is placed on the construction joints of integral abutment. Crystalline technique-based waterstops, whose information and implementation will be detailed later, are recommended.



Bridge Waterproofing Details Phase II

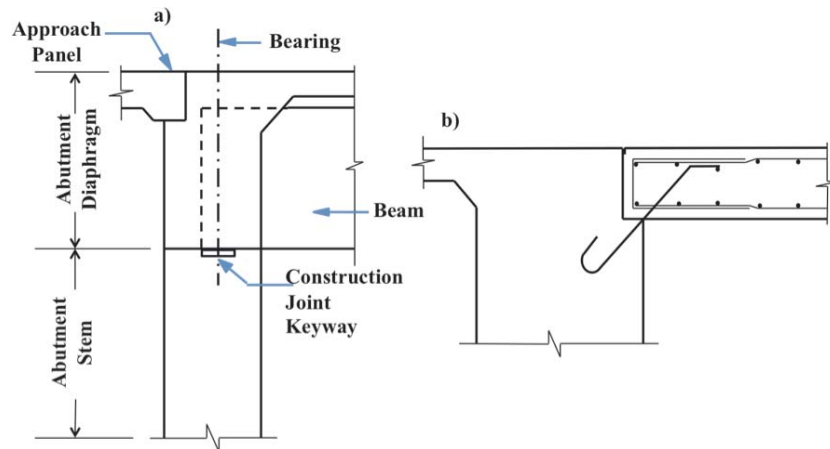


Fig. 7. Illustrations of a) an integral abutment and b) an approach slab tied with the integral abutment at paving notch.

However, despite their advantages in waterproofing capacity, integral and semi-integral abutments suffer from the significant stress redistribution triggered by temperature variation and many other time-dependent behaviors of concrete and prestressing tendons (e.g., the concrete creep and shrinkage, and the steel relaxation), many of which are still not fully understood. Therefore, the use of integral and semi-integral abutments is significantly limited by the geometrical and load restrictions, e.g., soil strata, skew angle and bridge length.

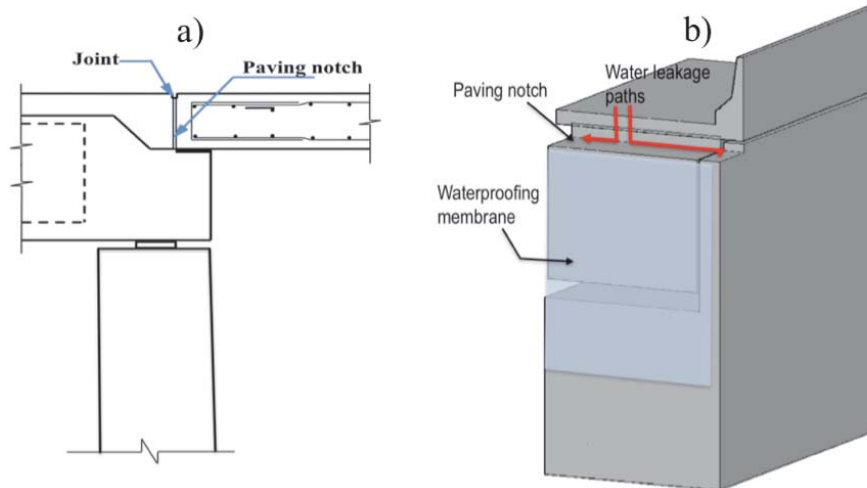


Fig. 8. a) Illustration of a cantilever abutment without backwall and b) the leakage path due to the existence of the paving notch.

To cover a broader range of soil strata, span lengths and skew angles, cantilever abutment is needed in bridge construction. Usually, there are two types of cantilever abutments, one with backwall and the other without. In the former one, the expansion joint is placed right over the bearings. Considering the hostile conditions that the expansion joint assembly is exposed to (Distlehorst and Wojakowski, 2005), this type of abutment leads to a low-redundancy and high-

Bridge Waterproofing Details Phase II

risk design for the waterproofing system and is not highly recommended. Currently, the more widely used abutment in PennDOT is the one without backwall; see Fig. 8a. In this abutment, the expansion joint is placed over a paving notch so that the water has to overcome the waterproofing membrane and rubberized sealing materials to reach the bearings, even when failure happens in the expansion joint assembly. Thus it provides a more robust and more economical design for the waterproofing system than the one with backwall.

However, due to the existence of the paving notch (Fig. 8b), the abutment/beam adjunction in this type of abutment is more complicated than that of the abutment with backwall. It is difficult to use waterproofing membrane to cover all the possible water leakage paths. For example, as shown in Fig. 8b, the waterproofing membrane has to be terminated at the bottom of the paving notch, and thus cannot protect the gaps between the cheekwalls and abutment. If damage happens in the expansion joint assembly, water will penetrate inside following the leakage paths (red lines) shown in Fig. 8b.

In the current PennDOT practice, rubberized sealing materials are used to fill these gaps. For these rubberized sealing materials, they maintain their locations purely by friction force. However, different from the relative movement of stretching and contracting in the direction normal to the sealing materials, the relative movement in the gaps between the paving notch and cheekwalls is in-plane slip, which generates significant shear in the sealing materials. Thus, similar to the compression seal in a bridge of a large skew angle, the risk of dislodgement is high for the rubberized sealing materials. Furthermore, unlike normal deformation, the shear deformation caused by the relative slip will generate angle changes in the sealing materials. This provides a direct path at corners for water to reach the bearings because waterproofing membrane cannot be installed at the paving notch; see Fig. 8b.

To remedy this problem, three preliminary designs are proposed to simplify the geometrical complexity at abutment/beam adjunction:

■ Design I

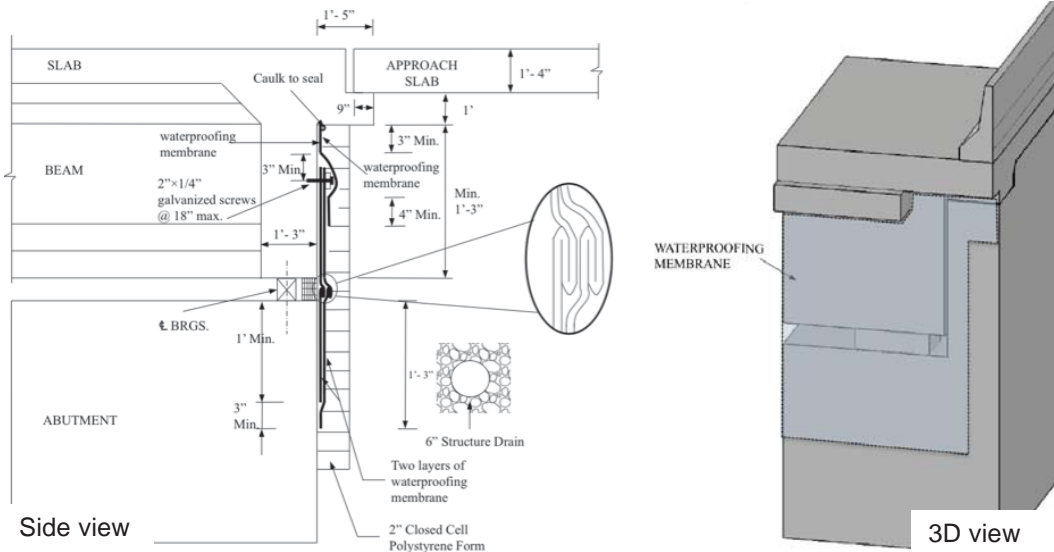


Fig. 9. Illustration of Design I for the enhanced abutment/beam adjunction.

Bridge Waterproofing Details Phase II

In this design, the deck slab is extended 1 foot and 5 inches away from the backside of the abutment and the approach slab is seated on it (Fig. 9). Here the thickness of the extension slab is preliminarily selected to be 2 ft and 4 inches. The extension of the deck slab brings a number of advantages in terms of waterproofing design. First, the expansion joint is moved away from the abutment. Thus, if damage happens in the expansion joint assembly, water can only get into the backfill, but cannot reach the bearings through the gaps between the cheekwalls and abutment. Second, the abutment/beam adjunction is greatly simplified by eliminating the paving notch. All the gaps, especially those between the abutment and cheekwalls, can be fully covered by the waterproofing membrane (Fig. 9). Finally, this design benefits the installation of waterproofing membrane because the surface is flat and there is no need to fold the waterproofing membrane at any joint. This is especially helpful for the construction of the overlap at the gap of beam seat. Since in this design this gap is one of the most important locations in the waterproofing system, two layers of membrane may provide a more durable and robust protection. Note that in this design, each membrane forms its own overlap as shown in Fig. 9.

■ Design II

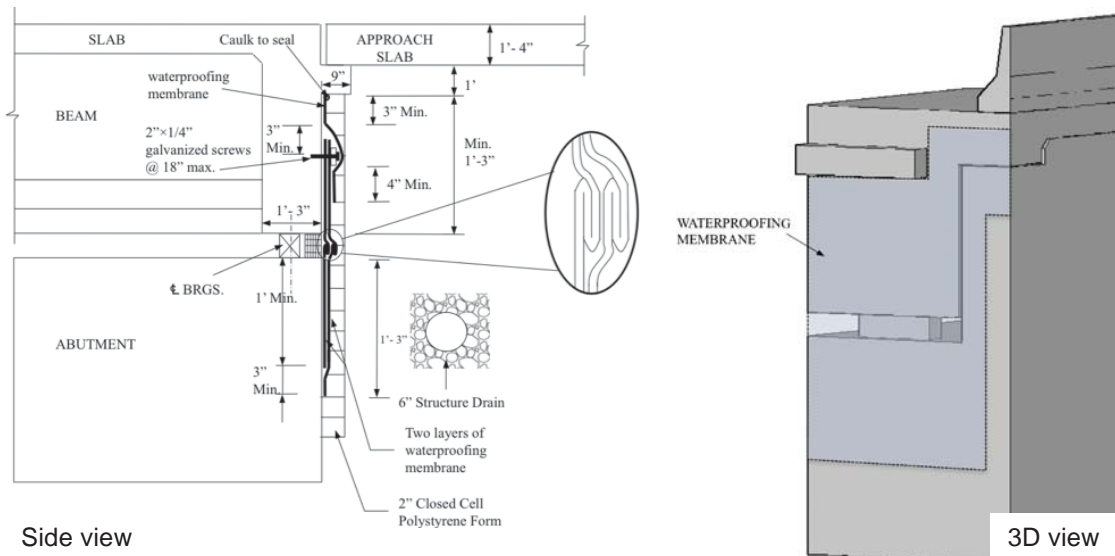


Fig. 10. Illustration of Design II for the enhanced abutment/beam adjunction.

In this design, the deck slab is not extended. Instead, a lip-shaped support is added to the diaphragm to replace the paving notch (Fig. 10). This modification can simplify the design and construction. But the tradeoff is that the expansion joint is unmoved. Thus, the risk of water leakage to the abutment is higher than that of Design I. Similar to Design I, the geometry of the abutment/beam junction is greatly simplified in this design. Waterproofing membrane can be installed to cover all the open gaps on the backside of the abutment and cheekwalls (Fig. 10). Since the surface is flat, a convenient installation of waterproofing membrane can be expected. At the gap of beam seat, overlaps similar to Design I are constructed.

■ Design III

In this design, the paving notch remains and the expansion joint is unmoved (Fig. 11). The only structural modification is that a step-like seat is created in the paving notch to carry the



Bridge Waterproofing Details Phase II

approach slab. Compared to the current practice, one benefit of this modification is that all the gaps can be fully covered by the waterproofing membrane now (Fig. 11). At the same time, this modification does not impose burdens on structural design because the forces are transmitted almost along the same path of the current design. However, as a tradeoff, the waterproofing membrane has to be folded during the installation; see the red region in Fig. 11. Furthermore, the waterproofing membrane may undergo significant in-plane shear, which does not exist in Designs I and II.

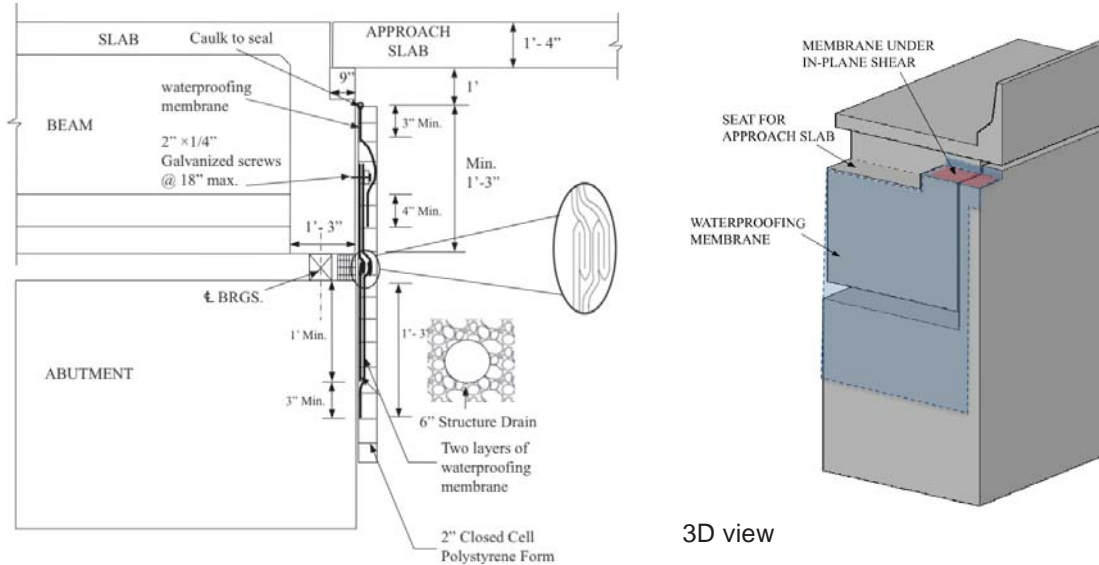


Fig. 11. Illustration of Design III for the enhanced abutment/beam adjunction.

In all these three designs, there are no backwalls. Pedestals are not needed to support the approach slab. Despite their different structural forms, the water leakage paths existing in the current practice are blocked by the waterproofing membrane in these designs. To evaluate these designs, preliminary numerical analyses were carried out. Two simple bridge models, one for Design I and the other for Design II, were constructed by using AASHTO Type III beams, which are commonly used in PennDOT. The lengths of both bridges are 52.5 ft. and both skew angles are zero. To investigate the longitudinal stress distribution in the end diaphragm and extension slab for Design I (or the lip support for Design II), the HL-93 live loading was considered. In the simulations, loads caused by trucks driving on and driving away from the bridge were both considered. In order to achieve the maximum moment and shear in the extension slab (or the lip support), the rear axles of the trucks were placed on the slab tip (or the lip support tip) in the simulations.

In Fig. 12, the profiles of longitudinal stress, shear stress and deflection are plotted for Designs I and II, respectively. Note that in Fig. 12 the color scale bars on the right represent the transition of stress from the positive values at the bottom (e.g. tensile stress) to the negative values (compressive stress) on the top. For deflection, the bars represent the transition from upward deflection to downward deflection. According to the simulation results, the stress level in the end diaphragm and extension slab (or lip support) does not lead to significant increase in reinforcement amount and placement. The vertical displacement of extension slab (or lip support) and end diaphragm is very small. The ratios of maximum deflection to cantilever

Bridge Waterproofing Details Phase II

length in both designs are much less than 1/1000, which is the ASSHTO limit of deflection-span ratio.

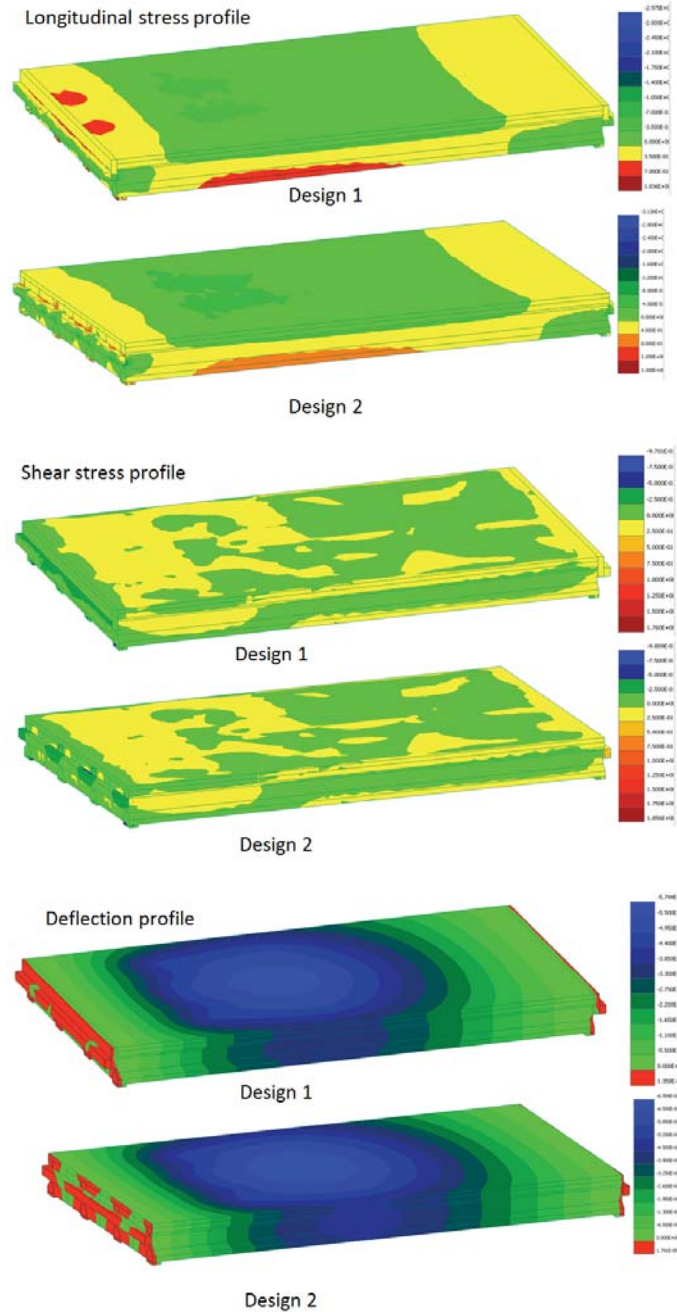


Fig. 12. Top: Longitudinal stress profiles; middle: shear stress profiles; and bottom: deflection profiles obtained by FEM simulations.

Bridge Waterproofing Details Phase II

The preliminary evaluation based on numerical simulations shows that the enhanced designs of abutment/beam adjunction, which are capable of improving the waterproofing system, are structurally solid. Thus, these designs can be applied to the current practice after their application scopes are further investigated.

3. Preliminary Investigation of Crystalline Waterstops

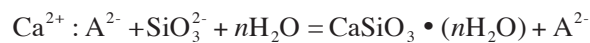
In the current practice of PennDOT, the conventional polymer-based waterstops, which take advantage of the extremely low water permeability of polymer, are widely used at construction joints to block water ingress. According to their working mechanisms, the quality of installation is of great importance for the conventional waterstops. Poor workmanship can easily lead to misalignment, dislocation, buckling, warping and overlapping of the polymer sheet when concrete is poured.

In Phase I, it was found that failure of the waterstops, likely caused by incorrect installation, was responsible for the water leakage observed at the construction joints in the end diaphragm of a young bridge. Another limitation of the conventional waterstops is that they cannot be applied to the old-new concrete interface. To anchor the polymer sheet in hardened concrete is costly and challenging in construction. Thus, it is not surprising that water leakage was found in the interfaces in Phase I.

In view of these disadvantages of conventional waterstops, it was recommended in Phase I to seek for high quality, economical and construction-friendly waterstops for abutments, diaphragms and old-new concrete interfaces. After an extensive literature review of the current advancement in waterproofing materials, it was found that waterstops based on crystalline techniques are promising candidates for the bridge waterproofing system.

Unlike the polymer-based waterstops, crystalline waterstops attain their waterstop capability by chemical reactions. By the reactions with water and chemicals in cement matrix, crystalline waterstops will generate a non-soluble and impermeable crystalline formation to resist water ingress. Thus, the way to implement them in construction is inherently different from the conventional polymer-based waterstops.

The primary chemical reaction of crystalline waterstops can generally be described as follows (Sprouts et al. 1994, Keck 2001, and Mather 2004):



here the free reactive group A^{2-} from crystalline waterstops is able to move with free water in concrete matrix. Once the group meet with the free $\text{Ca}(\text{OH})_2$ existing in the concrete, they will aggregate together to create a high concentration of $\text{Ca}^{2+}:\text{A}^{2-}$ compound, whose bond is relatively weaker than that of CaSiO_3 . Thus, in the crystalline formation zone, the A^{2-} will be replaced by the SiO_3^{2-} to form a sediment with an expanded volume, namely $\text{CaSiO}_3 \cdot (n\text{H}_2\text{O})$, which will fill the voids and pores. Again the released reactive group A^{2-} can move with water to generate the next crystalline formation when leakage approaches a new position. The key process of crystalline formation growth in concrete is illustrated in Fig. A1 in Appendix.

The unique mechanisms of crystalline waterstops inherently bring a number of advantages in performance and construction, which include:

1. Efficient installation in construction
2. Easy inspection before and after concrete pouring
3. Easy implementation for old-new concrete interface



Bridge Waterproofing Details Phase II

4. Adaption to curves and uneven surfaces
5. Resistance to high hydrostatic pressure
6. Low demand for protection during backfilling and steel placement
7. Resistance to corrosive agents
8. Tolerance to temperature variation

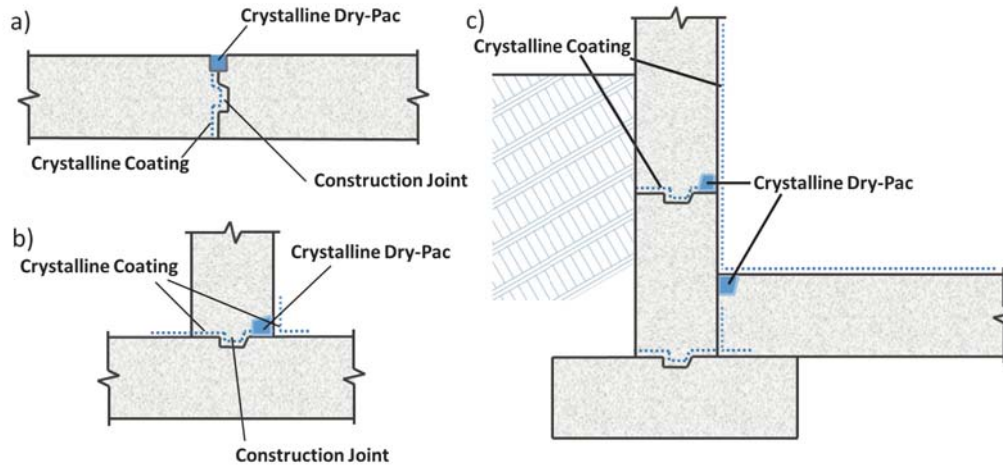


Fig. 13. Illustration of the implementation of Xypex crystalline waterstop for construction joints.

In addition, due to their construction-friendly nature (e.g., installation rate can be up to 100 ft. per hour based on the product manual), crystalline waterstops can considerably reduce the construction cost when compared to the conventional polymer-based waterstops. On the other hand, their unique working mechanisms make them unsuitable for joints undergoing significant relative movement. Their implementation also requires for certain protection and curing.

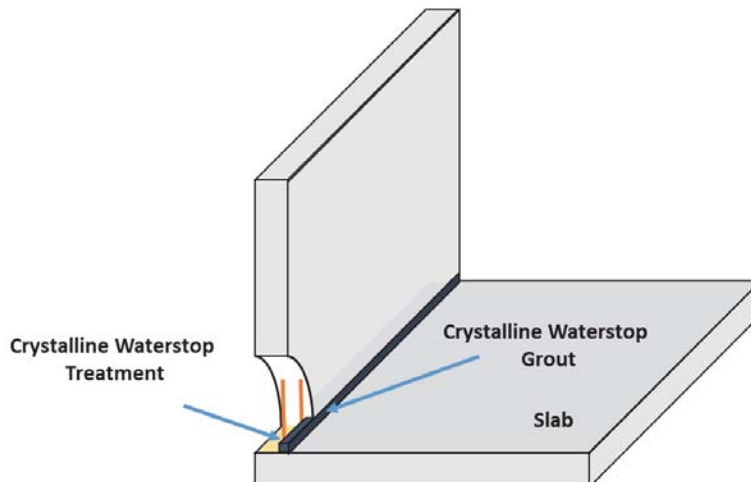


Fig. 14. Illustration of the external implementation of Krystol crystalline waterstop.

Bridge Waterproofing Details Phase II

Based on the availability and previous construction application, the preliminary investigation is focused on the crystalline waterstops supplied by Xypex and Krystol. Their implementation is illustrated in Figs. 13 to 15 respectively. It can be seen that for Xypex crystalline waterstop, the treatment consists of a slurry-like surface coat and a paste-like grout, which is also called Dry-Pack.

Similar to Xypex crystalline waterstop, Krystol crystalline waterstop also consists of surface slurry and grout. In Fig. 14, it shows the external implementation of Krystol crystalline waterstop, which is almost the same as Xypex crystalline waterstop. In addition, Krystol crystalline waterstop can be implemented internally, which is shown in Fig. 15. It can be seen that both crystalline waterstops are construction-friendly for both horizontal and vertical joints, applicable for old-new concrete interfaces, and insensitive to the position of steel bars.

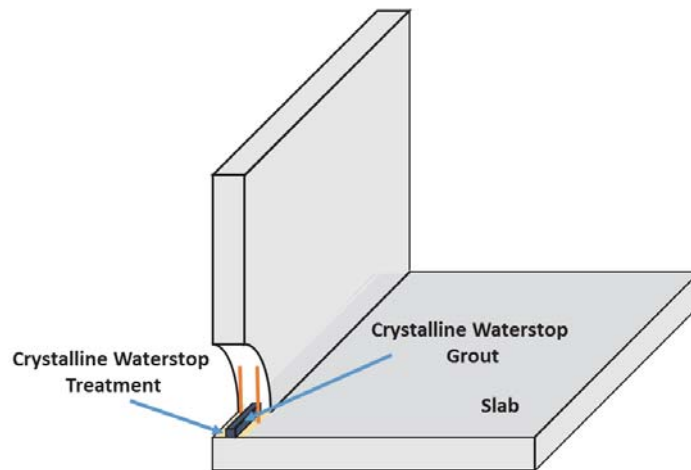


Fig. 15. Illustration of the external implementation of Krystol crystalline waterstop.

To evaluate their application in bridges, a number of tests are designed to examine their waterproofing capacity and construction efficiency.

■ Water tank test

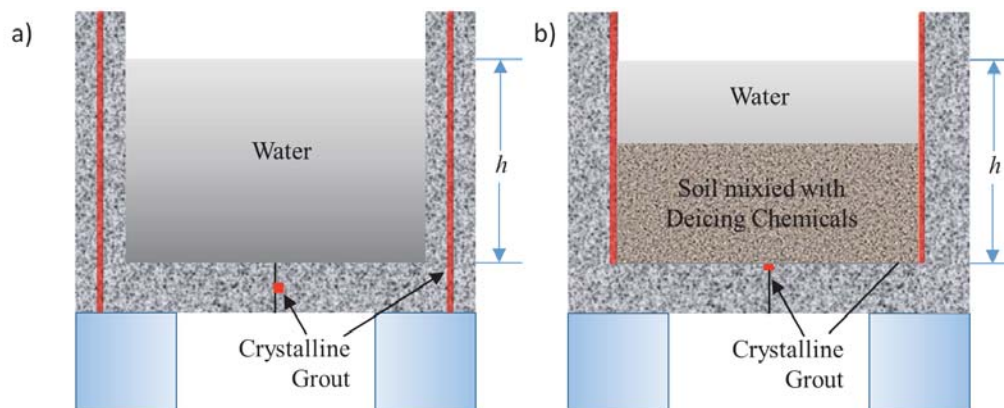


Fig. 16. Designs for water tank tests: a) without backfill and b) with backfill.

Bridge Waterproofing Details Phase II

The objective of this test is to examine the performance of the crystalline waterstops at different locations under a certain level of hydrostatic pressure. In this test design, several water tanks will be built; see Fig. 16. For each sidewall and the bottom slab of the tank, a construction joint will be introduced. Here vertical joints will be constructed in the sidewalls. Thus, each tank will contain both horizontal and vertical joints. After the construction of the tanks, water will be filled in for leakage test (Fig. 16a). To test the effects of backfill and chemical attack on the crystalline waterstops, soil and deicing materials will be filled in some of the tanks (Fig. 16b) to mimic the impacts induced by backfilling and environment.

■ Load test

The objective of this test is to evaluate the performance of crystalline waterstops when stress variation exists at the construction joints. Although the relative movement at construction joints is negligible, stress variation exists due to the vehicles travelling on the bridge. This test is designed to examine the performance of crystalline waterstops under similar loading conditions

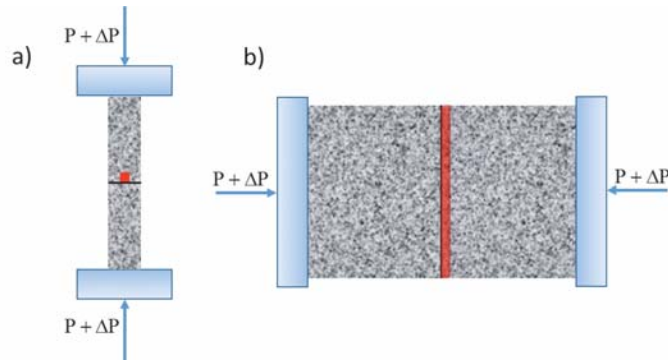


Fig. 17. Designs for cyclic loading tests: a) with a horizontal joint and b) with a vertical joint.

In this test design, two construction joints, one being vertical and the other being horizontal, will be constructed (Fig. 17). After construction, the concrete blocks will be put on the loading frame to undergo a certain number of cyclic loading. The amplitude of stress variation is preliminarily set as 10% of concrete strength. After the cyclic loading, the joints will be tested to examine if any leakage happened and the evaluation of the performance of the crystalline waterstops will be given based on the test results.

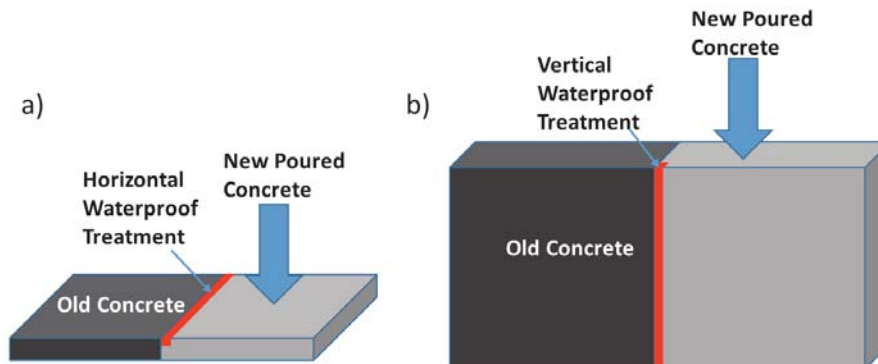


Fig. 18. Designs for old-new concrete interface tests: a) with a horizontal joint and b) with a vertical joint.

■ Old-new concrete interface test

The objective of this test is to examine the applicability of crystalline waterstops to the old-new concrete interfaces. In this test design, concrete blocks more than 1 year old (which are available at PITT) will be used as the old concrete. For each concrete block, a horizontal or a vertical joint will be prepared (Fig. 18). The crystalline waterstops will be applied to the surface of the old concrete. Then new concrete will be cast to form the old-new concrete interface, which will be tested to examine the waterproofing capacity of the crystalline waterstops.

4. Delamination Mitigation of Waterproofing Membrane

For cantilever abutment without backwall, waterproofing membrane is the only barrier protecting the open joint at beam seat against the water penetration from the backfill. Therefore, it is critical for the whole waterproofing system. To improve its waterproofing capacity, it was recommended in Phase I to construct an overlap to accommodate the beam movement without triggering the peeling stress at the joint corners.

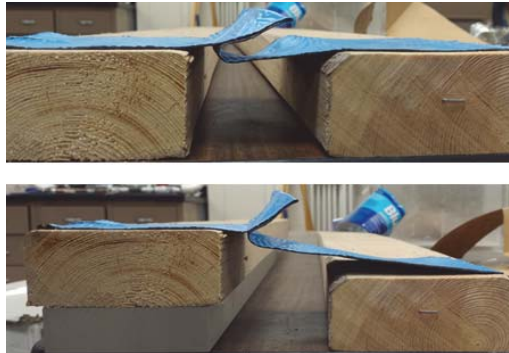


Fig. 19. Membrane sticking together at the overlap to form a stiffer double layer.

After the cover is peeled, the adhesive surface of waterproofing membrane will be exposed in construction. Without a proper treatment, the overlap of waterproofing membrane will glue together to form a stiffer double layer (Fig. 19). This double layer will significantly reduce the free movement of the overlap, and thus compromise its effect on delamination mitigation.



Fig. 20. Membrane treated with fiberglass powder.

To avoid this stiffer double layer, the self-bonding of the membrane must be prevented. To achieve this goal, fiberglass powder, dry fine sand, paper sheet, tape and paint spray were tested in the preliminary investigation. The test results showed that both fiberglass powder and dry fine sand were capable of preventing the self-bonding at overlap; see Figs. 20 and 21.

Bridge Waterproofing Details Phase II

Furthermore, no changes were noticed in the membrane flexibility after the membrane was treated with fiberglass powder or dry fine sand (Figs. 20 and 21). Thus, they are selected as candidates for the overlap construction. As for paper sheet, tape and paint spray, they did not provide satisfactory treatment. Their poor performance is shown in Fig. A2 to Fig. A4 in Appendix, respectively.



Fig. 21. Membrane treated with fine sand.

To further investigate the overlap construction with fiberglass powder and dry sand, experimental tests mimicking the movement at beam seat are designed; see Fig. 22. Based on the test results, the roadmap guiding the construction of the membrane overlap by using sand and fiberglass powder will be developed and examined.

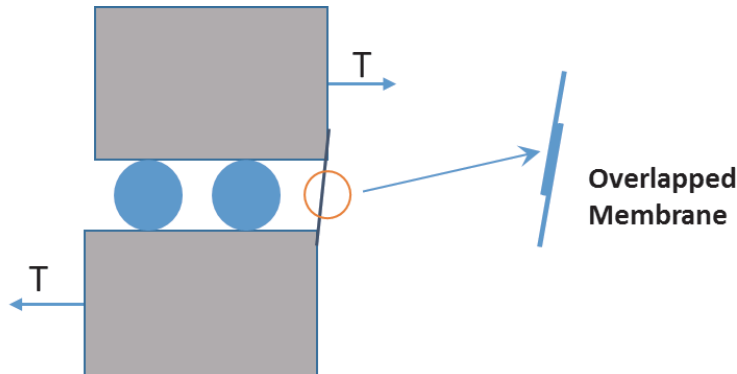


Fig. 22. Experiment to evaluate the overlap construction and delamination mitigation.

5. Evaluation of Header Materials

For cantilever abutment, expansion joint has to be used to accommodate the bridge movement due to temperature variation and other influences. For many bridges, even when the expansion joints are moved away from the abutments as proposed in Design I, the failure of expansion joint increases the risk of water leakage. Thus, ensuring the functionality of expansion joint is important for the bridge waterproofing system.

Header (or block-out) is a critical structural component in the expansion joint assembly. In PennDOT, Class AAAP concrete is exclusively used for expansion header. However, in Phase I, it was found that premature damage in headers (e.g., spalling and chipping off) was not unusual. Therefore, it was recommended to seek for stronger and more durable header materials to strengthen the expansion joint assembly.

Bridge Waterproofing Details Phase II

A recent field investigation supported by Kansas Department of Transportation (KDOT) shows that compared to concrete headers, elastomeric concrete headers seem to behave better *because much less spalling was observed* (Distlehorst and Wojakowski, 2005). The main concern about elastomeric concrete headers is rutting, which is negligible for concrete headers. It is well-known that rutting is primarily caused by 1) plastic deformation under overload, 2) consolidation or continued compaction under the action of traffic; 3) surface wearing; and 4) material deterioration. This implies that the performance of elastomeric concrete headers may be improved if reinforcement is provided to resist the rutting. In view of this, tests are designed to evaluate the performance of elastomeric concrete reinforced by steel wires.

The evaluation will be based on the comparison with the current practice. Here Class AAAP concrete and the elastomeric concrete supplied by *Delcrete* will be used. Their mix designs or compositions are tentatively selected as follows:

Class AAAP Concrete: Type I cement (493 lb); Class F fly ash (87 lb); sand (1245 lb); coarse aggregate (1756 lb); water/cement ratio (0.45).

Elastomeric Concrete: Decrete/delpatch DSB 1494 A (Isocyanate-terminated prepolymer); Delcrete/Delpatch DSB 1494 B (Polyol/Diamine blend); aggregate.

Since the rutting resistance is a collective result of the performance under impact, wearing and deterioration, a series of tests is developed to compare the performance of different header materials.

■ Charpy test

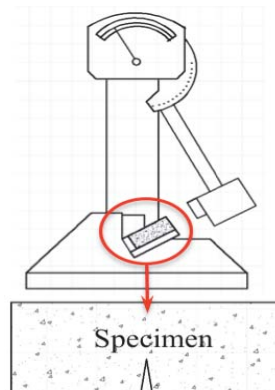


Fig. 23. Illustration of the specimen and the setup for Charpy test.

The objective of this test is to characterize the impact resistance of header materials. In this test design, a notched specimen is impacted by a striker (Fig. 23). To ensure that the measured value can be realistically extrapolated to a full-scale header, specimens of recommended size will be used (Gopalaratnam et al. 1984). To minimize the disturbance induced by the inertial oscillations (Gopalaratnam et al. 1984), a rubber pad will be installed based on the mass and stiffness ratios between the striker and specimen.

■ Abrasion test

The objective of this test is to characterize the resistance of header materials to wearing. Here abrasion test using rotating cutter method based on the ASTM standards will be employed. As shown in Fig. 24, cylindrical specimens will be cast and then loaded by a rotating-cutter equipped with dressing wheels at a rate of 200 r/min. Normal load condition will be adopted in

Bridge Waterproofing Details Phase II

the testing. To ensure a reliable comparison between different samples, the specimens will be cast in molds made of PMMA, which leads to surfaces of similar smoothness.

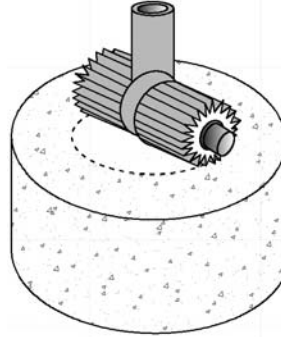


Fig. 24. Illustration of the specimen and setup for abrasion test.

■ Corrosion test

Coupled chemical attacks during service, especially deicing chemicals-related process, will accelerate degradation in headers to trigger structural failure. To characterize the corrosion resistance, specimens made of different header materials are designed to undergo accelerated corrosion test to mimic the coupled calcium leaching and salt attack in headers during service. In the test, prismatic specimens will be alternatively immersed (within an interval of 1 week) in NH_4NO_3 and Na_2SO_4 solutions of a concentration about 15%. After 3 months, the residual chemical-mechanical-physical properties of the degraded specimens will be examined to identify their resistance against the coupled deterioration. The setup of the corrosion test is plotted in Fig. 25.

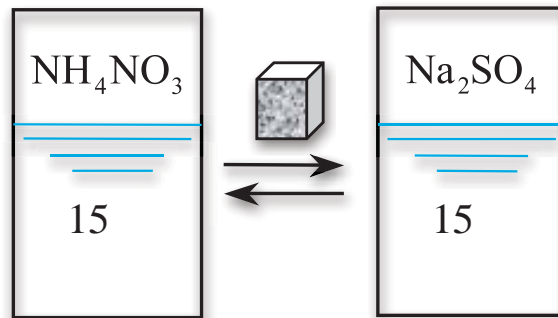


Fig. 25. Illustration of the specimen and setup for corrosion test.

■ Freeze-thaw test

The cycles of freeze-thaw pose a serious threat to the structural integrity of headers because of the cyclic dilating pressure caused by the phase change of water in the pores. To characterize the tolerance against freeze-thaw, specimens are designed to undergo a certain number of freezing/thawing cycles before their residual properties are examined (ASTM C666/C666M-15). As demonstrated in Fig. 26, specimens of different mixtures will undergo the same freezing/thawing cycles. During the test, measurements of the mass change and length variation will be made for each specimen after every 20 cycles and then comparisons will be made.

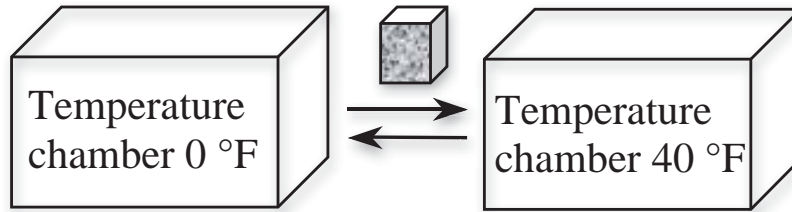


Fig. 26. Illustration of the specimen and setup for freeze-thaw test.

6 Preliminary Design of Sensing System

To ensure that the proper size is selected for the compression seal, which is critical for the lifetime of an expansion joint, the size variation of the joint during bridge service needs to be determined. Meanwhile, it is important to detect the water leakage so as to identify the source of failure, which is difficult to capture by visual inspection. Therefore, an integrated sensing system was recommended in Phase I to monitor the movement of expansion joints as well as to detect water leakage at critical locations.

To monitor the in-situ behavior of the subject, a sensing system, which is self-powered and capable of working outdoors, needs to be designed. As shown in Fig. 27, the preliminary design of this system consists of the following key components:

- Sensor heads to convert physical parameters to electrical/optical signals.
- Signal conditioning circuits to convert sensor signals into standard electric process signals (e.g., analog signals).
- Wireless transmitter to deliver the conditioned signals.
- A storage system to keep the data received.

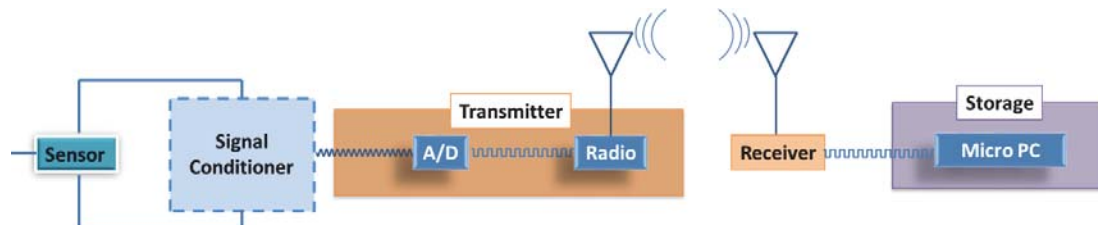


Fig. 27. Illustration of the key components in the sensing system.

To monitor the displacement of joints, electric displacement sensor heads are investigated. The initial focus is placed on Linear Variable Differential Transformer (LVDT) sensor and Differential Variable Reluctance Transducer (DVRT) sensor, both of which are capable of converting displacement measurements to electrical signals (Saxena and Seksena 1989, Mohammad et al. 1994, Crescini et al. 1998, Tariq et al 2002, Fleming et al. 1999, Hollis et al. 2000, Wright et al. 2001). Their working mechanisms are depicted in Fig. A5 and Fig. A6 in Appendix, respectively.

To detect the water leakage, two types of sensor heads are available. The first one is electric sensor, which takes advantage of its electric response to water contact. When any part of the sensor meets water leakage and absorbs a small amount of water, the AC resistance between the sensor electrodes will drop significantly, and thus can be used as output signals. Its working mechanism is illustrated in Fig. 28.

Bridge Waterproofing Details Phase II

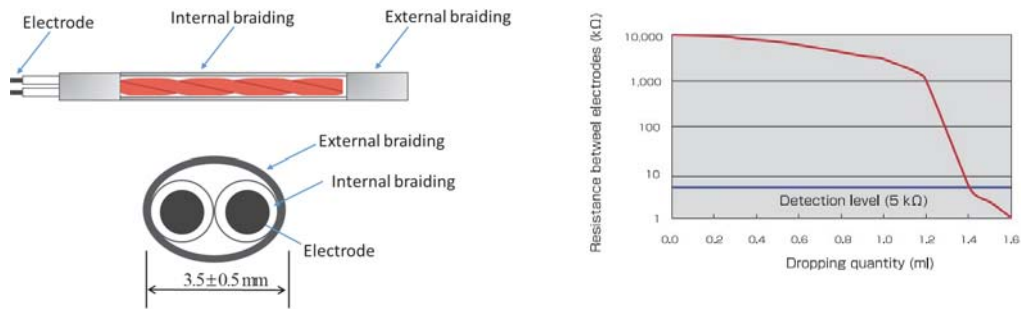


Fig. 28. Illustration of the structure of an electric sensor head and its electrical characteristics.

The second type is optical fiber, which is able to measure strain, temperature, pressure, moisture, and displacement by monitoring the intensity, phase or wavelength of the light travelling in the fiber (Merzbacher et al. 1996, Casas et al. 2003). Based on the physical sources being measured, the basic working mechanisms of optical fiber can be categorized into 1) intensity modulated; 2) phase modulated; and 3) wavelength modulated. The preliminary design of the optical fiber system is shown in Fig. 29, which consists of 1) light source (laser diode); 2) laser diode controller; 3) optical fiber sensor head; and 4) optical detector (to detect intensity, or wavelength changes in the sensor head).

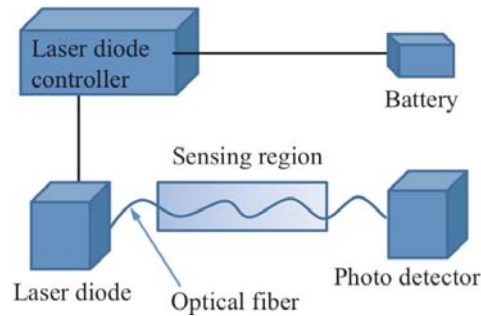


Fig. 29. Preliminary design of the optical fiber sensor system.

To condition and output the signals measured by the electric sensor heads, conditioning circuits need to be designed. The preliminary designs of the conditioning circuits are illustrated in Figs. A7 and A8 in Appendix. For the optical fiber sensor, a conditioning circuit is not needed because the optical detector will handle the output.

To integrate the sensor for displacement and the sensor for water leakage, an electrical system using electric sensor heads were designed; see Fig. 30. In this system, there are two conditioning circuits for the displacement sensor and water leakage sensor respectively. Here a multi-channel transmitter is used to receive and transfer the regularized signals from the LVDT sensor and the wire water leakage sensor. Batteries will be used to power the different components. To use the optical fiber sensor, a hybrid system was designed for the integrated sensing system; see Fig. 31. In this system, the water leakage is detected by the optical fiber system and the same multi-channel transmitter can be used to transfer the signals for water leakage.

Bridge Waterproofing Details Phase II

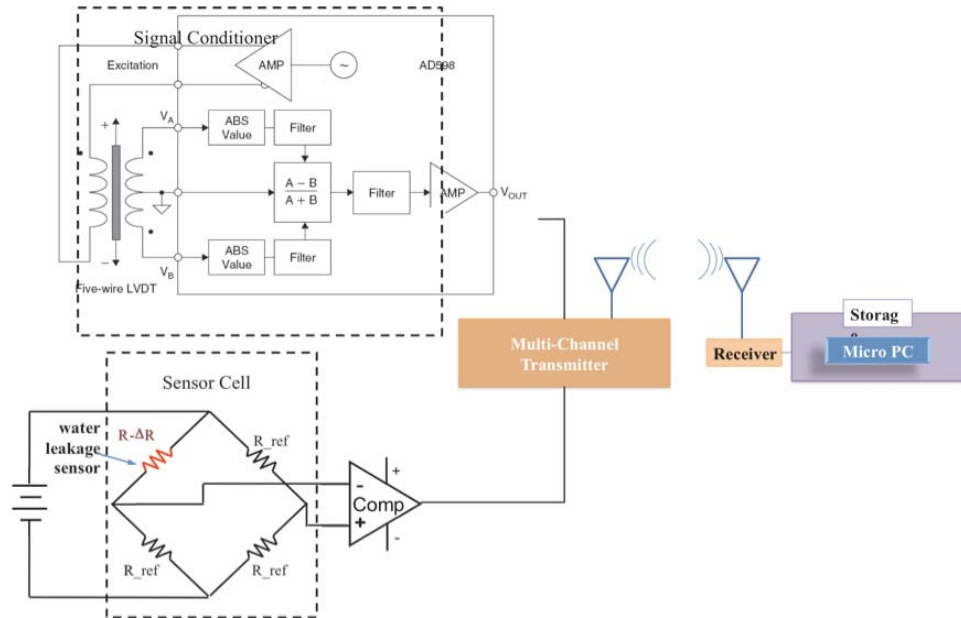


Fig. 30. Preliminary design of the electrical system.

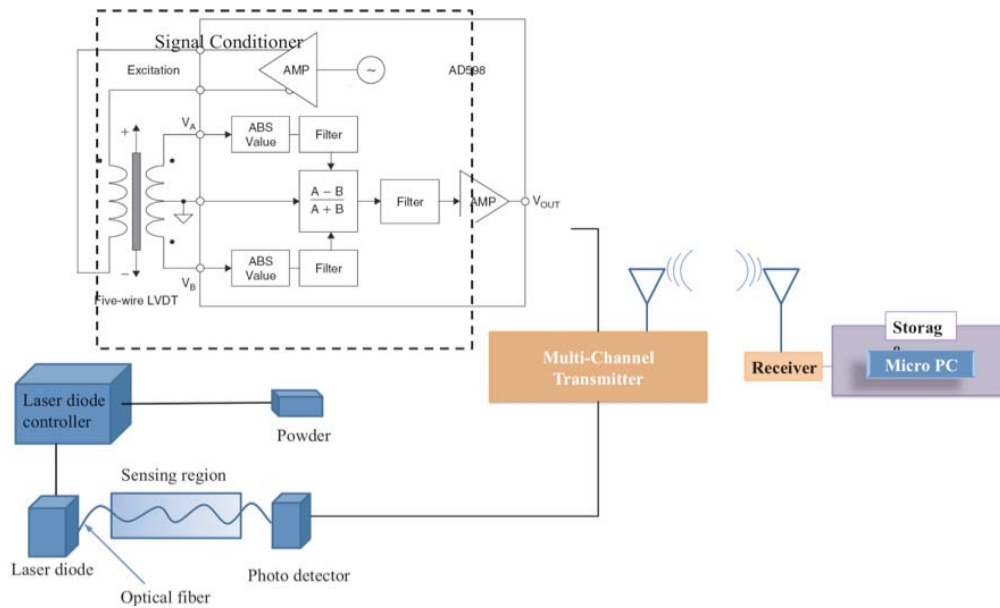


Fig. 31. Preliminary design of the hybrid system.

7 Summary

In this investigation, the recommendations proposed in Phase I are evaluated and the preliminary roadmaps to guide their implementation to practice are developed. The designs and evaluations include:

1. *Enhanced Abutment/beam Adjunction Design*: For integral abutment, crystalline waterstops are recommended for construction joints. For cantilever abutment, three enhanced designs are proposed to simplify the geometry at abutment/beam adjunction. These designs allow the waterproofing membrane to cover all the open gaps between beams, abutments and cheekwalls. Furthermore, the flat surface of the adjunction in the proposed designs provides convenience in membrane installation. Initial FEM analyses show that these designs will not lead to significant change of stress or deformation in the structure.
2. *Construction-friendly Waterstops*: For joints with negligible relative movement (e.g., construction joints), crystalline waterstops are recommended to replace the conventional polymer-based waterstops. The mechanisms of crystalline waterstops lead to an installation process that is construction-friendly. Experimental tests, which simulate the working conditions of bridges, are designed to assess their implementation.
3. *Membrane Delamination Mitigation*: The implementation roadmap focused on constructing an overlap at beam seat is developed to mitigate the delamination risk of waterproofing membrane. Materials preventing the occurrence of a stiffer double layer are assessed and experimental tests for construction process and delamination analysis are designed.
4. *Improved Header Materials*: Elastomeric concrete reinforced with steel wires will be implemented to improve the performance of headers. Tests are designed to quantify its key characteristics related to the resistance to rutting.
5. *Sensing System*: A roadmap to construct an integrated sensing system to monitor the expansion joint movement and detect water leakage is developed. The mechanisms of key components are studied and the approaches to fabricate sensor heads and conditioning circuits are proposed.

Following the roadmap proposed in this task, the characterizations and quantifications will be carried out in Tasks II and III for the abutment design, crystalline waterstops, membrane delamination mitigation and header materials. Concurrently, the components of the sensing system will be fabricated and the system will be tested and optimized.



Chapter 2 Design and Implementation I

1. Introduction

In Task I, three preliminary designs (I, II and III) were proposed to mitigate the risk of water leakage at abutment/beam adjunction. The preliminary evaluation shows that these three designs simplify the geometry of the adjunction so as to enable the gaps between the abutment, beam seat and cheekwalls to be fully covered by the waterproofing membrane. However, compared with the current practice, Designs I and II display some changes in structural forms. To ensure their applicability in the typical bridges of PennDOT, these two designs need more structural evaluations about the stress distribution and deformation development in the adjunction, which will be carried out in this task.

To overcome the limitations of conventional waterstops, as well as to achieve easy installation, crystalline waterstops, whose working mechanisms are very different from the conventional polymer-based waterstops, were preliminarily investigated in Task I. To evaluate the practical implementation of crystalline waterstops, experimental tests, mimicking the service conditions of waterstops in a bridge, are carried out in this task to complete the implementation roadmap.

To mitigate the risk of membrane delamination at open gaps, an overlap was designed in Task I to accommodate the relative movement. To complete the implementation roadmap, tests designed in Task I are carried out in this task to examine the installation easiness and assess the effectiveness of the overlap subject to in-plane and out-of-plane shear stress, both of which can be induced by the relative longitudinal movement of bridge beams.

A sensing system capable of detecting water leakage and monitoring expansion joint movement was outlined in Task I. In this task, the focus is placed on the sensing system monitoring the displacement of expansion joints. The completion of implementation roadmaps for the header materials and the sensing system for water leakage detection will be tackled in the next task – Task III.

2. Design of Abutment/beam Adjunction

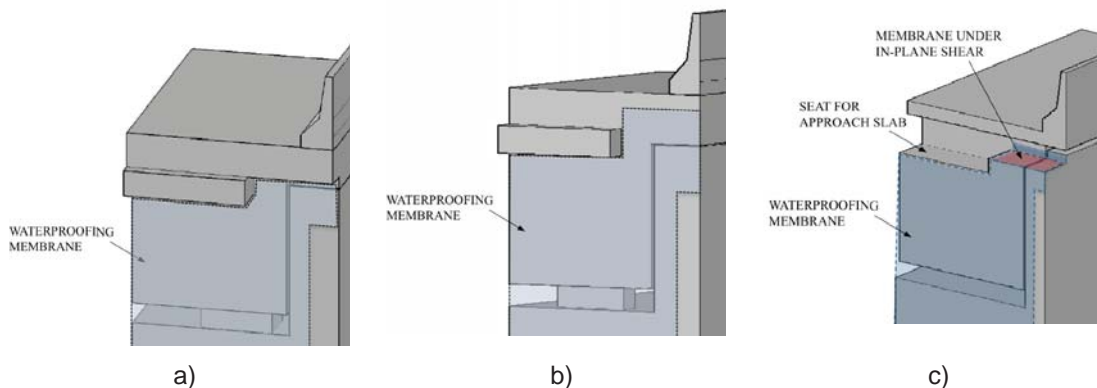


Fig. 32. Illustration of the enhanced designs of abutment/beam adjunction: a) Design I; b) Design II; and c) Design III.

Three designs, which are illustrated in Fig. 32, were proposed in Task I to improve abutment/beam adjunction. Among these three designs, Design III uses a modified paving notch

Bridge Waterproofing Details Phase II

to support the approach slab. Its structural form is almost the same as the current practice. Therefore, its application for the typical bridges in PennDOT should not result in significant difference in terms of structural analysis.

However, both Designs I and II show structural forms different from the current practice in PennDOT. In Design I, the deck slab is extended 1 foot and 5 inches away from the backside of abutment and provides a step-shaped seat for the approach slab; see Fig. 32a. While in Design II, the deck slab is not extended. But a lip-shaped support is added at the beam end for the approach slab; see Fig. 32b.

Table 2: matrix of models for Designs I and II

Girder or beam type	Case	Skew angle	Span (ft.)
AASHTO Type IV	1	0°	80
	2	0°	100
	3	30°	80
	4	30°	100
BD-662M (Bulb-T)	5	0°	80
	6	0°	100
	7	30°	80
	8	30°	100
BD-661 M (Box)	9	0°	80
	10	0°	100
	11	30°	80
	12	30°	100
Steel girder (W18X158)	13	0°	80
	14	0°	100
	15	30°	80
	16	30°	100

To ensure the safety and applicability of these two designs, numerical analyses based on finite element method (FEM) are employed to investigate the structural responses of bridges, especially the responses of the end diaphragm and extended slab (or lip-shaped support). In order to achieve a balance between the cost of numerical simulations and investigation scope, four typical girders used in PennDOT practice are selected to probe the performance of the enhanced designs for beam-abutment adjunction. In addition to the difference in beam cross-sections and materials, different skew angles and span lengths are selected for extending the scope of numerical investigation. The matrix of bridge models for both Designs I and II is listed in Table 2, where the type of girder, span length and skew angle for each model are described.

The models are built in the commercial program ATENA (Cervenka et al. 2003), a FEM program with advanced material models for concrete and steel structures. It has been demonstrated that this FEM program is capable of capturing the structural responses of reinforced and prestressed concrete structures. In the simulations, each bridge model contains two lanes, and two HL-93



Bridge Waterproofing Details Phase II

truck loads, which comply with AASHTO code (AASHTO 2012), are applied on the bridge. Based on the AASHTO code, the dynamic impact factor is set to be 1.75 for the trucks.

Based on the preliminary results in Task I, the most undesired scenario happens in abutment/beam adjunction when the loads are placed on the tip of extended slab or lip-shaped support. In view of this, the heavier axles of the two trucks are placed on the tip and the other axles on the bridge deck in the simulations. For each model, the number of girders or beams, which support the deck, is determined by the spacing given in PennDOT recommendations for typical practice.

For each type of girder or beam, only the critical case is presented here for each design. The results of other cases, characterized by different span lengths and skew angles, are given in the tables in Appendix. In Table 3, the main structural responses obtained for Design I using AASHTO Type IV girders (Case 2) are shown. In Table 4, the structural responses of Case 2 using Design II are presented. Similarly, the simulation results for Cases 6, 10, and 14 can be found in Tables 5 to 10 when Designs I and II are used respectively.

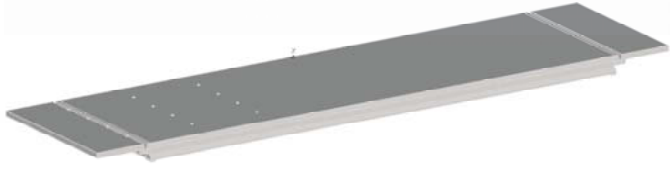
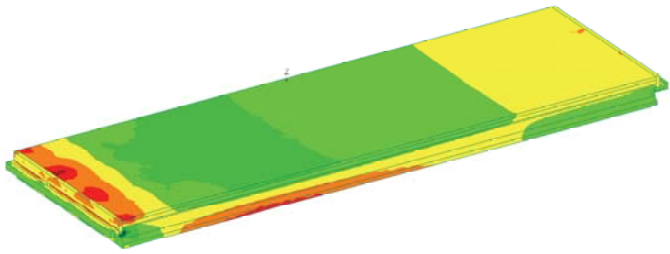
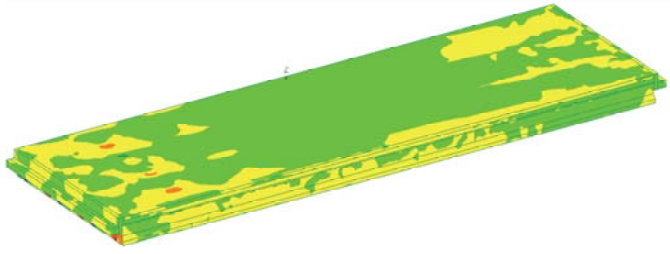
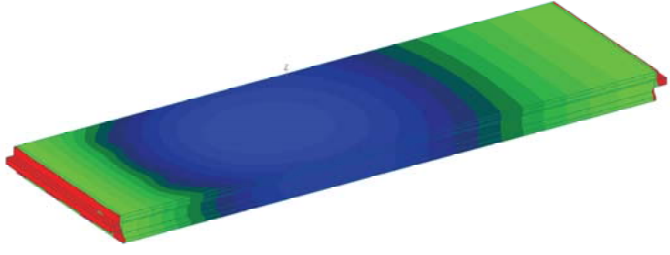
In the first row of these tables (as well as the tables in Appendix), the 3D computer model of the corresponding case is demonstrated. In the second row, the profile of normal stress induced by the trucks is depicted. In the third row, the distribution of shear stress is given. In the fourth row, the vertical deflection caused by the external load is presented. In the last row, a short summary of the numerical study is listed. Note that the color scale bars are not shown in these tables to save space. The representations of the colors in the models are similar to those in Fig. 12. For example, red color represents tensile stress for the normal stress profile (at the second row) and blue color means downward deflection in the deflection profile (at the fourth row). Based on these scale bars, the maximum values of interest can be attained from the simulations.

Based on the numerical results, it can be seen that for the typical concrete girders or steel beams used in PennDOT practice, Designs I and II will not cause excessive deflection, neither abnormal stress distribution leading to significant change in reinforcement amount and placement. Therefore, the safety and applicability of the bridges will not be compromised when the proposed designs are implemented to simplify the geometry of abutment/beam adjunction. Using the numerical results as benchmarks and utilizing AASHTO design methods for disturbed regions (e.g., strut-and-tie design method), a standard structural design of the extended slab and lip-shaped support can be achieved for bridges of different span lengths and skew angles.



Bridge Waterproofing Details Phase II

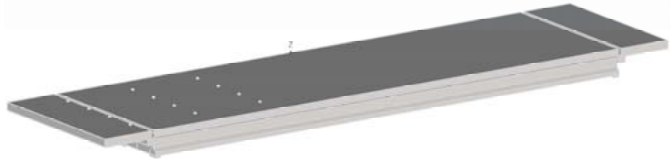
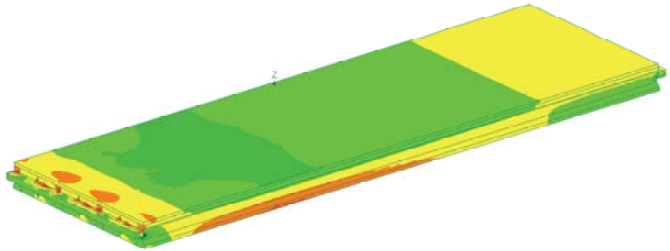
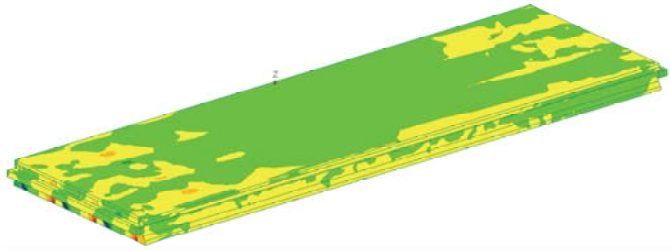
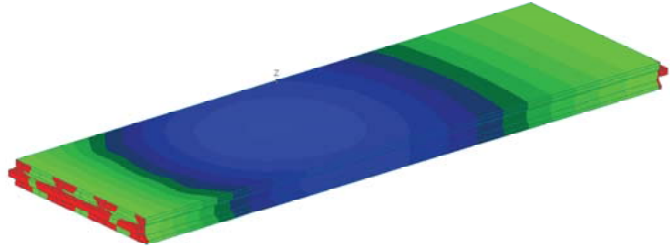
Table 3: Case 2 using Design I

Computer model	
Normal stress	
Shear stress	
Deflection	
<p>Span: 100 ft; Width: 30 ft; Skewed angle: 0°; Lanes: 2; Number of girders: 4 Maximum tensile stress: 0.05 ksi Maximum compressive stress: 0.11 ksi Maximum shear stress: 0.009 ksi Vertical deflection over length of extended slab: <1/1000</p>	



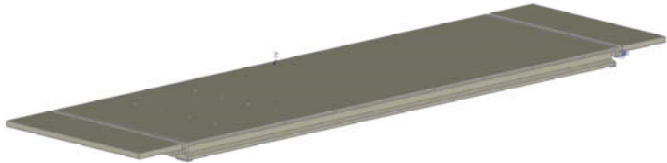
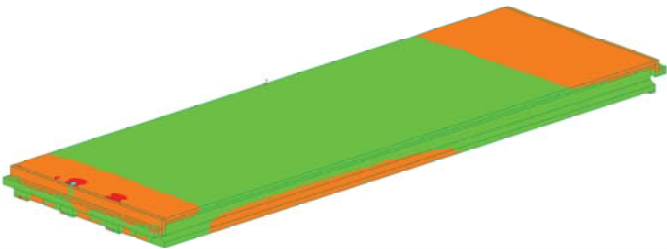
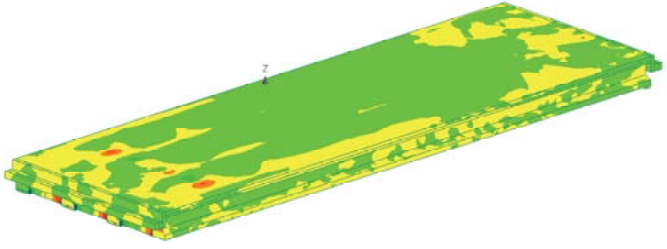
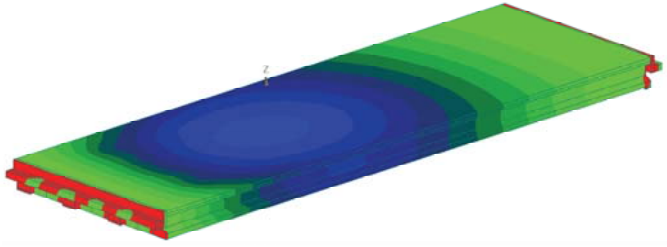
Bridge Waterproofing Details Phase II

Table 4: Case 2 using Design II

Computer model	
Normal stress	
Shear stress	
Deflection	
<p>Span: 100 ft; Width: 30 ft; Skewed angle: 0°; Lanes: 2; Number of girders: 4 Maximum tensile stress: 0.11 ksi Maximum compressive stress: 0.11 ksi Maximum shear stress: 0.016 ksi Vertical deflection over length of lip-shaped support: <1/1000</p>	

Bridge Waterproofing Details Phase II

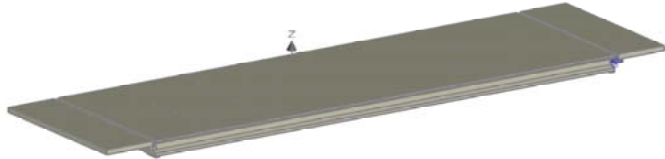
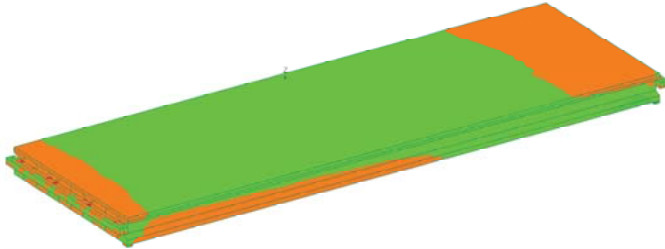
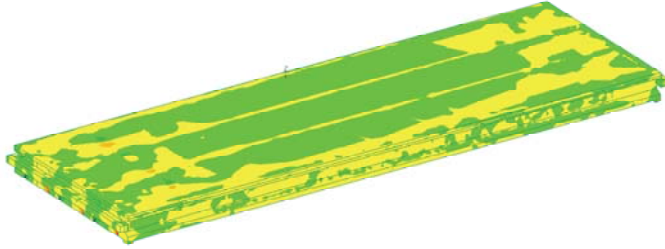
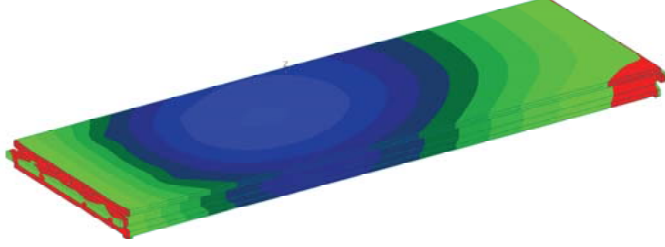
Table 5: Case 6 using Design I

Computer model	
Normal stress	
Shear stress	
Deflection	
<p>Span: 100 ft; Width: 30 ft; Skewed angle: 0°; Lanes: 2; Number of girders: 4 Maximum tensile stress: 0.05 ksi Maximum compressive stress: 0.13 ksi Maximum shear stress: 0.014 ksi Vertical deflection over length of extended slab: <1/1000</p>	



Bridge Waterproofing Details Phase II

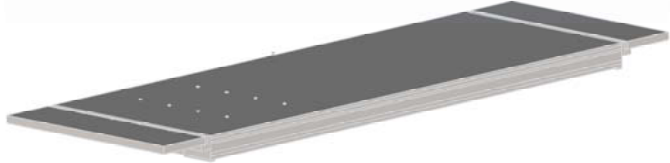
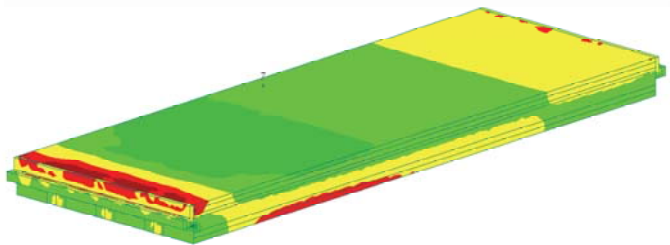
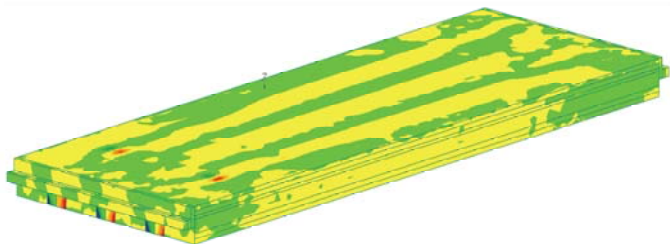
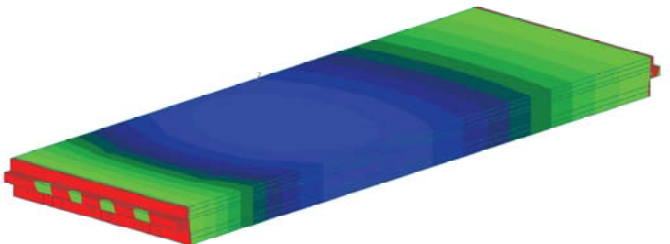
Table 6: Case 6 using Design II

Computer model	
Normal stress	
Shear stress	
Deflection	
<p>Span: 100 ft; Width: 30 ft; Skewed angle: 0°; Lanes: 2; Number of girders: 4 Maximum tensile stress: 0.12 ksi Maximum compressive stress: 0.11 ksi Maximum shear stress: 0.014 ksi Vertical deflection over length of lip-shaped support: <1/1000</p>	



Bridge Waterproofing Details Phase II

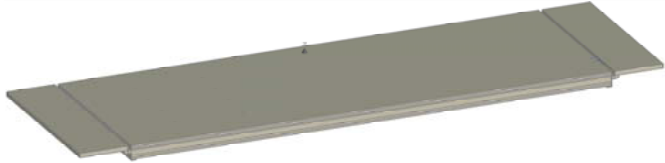
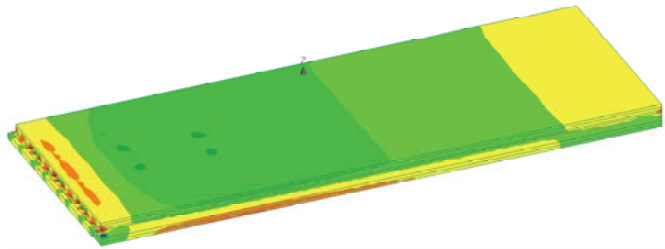
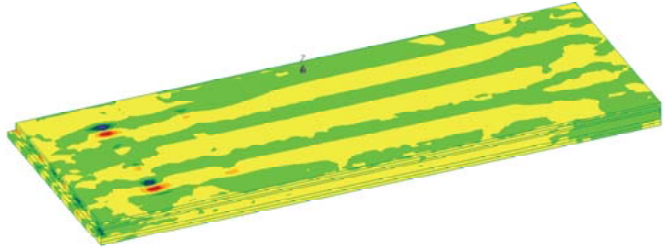
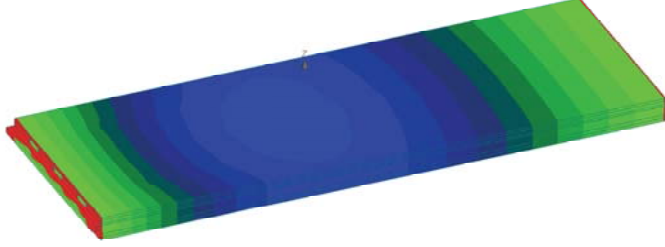
Table 7: Case 10 using Design I

Computer model	
Normal stress	
Shear stress	
Deflection	
<p>Span: 100 ft; Width: 30 ft; Skewed angle: 0°; Lanes: 2; Number of girders: 4 Maximum tensile stress: 0.05 ksi Maximum compressive stress: 0.13 ksi Maximum shear stress: 0.011 ksi Vertical deflection over length of extended slab: <1/1000</p>	



Bridge Waterproofing Details Phase II

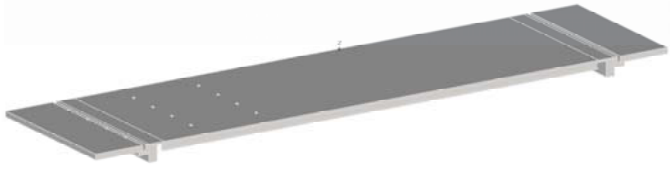
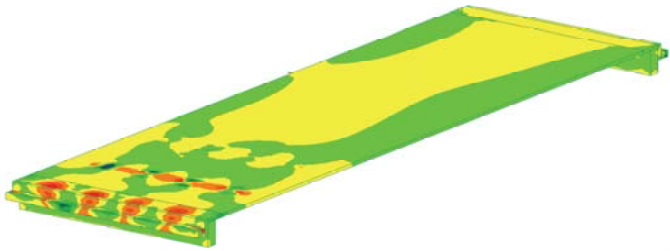
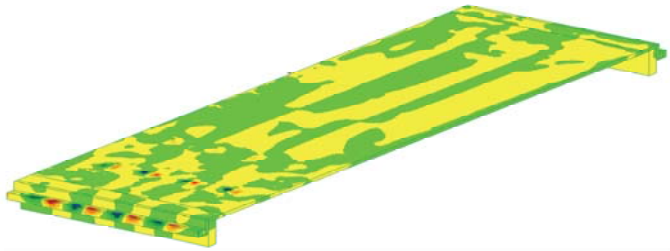
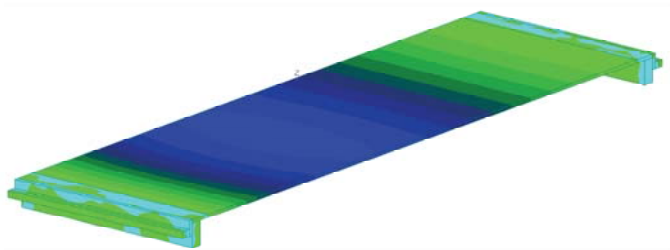
Table 8: Case 10 using Design II

Computer model	
Normal stress	
Shear stress	
Deflection	
<p>Span: 100 ft; Width: 30 ft; Skewed angle: 0°; Lanes: 2; Number of girders: 4 Maximum tensile stress: 0.10 ksi Maximum compressive stress: 0.10 ksi Maximum shear stress: 0.014 ksi Vertical deflection over length of lip-shaped support: <math><1/1000</math></p>	



Bridge Waterproofing Details Phase II

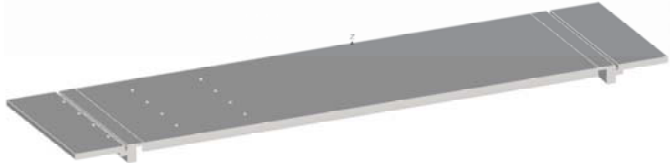
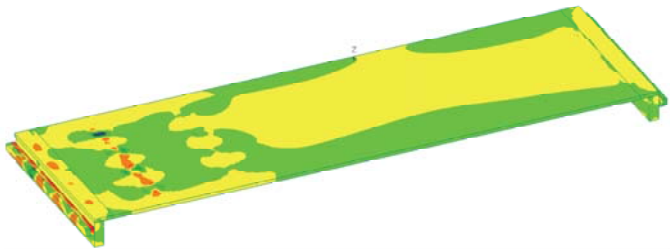
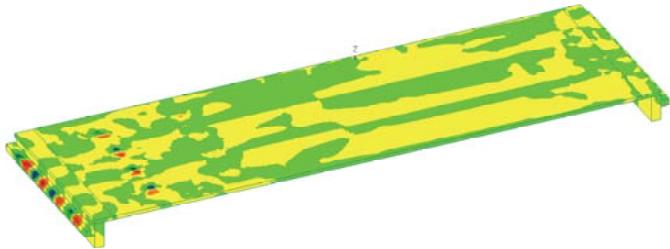
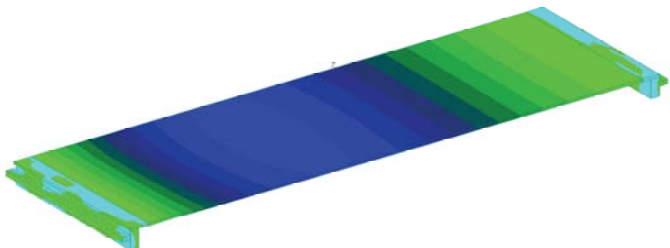
Table 9: Case 14 using Design I

Computer model	
Normal stress	
Shear stress	
Deflection	
<p>Span: 100 ft; Width: 30 ft; Skewed angle: 0°; Lanes: 2; Number of girders: 4 Maximum tensile stress: 0.05 ksi Maximum compressive stress: 0.10 ksi Maximum shear stress: 0.013 ksi Vertical deflection over length of extended slab: <1/1000</p>	



Bridge Waterproofing Details Phase II

Table 10: Case 14 using Design II

Computer model	
Normal stress	
Shear stress	
Deflection	
<p>Span: 100 ft; Width: 30 ft; Skewed angle: 0°; Lanes: 2; Number of girders: 4 Maximum tensile stress: 0.13 ksi Maximum compressive stress: 0.11 ksi Maximum shear stress: 0.016 ksi Vertical deflection over length of lip-shaped support: <1/1000</p>	



3. Implementation of Crystalline Waterstops

To complete the implementation map of crystalline waterstops, both Xypex and Krystol crystalline waterstops were used in the tests designed in Task I. In the tests, the procedure of casting concrete and installing crystalline waterstops strictly followed the instruction manuals for worksite implementation. Only the external implementation was investigated for Krystol waterstop. The internal implementation was not tested because it requires a minimum thickness of 6 in. for concrete sections, which may not be satisfied in bridge construction.

Based on the instruction manuals, a layer of crystalline slurry is first sprayed on the interface of joint. Then, the treatment is completed with the dry-pack (of Xypex) or crystalline grout (of Krystol) filled in the pre-formed groove to seal the joint. The recommended size of the groove should be as deep as $\frac{1}{4}$ of the thickness of concrete sections but no more than 1.25 in., and as wide as twice of the depth while no more than 2 in. The groove for dry-pack or grout can be formed by spacers made of materials of low water absorption, for example PMMA plastic.

The critical implementation steps in the test, which should be the same for real construction, are listed as follows (Xypex Concentrate Product Data 2004, Application Instructions Construction Joints and Details of Krystol 4.11 & 4.12, 2016):

◆ *Xypex treatment*

1. Clean the concrete surface with clean water and then make the concrete surface-dry;
2. Mix waterstop slurry, and then use a brush to pave it uniformly on the concrete surface (to form a layer about 0.04 in. thick), and then cure this layer for 48 hours before the casting of next part of the joint;
3. 24 hours after the second part of the joint is cast, clean the pre-formed groove in the joint with clean water and then make it surface-dry;
4. Pave the surface of groove with waterstop slurry uniformly;
5. Wait for at least 10 minutes, fill the groove with dry-pack grout and then apply the Xypex plug-N pack to make the surface flat;
6. Cure the treatment for 24 hours by light mist or wet burlap.

◆ *Krystol treatment*

Steps are similar to Xypex treatment except for the difference listed below:

1. The curing time for the slurry layer in the interface of concrete joint is shorter than Xypex waterstop; it is recommended to be 12-24 hours (24 hours were used in the test).
2. The Krystol grout is used to fill the groove, and then the slurry layer is brushed on the top of the grout to make the surface flat.

To prepare the crystalline slurry and grout, protocols were established in the tests, which can be used in construction. Compared to the instruction manuals, the protocols of preparing the waterstop slurries are slightly revised based on the research team's experience in the lab and the discussion with the technicians from the suppliers. The finalized mixing process is listed below (here all the mix ratios are by volume):

1. For Xypex slurry, the recommended mix ratio of Xypex concentrate powder to water is 2 : 1; for Xypex Dry-pack, the mix ratio is 4 : 1; for the Plug N Pack, it is 3 : 1. After mixing, stirring for about 1 minute to achieve a uniform slurry- or paste-like product.
2. For Kystol slurry, the recommended mix ratio of Krystol powder to water is 3 : 1; for Krystol Grout, the mix ratio is 4 : 1. After mixing, stirring for about 1 minute to achieve a uniform slurry- or paste-like product.



Water tank test

The water tank test is designed to examine the effectiveness of crystalline waterstops, as well as to evaluate the installation easiness. To mimic the real construction and service conditions, vertical and horizontal joints were constructed and water pressure was applied on these joints in the tests. The design of water tanks and the arrangement of the spacers for constructing the pre-formed grooves are depicted in Fig. 33, where the dimensions of the water tank are given and the sequence of concrete casting is illustrated.

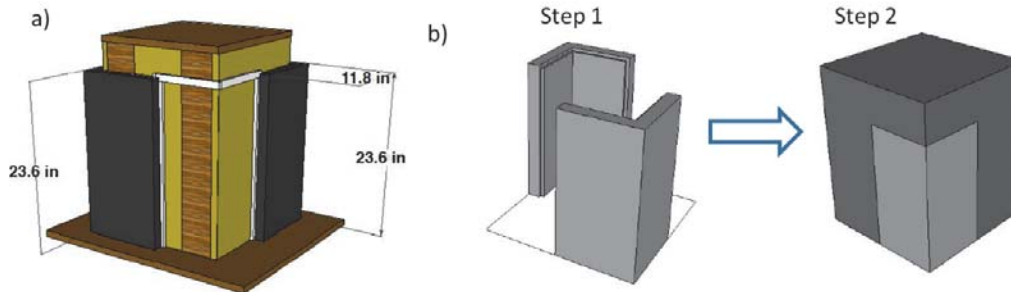


Fig. 33. a) The water tank design and the arrangement of plastic spacers and b) the sequence of concrete casting.

To make it easier to cast concrete and remove moulds and spacers, the horizontal construction joint in the bottom slab, which was initially proposed in Task I, is replaced by two horizontal joints at the bottom of sidewalls; see Fig 34. In addition, for each tank, there is a vertical joint, running from the bottom to the top, in each sidewall (Fig. 34).

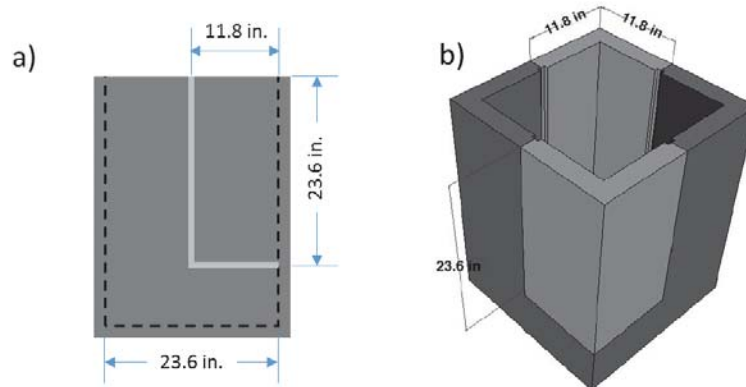


Fig. 34. a) The front view of the horizontal and vertical construction joints in a sidewall and b) the 3d plot of the horizontal and vertical construction joints.

Fig. 35 shows a water tank after the first casting of concrete. Two days after the concrete was cured, which is usually the case in construction, the crystalline slurries were applied on the surfaces of vertical and horizontal joints. The mixed slurries of Xypex and Krystol treatments are shown in Fig. 36, respectively.

Bridge Waterproofing Details Phase II



Fig. 35. The first casting of concrete in a water tank.



Xypex Slurry



Krystol Slurry

Fig. 36. Xypex and Krystol slurry mixture.

Then, the crystalline treatment was cured as instructed before the second casting of concrete. After that, the second part of the water tank was cast and the finished tank is shown in Fig. 37. Similarly, the curing of concrete lasted two days. Next, the dry-pack of Xypex treatment or grout of Krystol treatment was mixed (Fig. 38) and then used to seal the pre-formed grooves as instructed (Fig. 39).



Fig. 37. The second casting of concrete in a water tank.

Bridge Waterproofing Details Phase II



Xypex Dry-Pack



Krystol Grout

Fig. 38. The mixture of Xypex Dry-Pack and Krystol Grout.

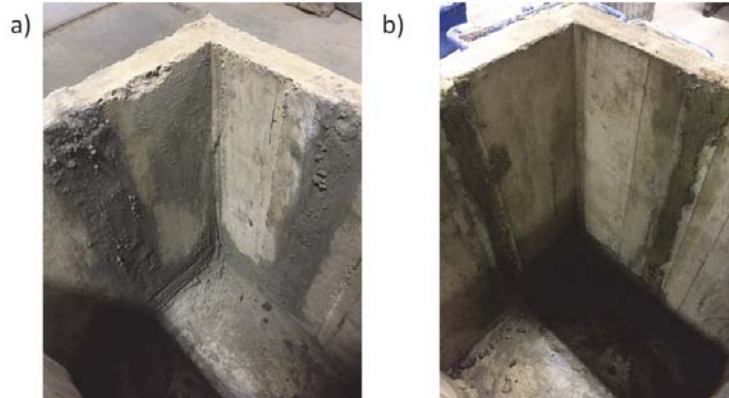


Fig. 39. Water tank treated with a) Xypex waterstop and b) Krystol waterstop.

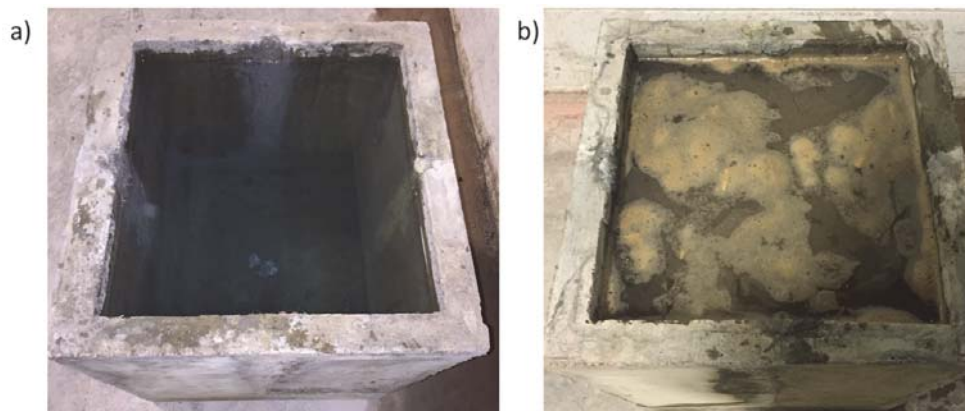


Fig. 40. Water tank tested with a) clean water and b) water, soil and deicing powder mixture.

Bridge Waterproofing Details Phase II

For each crystalline waterstop treatment, two water tanks were built, one filled with water and the other with water, soil and deicing powder (Fig. 40). The use of soil is to investigate the resistance of dry-pack of Xypex and grout of Krystol to the impact and friction induced by backfilling. The addition of deicing powder is to investigate the performance of crystalline waterstops under the typical chemical attack on bridge substructure.

The observation lasted 7 days. Every joint in each water tank was visually inspected twice per day. No water leakage was found in all the joints treated with the crystalline waterstops. This means that both crystalline waterstops worked well, even under water pressure, chemical attack and subject to backfill. To evaluate the easiness of implementation, an additional water tank was built for comparison. In this construction, a conventional polymer-based waterstop was used for all the joints; see Fig. 41a,b. The polymer-based waterstop was procured from W.R. Meadows (IL, USA), and its installation instruction is shown in Fig. 41c. The test result shows that the polymer-based waterstop also provided satisfactory service and no water leakage was found in any joints during the 7-day observation.



Fig. 41. a) The implementation of a polymer-based waterstop in the water tank; b) the water tank during test; and c) Illustration of the implementation of the polymer-based waterstop.

However, compared to the crystalline treatment, the installation of the polymer-based waterstop is much more demanding in terms of carefulness, skill and time. When concrete was poured, dislodgement and warping happened in all the joints, especially in the vertical joints. Therefore, the concrete casting had to be stopped frequently during the test to check and adjust the position of the polymer sheet. While for crystalline waterstops, this is not needed. Furthermore, after the concrete is poured, the position of polymer sheet embedded inside the concrete cannot be visually inspected. But for crystalline waterstops, the uniformity of slurry can be easily inspected before the second part of the joint is cast.

■ Cyclic loading test

Although the relative movement at construction joint is negligible, stress variation exists due to the vehicles travelling on the bridges. To investigate the effect of stress variation on the performance of crystalline waterstops, cyclic loading test, which was designed in Task I, was carried out on both Xypex and Krystol waterstops.

In the test, two concrete slabs were made. For each slab, there is a horizontal joint at middle. Since the concrete was designed to go through cyclic loading, a longer curing time, i.e., 7 days, was used for each batch of concrete. For both slabs, the joints in them were treated with Xypex and Krystol waterstops respectively. The procedure of implementation of crystalline waterstops is the same as that in the water tank test.

Bridge Waterproofing Details Phase II

To mimic the stress variation induced by traffic loads, a periodic load, characterized by a sinusoidal waveform, was used in the test. The frequency of cyclic load is 0.25 Hz, corresponding to vehicles traveling at a velocity about 20 mph. The stress exerted on the concrete slab is compressive, with an average of 25% of concrete strength and cycling from 15% to 35% of the concrete strength. The total number of cycles for each slab was selected to be 2000. Obviously, this number is much less than the cycles a bridge will experience in its lifetime. However, considering the facts that relatively high stress (35% of strength) was used in the test and the slabs were not reinforced by any steel bars, the selected cycle number is deemed to give a reasonable indication of the performance of crystalline waterstops subject to stress variation.

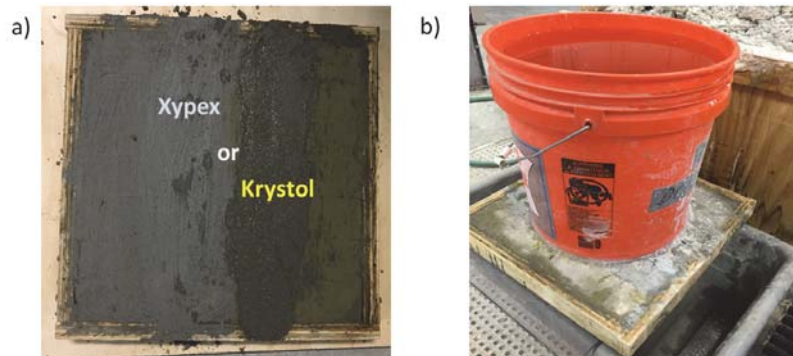


Fig. 42. a) Concrete plate containing a construction joint being treated by Xypex or Krystol waterstops and b) water leakage test before and after cyclic loading.

The test was carried out in two steps. In the first step, the slabs with joints treated with crystalline waterstops were made and cured; see Fig. 42a. Then, water leakage test was run to ensure the joints were watertight; see Fig. 42b. If no water leakage was found in the joint for 7 days, the slabs were placed on the loading frame for the second step. In the second step, the loading setup is shown in Fig. 43. After loaded for 2000 cycles, the slabs were moved out from the loading frame and water leakage test was repeated. This time, the joints were inspected visually twice per day for 7 days. The test results show that both crystalline waterstops performed well after cyclic loading. There was no water leakage found in the slabs.



Fig. 43. Concrete plate under cyclic loading.

Bridge Waterproofing Details Phase II

■ Old-new concrete interface

To evaluate the performance of crystalline waterstops in old-new concrete interface, where it is difficult to install the conventional, test designed in Task I was carried out. To form the old-new concrete interface, two concrete blocks stored in the environmental chamber for more than 3 years were used. The mixture design of these two concrete blocks is very different from the new concrete. For each block, two old-new interfaces were constructed; see Fig. 44. To form the groove for dry-pack of Xypex or grout of Krystol, a saw was used to produce a slot in each concrete block.

Then, Xypex and Krystol crystalline waterstops were applied to the old concrete blocks respectively. After the slurry was cured, new concrete was cast and then the groove was filled with dry-pack or grout. Water leakage test, which is similar to that used in the cyclic loading test, was subsequently carried out (Fig. 45).

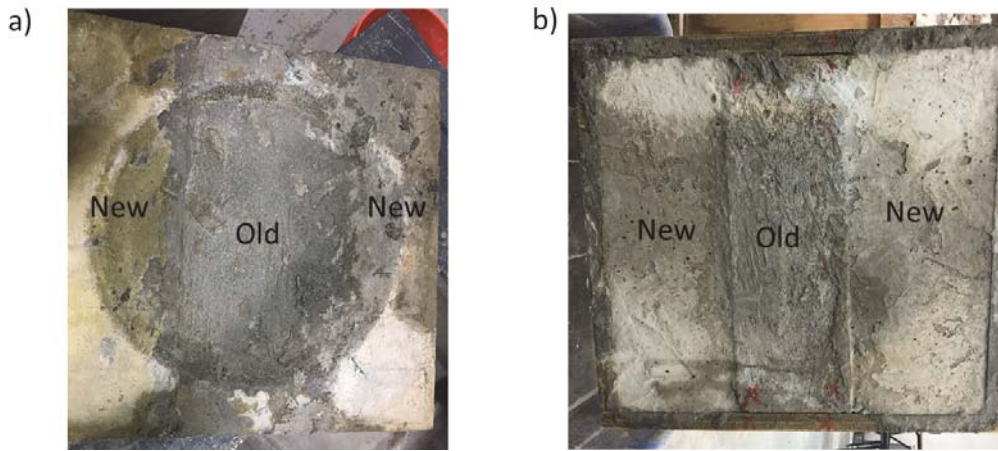


Fig. 44. a) The front view of the concrete old-new interfaces and b) the back view of the concrete old-new interfaces.

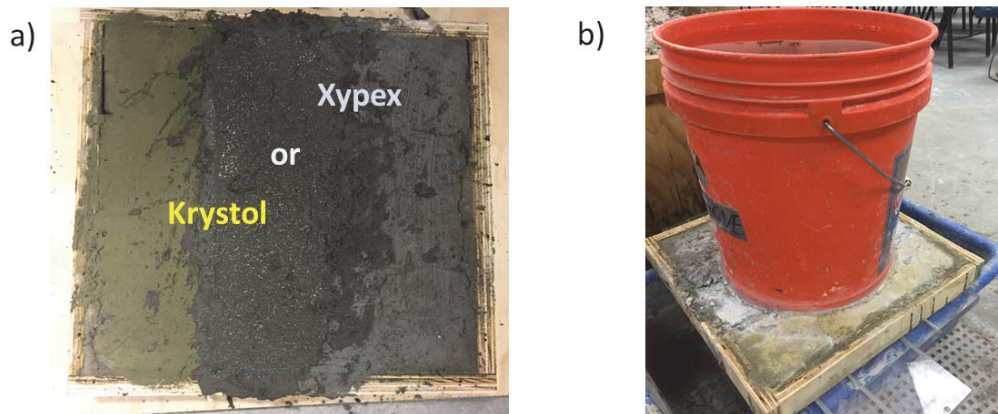


Fig. 45. a) The concrete plate with old-new concrete interface treated by Xypex or Krystol waterstop and b) water leakage test setup.

Bridge Waterproofing Details Phase II

In the following two weeks, no sign of water leakage was observed in any of the old-new concrete joints. It means that the crystalline waterstops are capable of sealing the gap between the old and new concretes. Considering the extreme difficulty lies in the implementation of the conventional waterstops in old-new concrete interface, the crystalline waterstops provide a promising alternative solution to this problem.

Based on the experimental results, the effectiveness and construction-friendliness of crystalline waterstops can be assessed. The performance of crystalline waterstops is good in all the designed tests. Compared with the conventional waterstops, the installation of waterstops is more efficient. Due to their inherent working mechanisms, curing time is needed for crystalline waterstops. This may demand for careful construction management to avoid prolonging the total construction time.

4. Construction of Overlapped Waterproofing Membrane

Based on the preliminary investigation in Task I, fiberglass powder and dry fine sand are selected to construct the membrane overlap at beam seat. The steps of overlap construction used in the tests include:

1. Fiberglass powder or fine sand is prepared;
2. A sharp blade, guided by a straightedge, is used to cut the cover, which is then peeled off to expose the adhesive surface of membrane;
3. The size of the exposed portion is determined based on the maximum relative movement at the gap. For example, if the designed maximum relative movement is 0.5 in., the exposed portion can be selected to be 1 in. plus the gap size to form an overlap to accommodate both the in-plane shear and out-of-shear induced by this movement;
4. After fiberglass powder or fine sand is applied, the rest of the cover of the membrane is peeled off and the membrane is then glued on the concrete surfaces;
5. Examine the bond quality before testing.

Two types of tests were conducted in this subtask to examine the installation efficiency and the effectiveness of the overlap. For comparison, membrane without overlap was also tested under the same conditions.

■ Setup for out-of-plane shear



Fig. 46. Experimental setup for the out-of-plane shear test.

Bridge Waterproofing Details Phase II

Fig. 46 shows the experimental setup for the delamination test. Two 2.75×2.75×14 in. rectangular concrete beams were cast and then utilized to simulate the gap at beam seat in cantilever abutment. Several steel rollers were placed on the steel blocks, which were used to simulate the beam seat, to allow the sliding of the concrete beam on the top. The size of the gap is 2.5 in.

■ No overlap

As a benchmark, the gap was first covered by membrane without overlap. Fig. 47 shows the setup of the test. After the quality of the bond between the concrete and membrane was visually inspected to ensure there was no wrinkles and misalignment, the top beam was pushed forward to generate a relative slip. In this test, it was found that significant delamination occurred when the relative movement reached 0.4 in. The images of delamination captured by a high-resolution microscopy system are shown in Fig. A9 in Appendix.

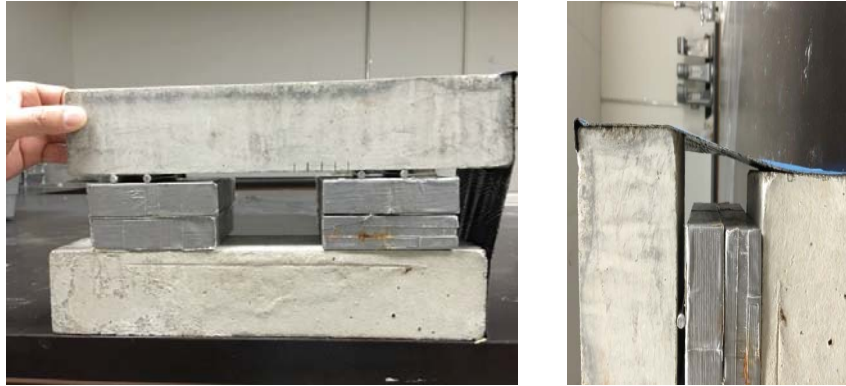


Fig. 47. Delamination of waterproof membrane without overlap at 0.4 in. slip.

In addition, another test, which used a longer piece of membrane to cover the same gap, was carried out to investigate the effect of self-stickness of membrane; see Fig. 48. To accommodate the relative movement, the length of the membrane covering the gap was selected to be 4 in., 1.5 in. longer than the gap size. However, due to the self-stickness of membrane, most part of the sticky surface was glued together to form a double layer (Fig. 48). In this test, significant delamination was found when the relative movement was about 0.8 in. This small improvement was due to the extra length provided by the unglued part of membrane.



Fig. 48. Delamination of waterproof membrane with a double layer formed by self-stickness.

■ Overlap treated with fiberglass powder

Fig. 49 shows the process of treating the adhesive surface of waterproofing membrane with the shredded fiberglass powder. In this test, an overlap, about 0.75 in. long, was designed to accommodate the relative movement of the concrete beams. To form this overlap, the construction steps listed above were followed and no problems were found during the construction. Since the middle portion was treated with fiberglass powder, the surface of membrane was no longer sticky and an overlap was naturally formed. In this test, the overlap hung at the gap freely. In real construction, polystyrene foam layer will be used to protect the membrane, which will provide support to fix the overlap.

After the overlap was made and the bond quality was examined, relative movement was introduced. With the help of overlap, no delamination was observed, even when the slip reached 2.8 in. Delamination of membrane was found when the relative movement was up to 3.2 in. (Fig. 49). Compared to the membrane without overlap or with a double layer, the use of fiberglass powder significantly improves the resistance of membrane to out-of-plane shear. Thus, the risk of delamination is significantly mitigated.

■ Overlap made with dry fine sand

Fig. 50 shows the process of covering the adhesive surface of waterproofing membrane with dry fine sand. Following the same construction process, a portion of cover was peeled off at first and then fine sand was uniformly applied on the exposed surface with the aid of a brush. An overlap, similar to the membrane treated with fiberglass powder, was automatically formed; see Fig. 50. When the top beam was pushed forward, the membrane showed an enhanced capacity to accommodate the relative movement. No delamination was observed when the top beam moved 2.8 in. forward. Significant delamination occurred when the relative movement reached 3.2 in.; see Fig. 50.

Bridge Waterproofing Details Phase II



Fig. 49. Experiment of waterproof membrane with an overlap treated with shredded fiberglass powder: a) treatment of shredded fiberglass powder; b) overlap formed at the gap; c) no delamination at 2.8 in. slip; and d) delamination appears at 3.2 in. slip.

Bridge Waterproofing Details Phase II

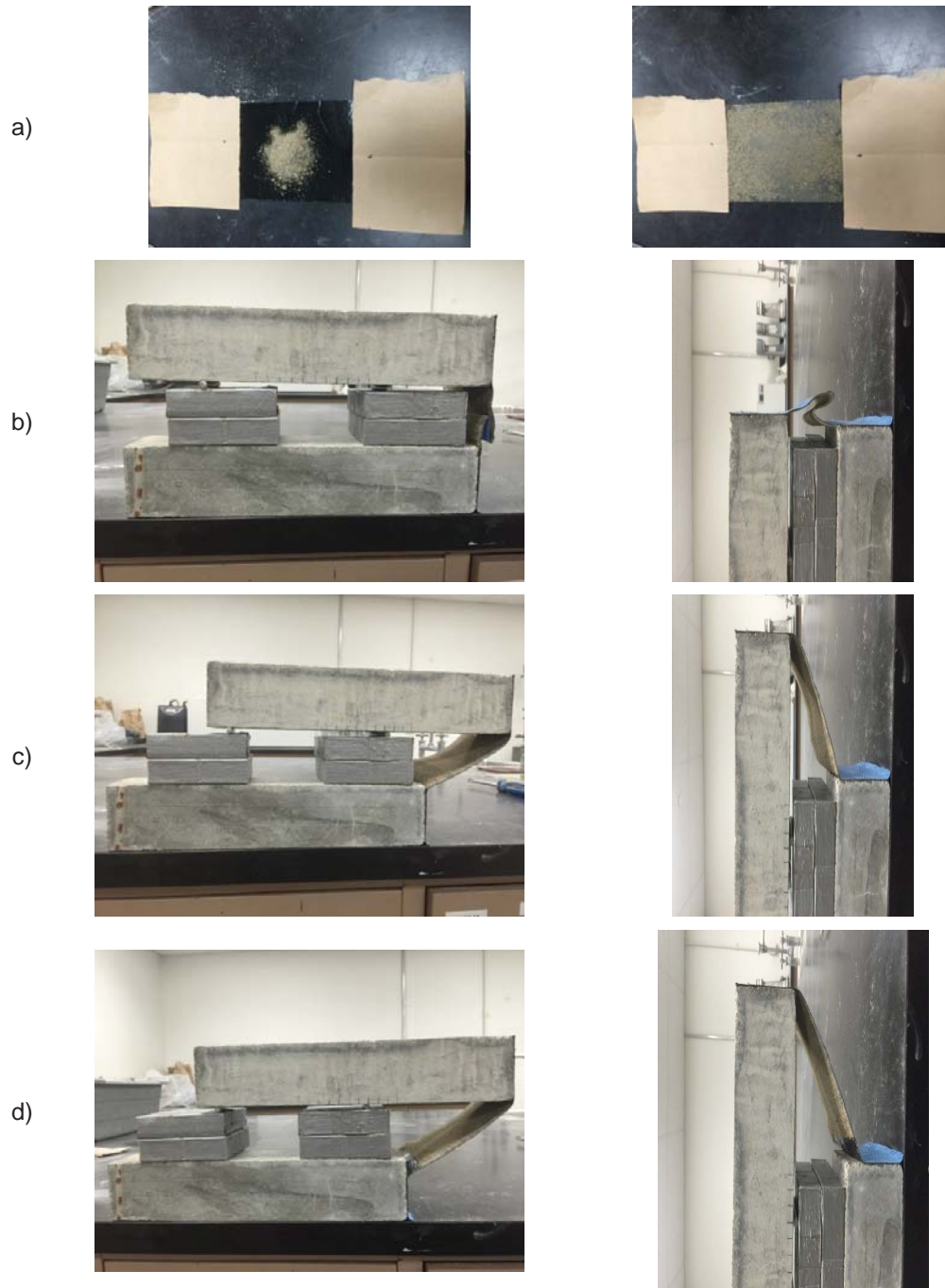


Fig. 50. Experiment of waterproof membrane with overlap treated with dry fine sand: a) treatment of dry fine sand; b) overlap formed at the gap; c) no delamination at 2.8 in. slip; and d) delamination appears at 3.2 in. slip.

■ In-plane shear

The experimental setup shown in Fig. 51 was used to test the resistance of the overlap to in-plane shear, which may happen in the waterproofing membrane (e.g., the red region in Design III in Fig. 3). In this setup, two concrete beams, placed in parallel to each other, were used to simulate the abutment and cheekwall. The gap between the beams was selected to be 1.2 in. The gap between the beams was covered by a piece of waterproofing membrane. When one beam was fixed and the other was pushed forward, in-plane shear was generated in the membrane.

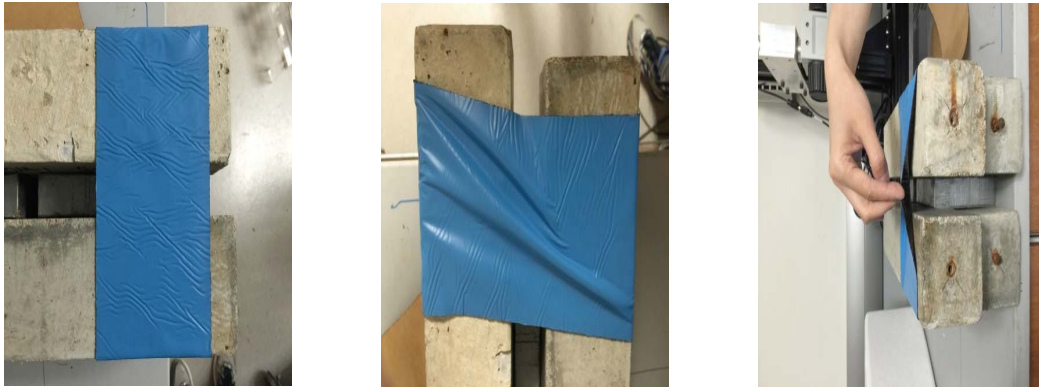


Fig. 51. In-plane shear in the waterproof membrane without overlap.

In the test, membrane without overlap was tested first to serve as a benchmark. After the bond quality was examined, one beam slid forward to trigger in-plane shear in the membrane. It was found the tolerance of the membrane to in-plane-shear was very low and significant delamination was found when the relative movement was only 0.4 in; see Fig. 51.



Fig. 52: In-plane shear of the waterproof membrane with a treated overlap.

Then fiberglass powder and fine sand were used to form the overlap at the gap (Fig. 52). The procedure to generate this overlap is the same as that for out-of-plane shear. In this test, the size of the overlap was 0.8 in. for both the fiberglass powder treatment and fine sand treatment. The test showed that the tolerance of membrane to in-plane shear was substantially improved. No delamination was observed when the relative movement reached 0.4 in. Delamination

Bridge Waterproofing Details Phase II

occurred when the relative movement was 0.8 in.; see Fig. 52. Thus, the capacity of membrane to resist in-plane shear was almost doubled.

Compared to the out-of-plane shear, the improvement brought in by the overlap is less. This is due to the different unfolding mechanisms of the overlaps in these two different types of relative movement. For out-of-plane shear, the overlap is fully unfolded with the increase of relative movement. Thus, it takes full advantage of the extra length reserved in the overlap. While for in-plane shear, the overlap cannot be fully unfolded with the relative movement (Fig. 52). Thus, the extra length reserved in the overlap can only be partially exploited.

5. Displacement Monitoring System

In Task I, an electric sensor system, which consisted of sensor head, signal conditioner, data transmitter and receiver, and data storage, was designed to monitor the expansion joint. To complete the implementation roadmap, the sensor system was assembled and tested here.



Fig. 53. LDI-119-150-A20A sensor head procured from OMEGA Engineering.

A LVDT (Linear Variable Differential Transformer) displacement sensor head, namely LDI 119-150-A20A (Fig. 53), was procured from OMEGA Engineering (Connecticut, USA). The length of the sensor is about 8.5 in., suitable for typical expansion joints. Its operation temperature ranges from -4°F to 185°F , sufficient to cover the typical annual temperature fluctuation in Pennsylvania. Its maximum measuring range is 6 in., with an error less than $\pm 0.25\%$. The housing material protecting the sensor is aluminum, which makes it suitable for outdoor use.

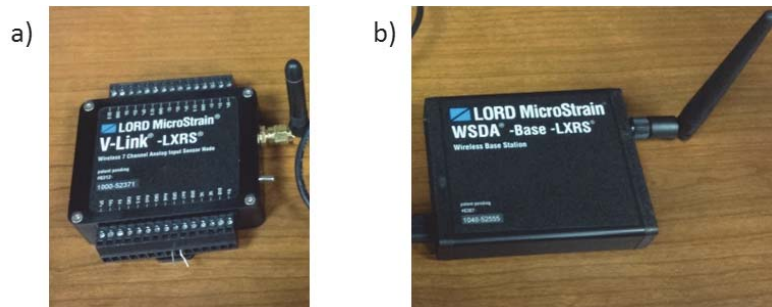


Fig. 54. The wireless signal transmission combo: a) V-Link transmitter and b) WSDA base station.

The wireless signal transmitter and receiver combo was procured from LORD Sensing (Vermont, USA). This combo, namely V-link/WSDA (see Fig. 54), allows the signal of the sensor to be sent to the storage at base station. Thus, remote monitoring can be realized in practice. The operation temperature of the combo ranges from -40°F to 185°F (LORD User Manual V-

Bridge Waterproofing Details Phase II

Link-LXRS, LORD Product User Manual WSDA-1500-LXRS, 2015), sufficient for the typical temperature condition in Pennsylvania. The range of receiver is within 1.2 miles for remote data transmission. In this combo, the receiver also plays the role of storage. It contains a storage component of size = 4 GB (LORD Product User Manual WSDA-1500-LXRS, 2015) for data storage. Later, the data can be downloaded in a computer for analysis. Furthermore, another advantage of this wireless transmitter/receiver combo is that it contains 7 more channels to accommodate more input signals, which makes it possible to integrate the water leakage detection into the same system later.

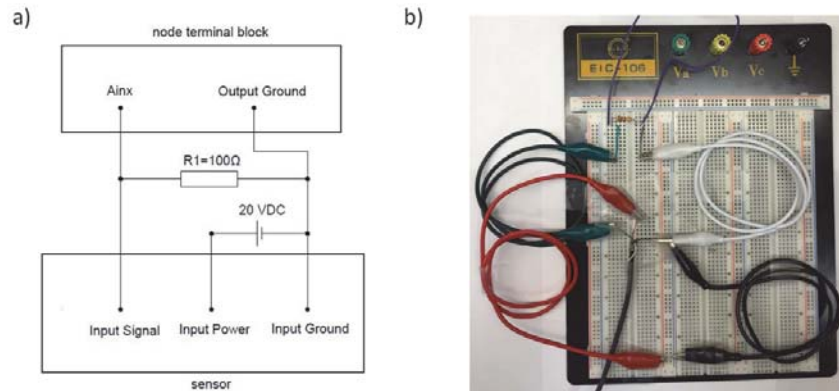


Fig. 55. a) The blueprint of the signal conditioning circuit and b) the real assembly of the signal conditioning circuit.

To convert the sensor measurements to signals that can be read and transmitted by the combo, a conditioning circuit was designed. The design blueprint of the circuit is shown in Fig. 55a and its final assembly is shown in Fig. 55b.

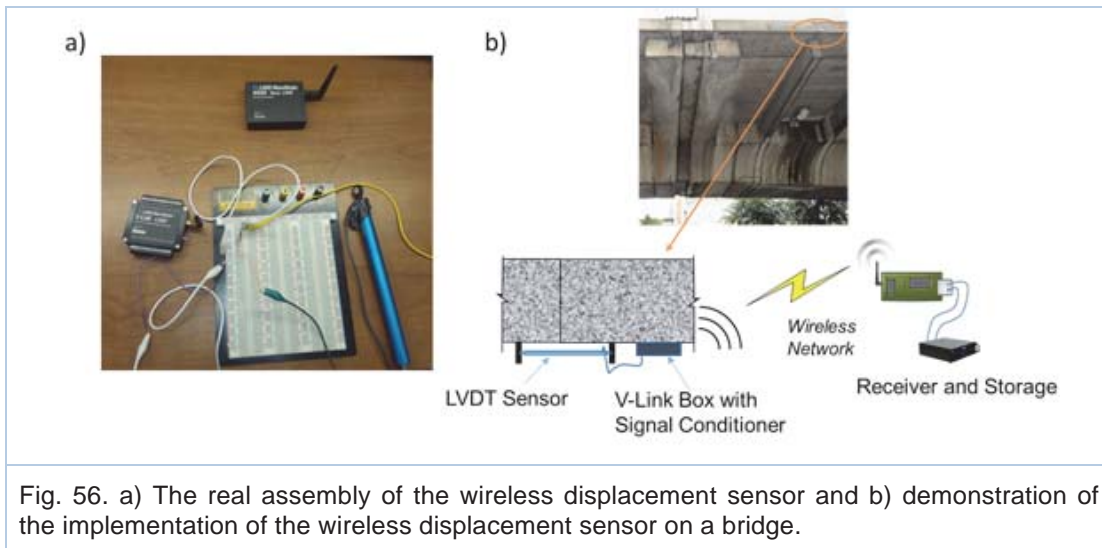


Fig. 56. a) The real assembly of the wireless displacement sensor and b) demonstration of the implementation of the wireless displacement sensor on a bridge.

The assembled sensor system is illustrated in Fig. 56a. The application of this system to a bridge is schematically illustrated in Fig. 56b. To examine its application in bridge engineering,



Bridge Waterproofing Details Phase II

tests were carried out. The accuracy and sensitivity of the system was tested at first. As shown in Fig. 57, the sensor head was installed in a loading frame capable of controlling the displacement of its piston. In the test, the receiver was placed about 50 ft. away from the transmitter, which was connected to the sensor head by wires. During the test, the movement of the piston was measured by the sensor and then the captured signal was sent to the receiver. Fig. 58 shows two different types of periodic displacement waveforms input to the piston by the controller of loading frame.



Fig. 57. The installation of the sensor head on the loading frame.

In the waveform shown in Fig. 58a, a frequency of 16 Hz was selected to transmit the signal of sensor head to the receiver. This means that every second, 16 measurements were made and sent to the receiver. For the waveform in Fig. 58b, the recording rate was set to be 8 Hz. When compared with the real input, the system captured the piston movement accurately, despite the background noise existing in the lab. In addition, the sensitivity of the system is acceptable. This is documented by the errors at the peaks and valleys, where the moving direction of the piston changes suddenly. The change of direction, characterized by the peaks and valleys in the waveforms, are well captured in the measurements. For example, the errors at the peaks and valleys of both waveforms are less than 5%.

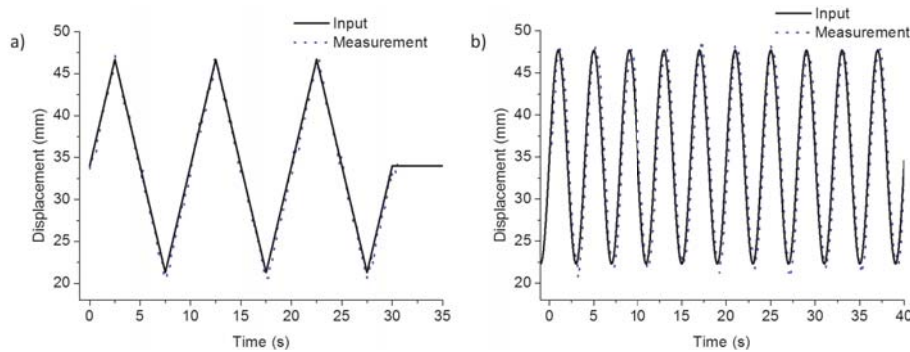


Fig. 58. a) The comparison of the input and measurement for ramp periodic displacement and b) the comparison of the input and measurement for sinusoidal periodic displacement.

Then the data transmission was tested. It is important to adjust the recording rate in the receiver based on the implementation. For an expansion joint, it is not necessary to monitor its

Bridge Waterproofing Details Phase II

movement at a rate of every second. It is more realistic to record the measurements every hour or every half hour. In Fig. 59, the options for the recording rate, which dictates the data transmission frequency, are shown.

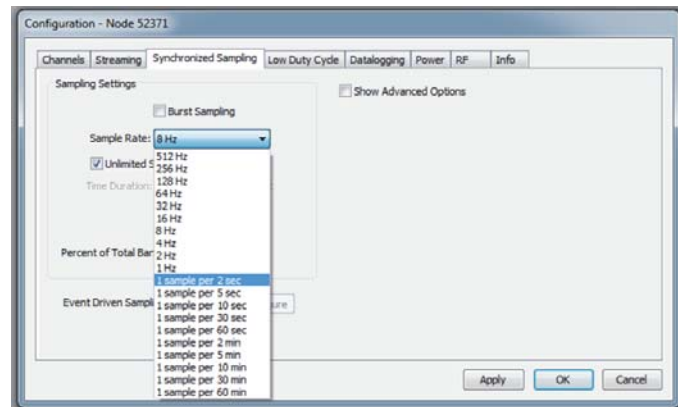


Fig. 59. Configuration menu showing multiple options for sampling rate.

In the test, the transmitter/receiver combo was supported by an internal rechargeable Lithium Polymer (Li-Po) battery, which is capable of working consistently up to 7000 hours. The sensor head was supported by a YUASA YTX-9 rechargeable battery system used in the structural lab at PITT. In real implementation, this battery can be replaced by an YTX20H rechargeable battery (which can last 5 weeks or longer) or by a solar panel.

6. Summary

In this task, the designs and implementation roadmaps of abutment/beam adjunction, crystalline waterstops, membrane delamination mitigation and LVDT monitoring system were assessed. The experimental and numerical results show that:

- *Abutment/beam Adjunction Design:* The changes of structural forms in Designs I and II will not cause excessive deflection and high stress in the end diaphragm and extended slab (or lip-shaped support). Designs I, II and III can be used for concrete girders and steel beams commonly used in the current practice. Based on the numerical results, a standard structural design may be achieved and used for bridges of different lengths and different skew angles.
- *Crystalline Waterstops:* The effectiveness and construction-friendliness of crystalline waterstops were tested by a series of tests mimicking the service conditions of construction joints in bridges. The implementation roadmap of the crystalline waterstops is established. The use of crystalline waterstops is composed of steps including mixing, installation and curing. In real construction, the curing of crystalline waterstops should be considered in construction management.
- *Overlap of Waterproofing Membrane:* The effectiveness of overlap on delamination mitigation was tested by both in-plane and out-of-plane shear tests. The procedure to generate an overlap by fiberglass or dry fine sand was outlined. The test results show that the overlap can significantly improve the resistance of membrane to delamination.
- *Displacement monitoring System:* A displacement monitoring system was assembled and its accuracy and sensitivity was tested. The system, powered by battery and



Bridge Waterproofing Details Phase II

capable of working outdoors, is able to measure the relative displacement of expansion joint and transmit the measurements to a remote receiver based on the prescribed recording rate.



Chapter 3 Design and Implementation II

1. Introduction

To remedy the inadequacy existing in the current bridge waterproofing system, some preliminary designs were conducted in Task I. In this task, the focus is placed on the improvement of header materials and the development of an integrated sensing system, which is capable of detecting water leakage.

Currently, there are two types of header materials widely used for expansion joints in practice, one of which is cement-based and the other is resin-based. A recent field investigation showed that elastomeric concrete header performed better than concrete one, except the resistance to rutting (Distlehorst and Wojakowski 2005). Based on the mechanisms of rutting, it is rational to assume that the resistance to rutting may be improved if elastomeric concrete header is reinforced. To assess this concept, experimental tests were conducted in this task to investigate the effect of reinforcement on the performance of elastomeric concrete.

In the preliminary design, an integrated system capable of detecting water leakage was proposed. To assess the functionality of this system as well as examine its applicability in an outdoor environment, the water leakage detection system was fabricated and tested in this task.

2. Evaluation of Header Materials

Based on the preliminary investigation in Task I, the investigation of header materials was focused on Class AAAP concrete, elastomeric concrete and steel wire-reinforced elastomeric concrete in this task. Five types of tests, including uniaxial compressive test, Charpy test, abrasion test, freeze-thaw test and corrosion test, were designed and conducted to investigate their properties of strength, impact resistance, wearing resistance and durability, which are closely related to the resistance to rutting.

■ Header Materials Tested

Based on the trial tests, the mix design for the Class AAAP concrete was adjusted. The water-cement ratio (w/c) of the Class AAAP concrete was changed to 0.4. Ordinary Type I Portland cement was used, and 20% of the cement was replaced by Pozzolan (Type C-Ash). The mass ratio of cement : sand : gravel was designed to be 1 : 2 : 3.

The elastomeric concrete used in this study is a 2-part polyurethane patching material mixed with aggregates. It was provided by D.S. Brown Company. The 2-part polyurethane material is comprised of Delcrete/Delpatch DSB 1494A (Isocyanate-terminated prepolymer) and Delcrete/Delpatch DSB 1494B (Polyol/Diamine blend).

For the steel wire-reinforced elastomeric concrete, the same elastomeric concrete supplied by Delcrete was used. The steel wires, with a diameter equal to 1/8 in., were made of structural steel obtained from McMaster-Carr.

■ Specimen Casting and Test Arrangement

To take into account the age sensitivity of concrete, two batches of Class AAAP concrete were used in this study. The first batch was cured for 7 days before the testing, and the second batch



Bridge Waterproofing Details Phase II

for 28 days. Based on the observed responses at these two ages, the concrete performance at a different age may be estimated by interpolation.

The specimen dimensions for each test are shown in Fig. A10 in Appendix. The mixing and casting of Class AAAP concrete followed the standard ASTM recommendations (ASTM C192/C192M-16a). The specimens were demolded 24 hours after casting and then cured under standard conditions (99% relative humidity and about 68°F). The arrangement of specimens of the Class AAAP concrete is listed in Table 11.

Table 11. Test arrangement for the Class AAAP concrete.

Curing duration	Test type	Number
7 days	Abrasion test	3
	Compression test	3
	Charpy test	0
	Freeze-and-thaw test	2
	Corrosion test	0
28 days	Abrasion test	3
	Compression test	3
	Charpy test	3
	Freeze-and-thaw test	2
	Corrosion test	6

Due to the unique material composition, the procedure to cast elastomeric concrete is different from that of concrete. In this study, the casting of elastomeric concrete followed the recommendation provided by the supplier. The key steps include:

1. Pour 3000 ml Part A and 1500 ml Part B into separate measuring buckets;
2. Add Part A and Part B to a clean, 5-gallon bucket;
3. Start the heavy duty pail mixer at low speed;
4. Start to add one bag of aggregates (31 lbs) gradually into the mixer;
5. Increase mixer speed to medium and continue mixing for 4 minutes;
6. Stop mixing when the material is evenly wet throughout, and then pour the material into the molds.

Table 12. Test arrangement for the elastomeric concrete.

	Steel wire ratio	Test type	Number
Elastomeric concrete	0	Abrasion test	3
		Compression test	3
		Charpy test	3
		Freeze-and-thaw test	2
		Corrosion test	6
	0.5%	Abrasion test	3
		Compression test	3
		Charpy test	3
		Freeze-and-thaw test	2
		Corrosion test	6
	1%	Abrasion test	3
		Compression test	3
		Charpy test	3
		Freeze-and-thaw test	2
		Corrosion test	6



Bridge Waterproofing Details Phase II

Vibration and curing are not needed for elastomeric concrete. Thus, the specimens were stored in their molds only for 2 days before they were demolded and tested. The arrangement of tests on the elastomeric concrete specimens with or without reinforcement is listed in Table 12. Their specimen dimensions are the same as those of Class AAAP concrete (see Fig. A10).

For steel wire-reinforced elastomeric concrete, two steel wire ratios, namely 0.5% and 1%, were selected to investigate the effect of reinforcement content. Since the elastomeric concrete is sticky, low steel wire ratios were used to avoid the compromise of flowability during casting. In the test, attention was paid when the elastomeric concrete was cast on the frames made of steel wires to avoid any segregation.

■ Abrasion Test

In order to determine the abrasion resistance of the three header materials, a standard test method following the ASTM C944/C944M procedure was employed to test the specimens.

Specimens

For the specimens made of Class AAAP concrete, no reinforcement was added. For the specimens made of elastomeric concrete, the steel wire ratios were 0, 0.5% and 1%, respectively. For the nonzero steel wire ratios, the wires were placed horizontally and vertically with a spacing of 1 in. to form a frame; see Fig. 60b,c. Since the maximum aggregate size is 0.2 in. for the elastomeric concrete, the spacing of steel wires, which is 1 in. wide (about five times larger than the aggregate size), is sufficient for the free pass of aggregates and will not cause any segregation of elastomeric concrete during casting. For the elastomeric concrete specimens of 0.5% reinforcement ratio, the layout of steel frames is shown in Fig. 60b; while for 1% ratio, the layout is shown in Fig. 60c.

Test setup and procedure

All tests followed the ASTM recommendations (C944/C944M), based on which the cylindrical specimen tested on the abrasion device must be held by a clasper (Fig. A11a in Appendix). The abrasion device is a drill press, which is able to hold the specimen on the platform, rotate the cutter head at a speed up to 200 r/min, and vertically exert an external load of 22 lb. (98 N) on the surface of the specimen (Fig. A11b). The surface roughness of the rotating cutter head is illustrated in Fig. A11b. The cutter head can provide a circular contact area of a diameter= 3.25 in. for abrasion on the specimen surface.

Test results

The abraded surfaces of the Class AAAP concrete specimens at the end of each 2-min period are shown in Fig. 61. For the first batch of Class AAAP concrete specimens, the average loss of weight at the end of each abrasion period is 3.1, 2.5, and 2.5 grams, respectively. Correspondingly, the fractions of weight loss are 0.10%, 0.08% and 0.08%, respectively. In addition to the weight loss, moderate wearing can be found on the contact surfaces. For the second batch cured for 28 days, the average loss of weight at the end of each abrasion period is 2.1, 1.6, and 1.4 grams, respectively. The corresponding fractions of weight loss are 0.06%, 0.05% and 0.04% respectively. Similarly, moderate wearing can be found in some areas of the contact surfaces. When the two batches of specimens are compared, the results show that a longer curing will improve the abrasion resistance of Class AAAP concrete.



Bridge Waterproofing Details Phase II

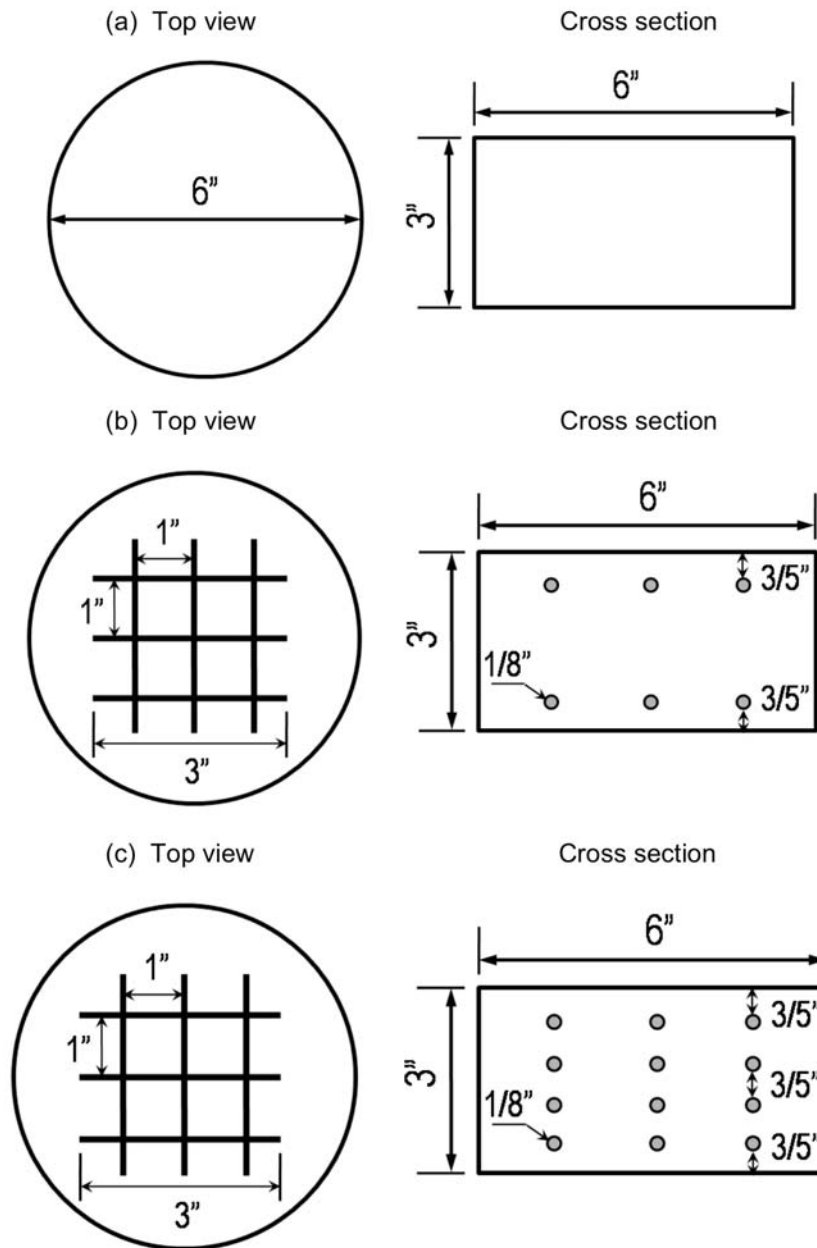


Fig. 60. Specimens for the abrasion test: a) without steel reinforcement; b) with 0.5% steel wires; and c) with 1% steel wires.

Bridge Waterproofing Details Phase II

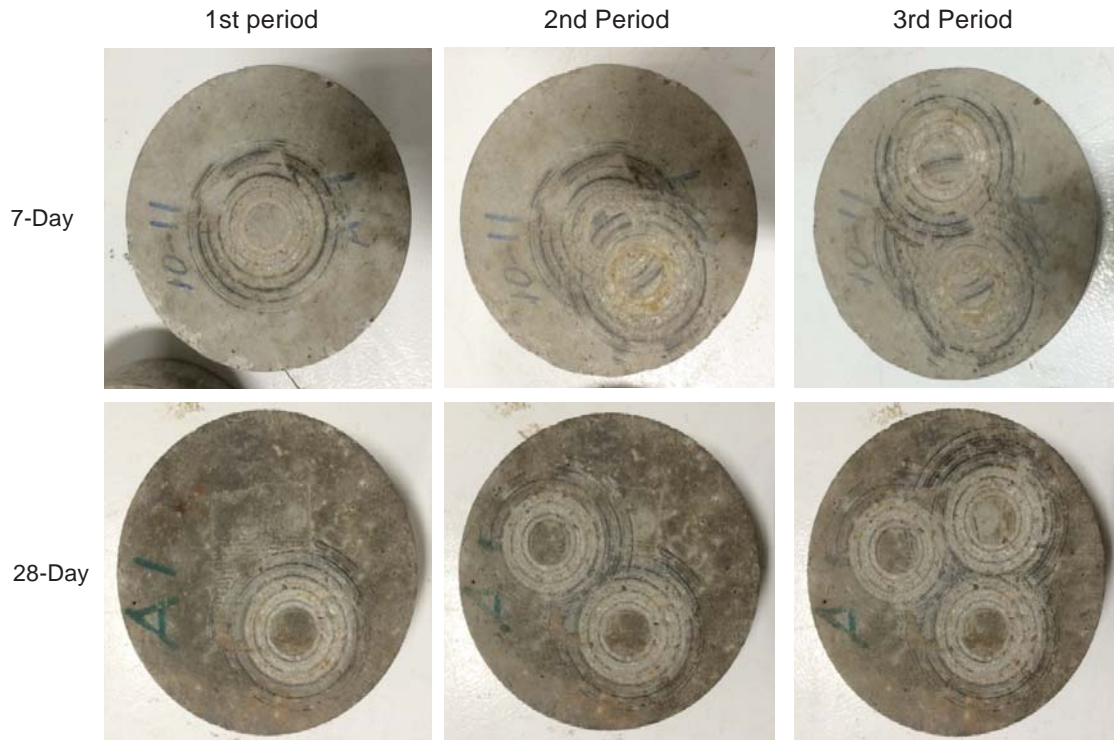


Fig. 61. Abraded surfaces of the Class AAAP concrete specimens

The abraded surfaces of elastomeric concrete specimens without steel wires at the end of each 2-min period are shown in Fig. 62. For specimens with steel wires (0.5% and 1%), the abraded surfaces are shown in Fig. A12 and Fig. A13 respectively. Based on the measurements, it transpires that for the elastomeric concrete specimens without steel wires, the average loss of weight after each abrasion is 0.5, 0.4 and 0.4 grams, and the corresponding fractions of weight loss are 0.02%, 0.02% and 0.02% respectively. In addition to weight loss, sign of light wearing can be found on the contact surfaces. After the addition of 0.5% steel wires, the average loss of weight at the end of each abrasion period is changed to 0.4, 0.4 and 0.5 grams, respectively. Correspondingly, the fractions of weight loss are 0.02%, 0.02% and 0.02% respectively. Based on visual inspection, the wearing of contact surfaces is negligible. If the steel wires are increased to 1%, the average loss of weight will be reduced to 0.2, 0.2 and 0.2 grams respectively. The corresponding fractions of weight loss are 0.01%, 0.01% and 0.01% respectively. Also, the wearing of contact surfaces is negligible. The significant drop of weight loss fraction indicates that the steel wire reinforcement is helpful for enhancing the abrasion resistance of elastomeric concrete.

Comparison and Summary

The test results show that the Class AAAP concrete specimens cured for 7 days have the greatest weight loss among the header materials tested. If the curing is extended to 28 days, the weight loss is reduced but is still substantially greater than that of the specimens made of elastomeric concrete. Among the specimens made of elastomeric concrete, the addition of steel wires mitigates the weight loss induced by abrasion. When 1% reinforcement is added, the

Bridge Waterproofing Details Phase II

weight loss is almost reduced by 50% when compared with the elastomeric concrete specimens without steel wires. Combined with the degree of wearing observed on the contact surfaces, the test results show that the elastomeric concrete performed better than the Class AAAP concrete in the abrasion test. Furthermore, adding steel wires improves the abrasion resistance of elastomeric concrete



Fig. 62. Abraded surfaces of the elastomeric concrete specimens without steel wires.

■ Uniaxial Compression Test

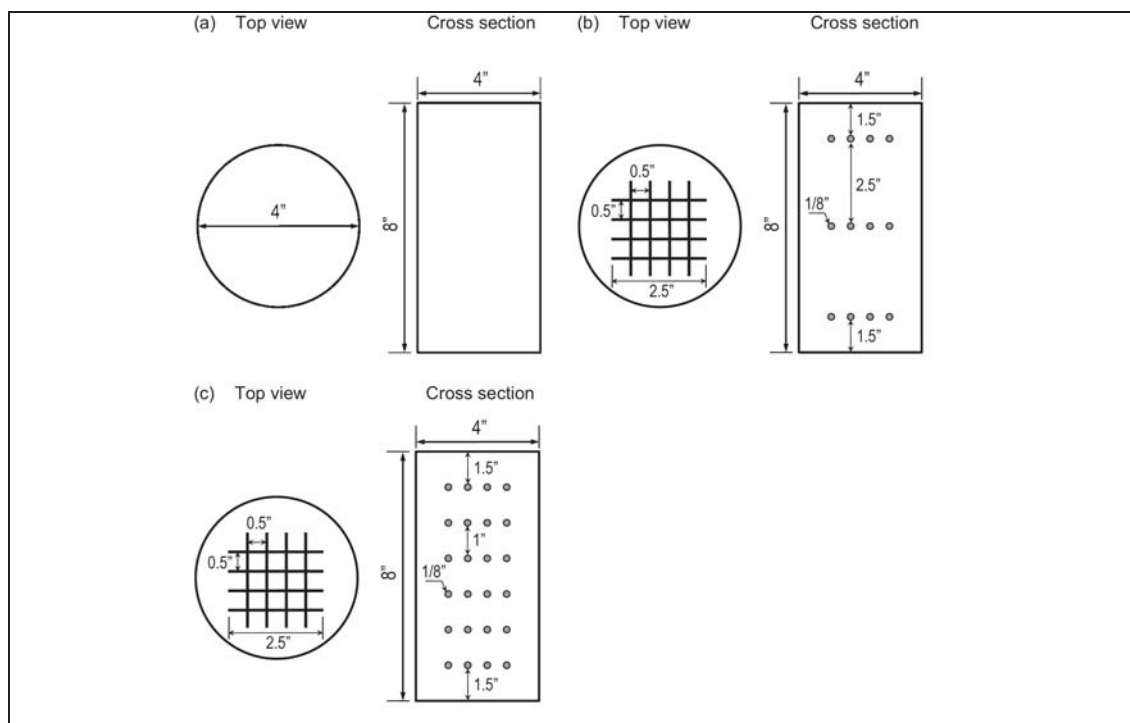


Fig. 63: Elastomeric concrete cylinders: a) without steel wires; b) with 0.5% steel wires; and c) with 1% steel wires.

Bridge Waterproofing Details Phase II

In order to determine the compressive strength of the header materials under investigation, a standard method following the ASTM C39/C39M – 16b procedure was adopted in the uniaxial compression test.

Specimens

The dimensions of all specimens are shown in Fig. 63a. For specimens reinforced with 0.5% and 1% steel wires, the steel frames and their layout are shown in Fig. 63b,c respectively. The steel wires used here are the same as those used in the abrasion test.

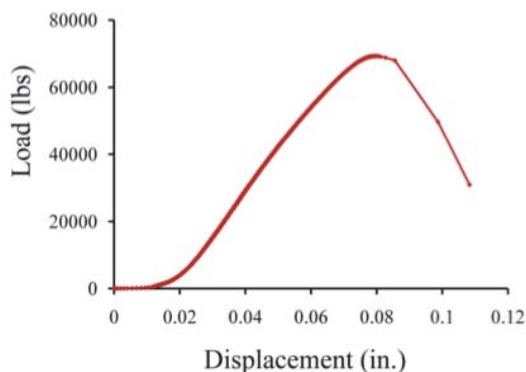


Fig. 64. The typical load-displacement curve obtained for Class AAAP concrete.

Test results

Following the ASTM recommendations (C39/C39M – 16b Standard), a complete load-displacement curve was recorded during each test and the peak load, as well as the compressive strength, was determined based on the obtained curve (Fig. 64). According to the experimental records, the average 7-day compressive strength is 4087 psi for the first batch, and the average 28-day strength is 5318 psi for the second batch. The strength ratio between these two ages is 1.30, which is comparable to the typical values reported for Class AAAP concrete. For Class AAAP concrete, a well-defined fracture pattern was found after the peak load.

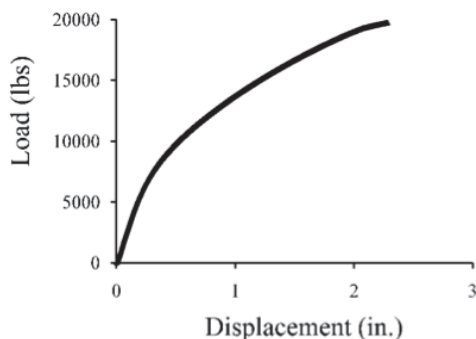


Fig. 65. The typical loading-displacement curve obtained for elastomeric concrete.

Bridge Waterproofing Details Phase II

Unlike Class AAAP concrete and normal concrete, which are typical quasibrittle materials, elastomeric concrete is more ductile. Thus, its failure pattern is very different from that of Class AAAP concrete. Instead of fracturing, the failure of an elastomeric concrete cylinder is characterized by a substantial lateral expansion. During each test, a complete load-deflection curve was recorded for each cylinder, and the peak load, as well as the compressive strength, was obtained based on the recorded curve (Fig. 65). The average compressive strength of elastomeric concrete specimens with reinforcement ratios of 0, 0.5% and 1% is 1534, 1562, and 1602 psi, respectively. The corresponding displacement at failure is 2.55 in., 2.57 and 2.58 in. respectively. The test results show that the addition of steel wires slightly enhances both the strength and ductility of elastomeric concrete.

Comparison and summary

In Table 13, the recorded average compressive strength and displacement at peak load are listed for each type of specimens. It can be seen that the strength of Class AAAP concrete is much higher than that of elastomeric concrete. On the other hand, elastomeric concrete is much more ductile than Class AAAP concrete. The displacement of elastomeric concrete at peak load is about 21 times greater than that measured for the Class AAAP concrete specimens. Note that in the specimen fabrication, the steel wire frames were placed normal to the compressive load in this study. If the frames are placed along the loading direction, it is rational to assume that the compressive strength of elastomeric concrete will be significantly improved.

Table 13. Results of the uniaxial compression test.

Material	Specimen Type	Compressive strength (psi)	Displacement at peak load (in.)
Class AAAP Concrete (w/c=0.4)	7-day curing	4087	0.11
	28-day curing	5318	0.12
	No Reinforcement	1534	2.55
Elastomeric Concrete	0.5% Reinforcement	1562	2.57
	1% Reinforcement	1602	2.58

■ Charpy Test

In order to measure the capacity of energy absorption when a specimen is struck and broken by impact, a modified method based on the ASTM A370-16 recommendation was employed to test the beam specimens made of Class AAAP concrete and elastomeric concrete.

Specimens

The dimensions of specimens are shown in Fig. 66a. For each elastomeric concrete specimen of reinforcement ratio = 0.5%, only one steel wire of a diameter = 1/8 in. was used and it was placed along the centerline of the beam specimen; see Fig. 66b. For each elastomeric specimen of reinforcement ratio = 1%, two steel wires were placed longitudinally and the spacing between them was about 0.79 in.; see Fig. 66c.



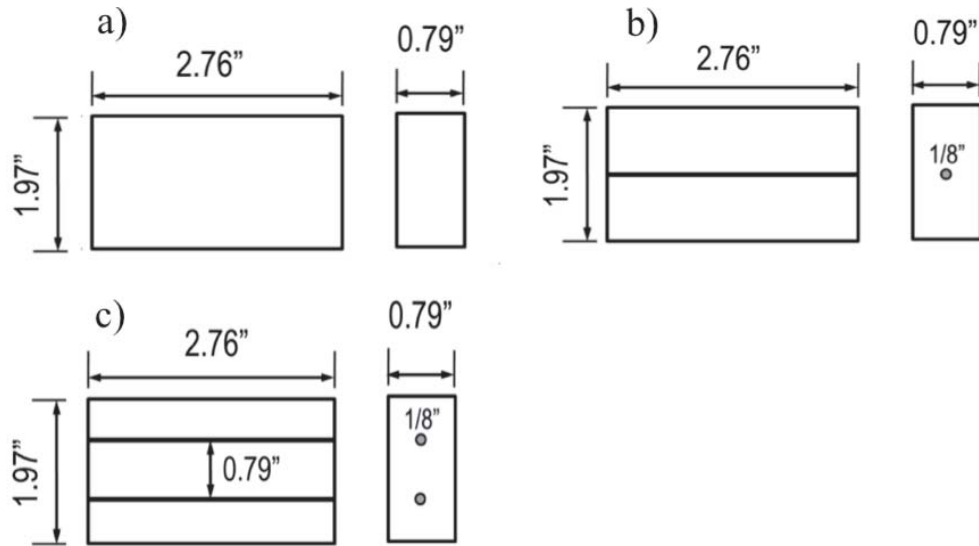


Fig. 66. Design of Charpy test specimens.

Test setup and results

Fig. 67 shows the experimental setup of Charpy test. The impact was generated by the free drop of the swing pendulum on a Charpy impact machine; see Fig. 67a. The specimen was fixed on the steel fixture shown in Fig. 67b at the bottom of the Charpy impact machine.

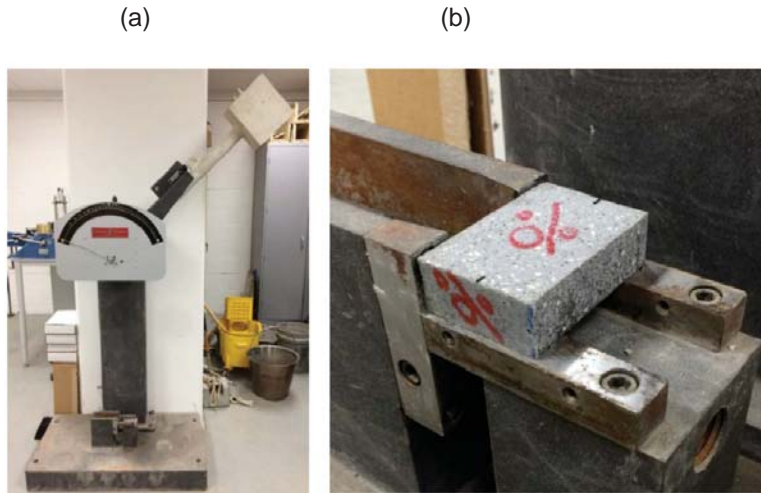


Fig. 67: Setup of Charpy test.

Bridge Waterproofing Details Phase II

The average value of absorbed energy of the Class AAAP concrete beams is 178 lb-ft, while the average values of elastomeric concrete beams with 0, 0.5% and 1% reinforcement ratios are 150, 186 and 191 lb-ft, respectively. The typical fracture patterns of an elastomeric concrete specimen after impact are shown in Fig. 68.



Fig. 68. Elastomeric concrete specimen (1% reinforcement) after impact

Comparison and summary

The recorded values of energy absorption are listed in Table 14 for all the specimens. The results show that the Class AAAP concrete displayed higher impact resistance than the elastomeric concrete. However, the addition of steel wires enhances the impact resistance of elastomeric concrete. For example, when the reinforcement ratio approaches 0.5%, the absorbed energy of elastomeric concrete is higher than that of Class AAAP concrete.

Table 14. Charpy test results

Material	Specimen type	Absorbed energy (lb-ft)
AAAP Concrete	28-day curing	178
	No reinforcement	150
Elastomeric Concrete	0.5% reinforcement	186
	1% reinforcement	191

■ Corrosion Test

The ability to resist chemical attacks is one of the essential aspects determining the durability of header materials. In this test, the performance of the selected header materials subject to calcium leaching was studied.

Specimens

All the specimens are cubes; see Fig. 69a. For the reinforcement ratio = 0.5%, the placement of steel wires is shown in Fig. 69b; for the reinforcement ratio = 1%, it is shown in Fig. 69c.

Bridge Waterproofing Details Phase II

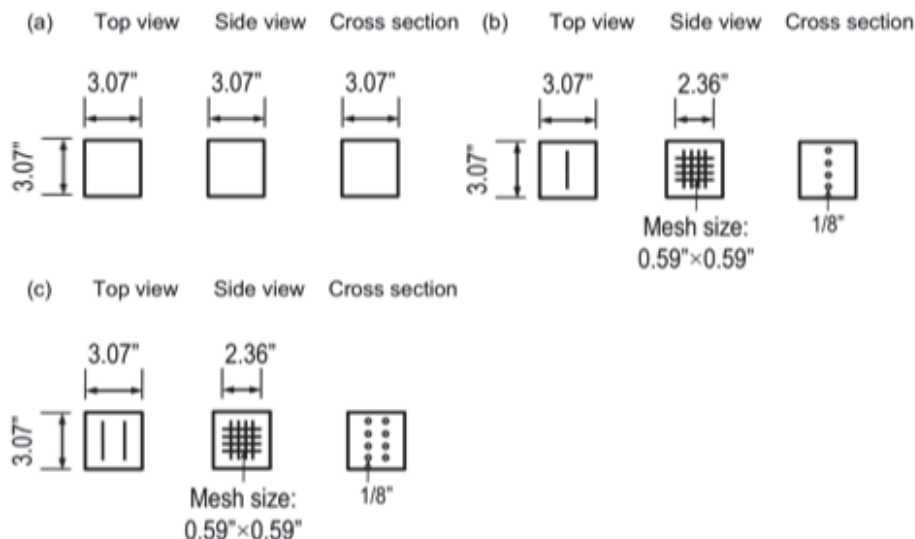


Fig. 69. Design of Corrosion test specimens

Test setup and results

To trigger calcium leaching in the specimens, ammonium nitrate solution of 10% concentration, was used. Two containers were used for the corrosion test. The first container was filled with clean water, and the second one was with 10% ammonium nitrate solution. The specimens made of each type of header materials were divided into two groups. The first group was immersed in clean water, while the second was immersed in the ammonium nitrate solution; see Fig. 70.

After 30 days, all the cubes were removed from the containers and uniaxial compression test was conducted to measure their strength. Here the cubes in the clean water served as benchmarks, based on which the strength loss due to calcium leaching was estimated. For Class AAAP concrete specimens, the average compressive strength of the cubes in the clean water is 6875 psi. After calcium leaching, the measured average compressive strength is 5850 psi. This means that after 30-day leaching in 10% ammonium nitrate solution, the strength loss is as much as 17.52%.

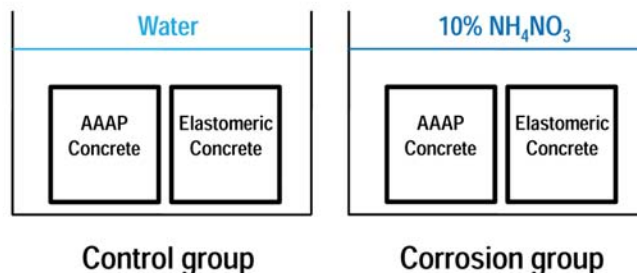


Fig. 70. Illustration of the corrosion test.

Bridge Waterproofing Details Phase II

For the elastomeric concrete cubes in the clean water, the average compressive strength is 1723, 2311, and 2354 psi for the reinforcement ratios of 0%, 0.5% and 1%, respectively. After leaching for 30 days, the compressive strength slightly drops to 1656 psi, 2283 psi, and 2337 psi respectively. It means the corresponding strength loss is only about 4.1%, 1.2% and 0.1%, respectively.

Comparison and summary

The strength of the two groups is listed in Table 15. It can be seen that after leaching for 30 days, the strength loss is significant for the Class AAAP concrete specimens. This means that the resistance of Class AAAP concrete to calcium leaching is not high. On the other hand, the strength loss of the elastomeric concrete specimens is insignificant. This indicates that elastomeric concrete will provide a better performance under calcium leaching. Furthermore, the measured strength of the specimens with different reinforcement ratios shows that the addition of steel wires will further improve the corrosion resistance of elastomeric concrete.

Table 15. Strength of the cubes

Materials	Specimen Type	Corrosion Group	Control Group	Strength loss (%)
		(10% NH ₄ NO ₃)	(Water)	
		Compressive strength (psi)		
Class AAAP Concrete	28 Day	5850	6875	17.52
	No Reinforcement	1656	1723	4.05
Elastomeric Concrete	0.5% Reinforcement	2283	2311	1.23
	1% Reinforcement	2337	2354	0.07

■ Freeze-thaw Test

The resistance to frost is an important indicator of the durability of header materials. Here the fast freezing method recommended by Zhang et al. (2008) was adopted and the freeze-thaw test was conducted for Class AAAP concrete and elastomeric concrete specimens.

Specimens

In the freeze-thaw test, all the specimens are prisms and their dimensions are shown in Fig. 71a. For specimens of reinforcement ratios = 0.5% and 1%, the placement of steel wires is shown in Fig. 71b,c respectively.

Test setup and results

In the freeze-thaw test, all the specimens underwent the same temperature history. During the freeze-thaw test, the weight of specimens was measured after every 20 freeze-thaw cycles. For the Class AAAP concrete prisms cured for 7 days, the change of weight is plotted in Fig. 72a. It can be seen that the weight loss increases almost linearly with the freeze-thaw cycles and then slows down. After 120 cycles, the average weight loss of prisms is about 0.7%. For the Class



Bridge Waterproofing Details Phase II

AAAP concrete prisms cured for 28 days, their weight loss is plotted in Fig. 72b. The weight loss is not significant until 40 cycles. Then the loss of weight accelerates and it reaches 0.4% after 120 cycles. It indicates that longer curing will improve the frost resistance of Class AAAP concrete.

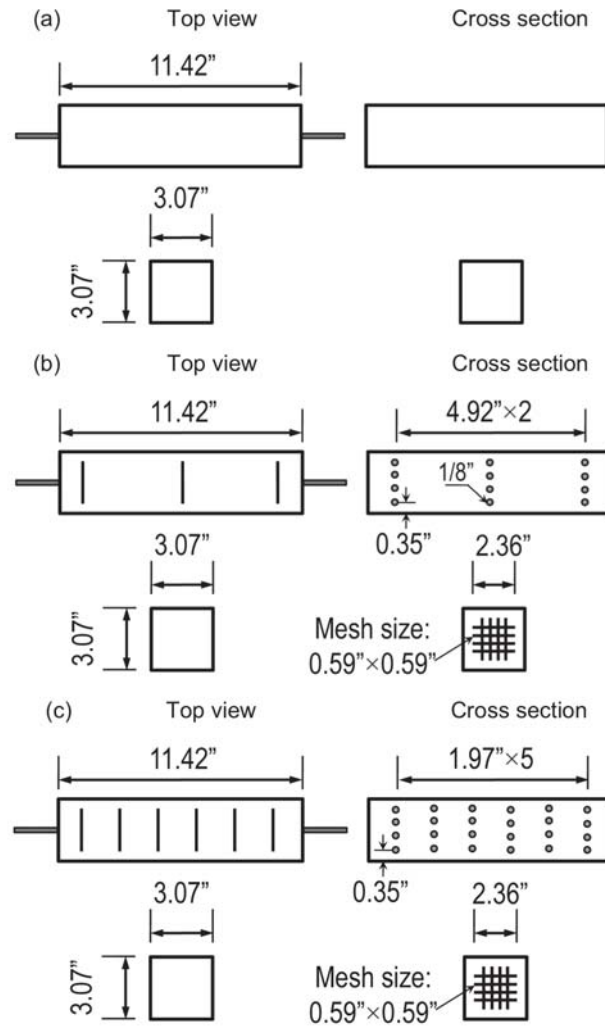


Fig. 71. Design of Freeze-thaw test specimens: a) specimens without stirrups; b) specimens of 0.5% steel wires; and c) specimens of 1% steel wires.

The average change of weight for the elastomeric concrete prisms is plotted in Fig. 73. For the prisms without steel wires, the weight loss is very small (Fig. 73a). After 120 cycles, the average weight loss is only about 0.04%. For the prisms reinforced by steel wires, weight loss is not observed; see Fig. 73b,c. This means the addition of steel wires improves the frost resistance of elastomeric concrete.

Bridge Waterproofing Details Phase II

The length of specimens was also measured after every 20 freeze-thaw cycles; see Fig. 74. For the Class AAAP concrete prisms cured for 7 days, the change of length is plotted in Fig. 74a. It can be seen that the change of length increases with the freeze-thaw cycles. After 120 cycles, the average length change of prisms is about 0.1%. For the Class AAAP concrete prisms cured for 28 days, their change of length is plotted in Fig. 74b. Noticeable change happens after 40 cycles. The difference reaches about 0.07% after 120 cycles. It also indicates that longer curing will improve the frost resistance of Class AAAP concrete.

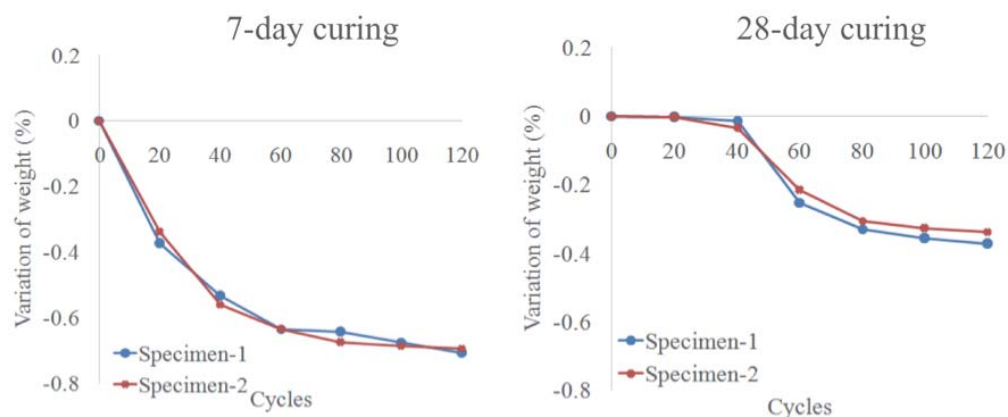


Fig. 72. Weight loss of Class AAAP concrete specimens.

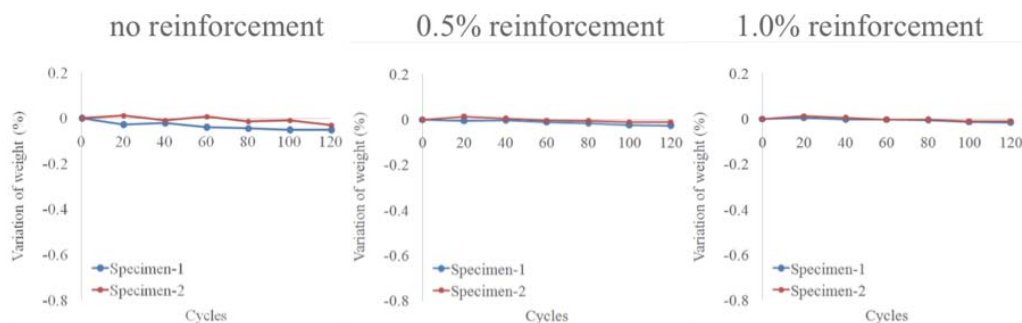


Fig. 73. Weight loss of elastomeric concrete specimens.

The average change of length for the elastomeric concrete prisms is plotted in Fig. 75. For the prisms without steel wires, the change is very small (Fig. 75a). After 120 cycles, the average change of length is only about 0.01%. For the prisms reinforced by steel wires, the changes of length are negligible for 0.5% and 1% reinforcement ratios, respectively; see Fig. 75b,c. This further indicates the addition of steel wires improves the frost resistance of elastomeric concrete.

Bridge Waterproofing Details Phase II

Comparison and summary

Based on the tests for 120 cycles, it can be seen that elastomeric concrete shows better frost resistance than Class AAAP concrete. Furthermore, the addition of steel wires improves the capacity of elastomeric concrete to resist freeze-thaw.

■ Summary

In this investigation, tests including uniaxial compression test, Charpy test, corrosion test, abrasion test and freeze-thaw test were conducted. The test results show that the reinforcement provided by steel wires improved the resistance of elastomeric concrete to these physical and chemical attacks. It implies that the reinforcement will improve the resistance of rutting. Furthermore, the tests also indicate that if the steel wires are placed along the loading direction, the compressive strength of elastomeric concrete will be enhanced.

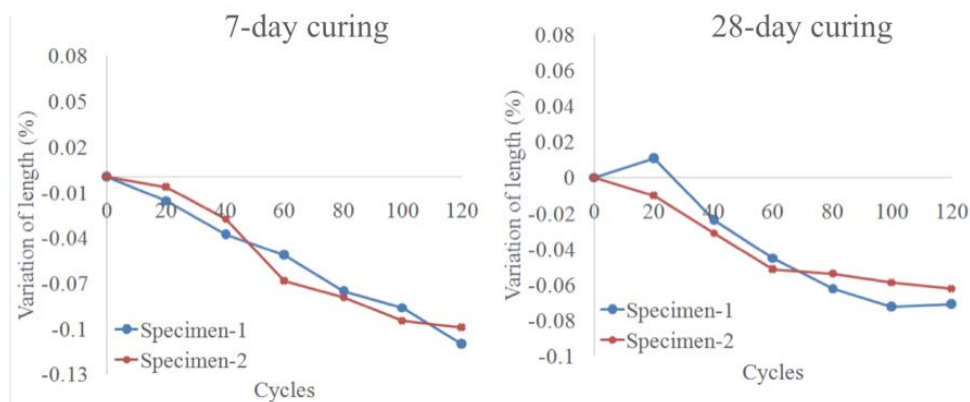


Fig. 74. Length variation of Class AAAP concrete specimens.

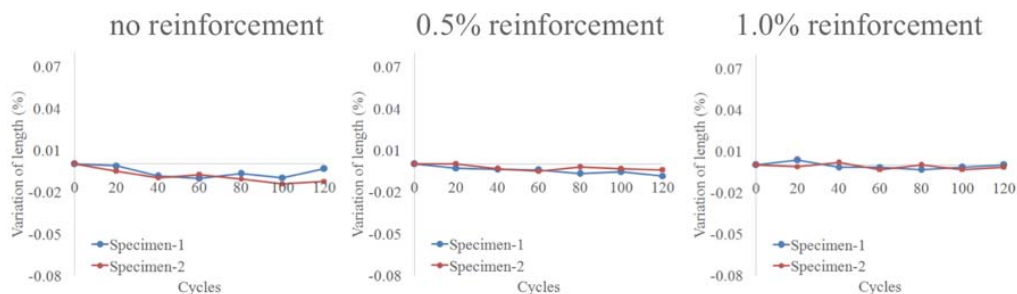


Fig. 75. Length variation of elastomeric concrete specimens.

3. Water Leakage Detection System

To integrate the function of water leakage detection with the existing displacement monitoring system, a new system featured with sensor heads capable of detecting water leakage was developed. This new system is able to work simultaneously with the existing system by sharing the same transmitter/receiver combo.



■ Electric Sensor for Water Leakage Detection

To fabricate an electric system, the patented SeaHawk sensor head from RLE technology was selected. This electric sensor head is like a rope (Fig. 76). It has a diameter less than $\frac{1}{4}$ in., and its ends are 0.96 in. in diameter (Figs. 77 and 78). This sensor head is able to work at an environment with temperature ranging from 32 °F to 167 °F, and humidity ranging from 5% to 95%. It can be stored at temperature ranging from -22 °F to 185 °F. Thus, it is suitable for the bridges in Pennsylvania, which has very low temperature in winter.

The sensor head consists of four single colored wires, which are numbered as 1 (white), 2 (black), 3 (green) and 4 (red), respectively; see Fig. 79. Once water or other liquid contacts with the sensor head, the resistance of the wires will change accordingly, and correspondingly, an electric-magnetic change in the circuit will be excited.



Fig. 76. SeaHawk sensing cable with clips for fixing its position.

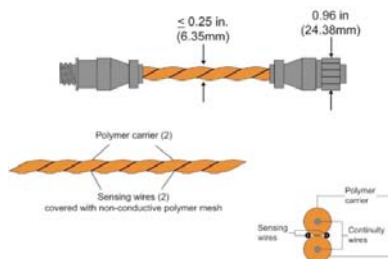


Fig. 77. Size of the sensor



Fig. 78. Ends of the sensor.

To make it suitable for outdoor applications, storable signals must be output by the controller LD310. To achieve this, a design was conducted to improve this controller. This improvement was achieved by taking advantage of the leakage relay switches in the controller. One leakage relay switch in the controller has three output ends, whose status is normally closed (NC), common (C) and normally open (NO) respectively. Once the water leakage is detected, the switch will alter from connecting NC and C to connecting C and NO. If the contact with water disappears, this relay switch will go back to the normal open status instantaneously. Thus, this property of relay switch can be utilized to generate analog voltage signal to detect water leakage.

Bridge Waterproofing Details Phase II

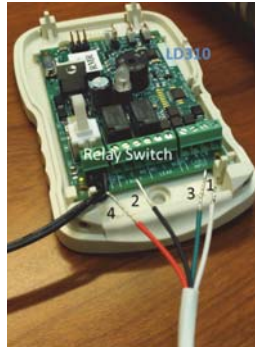


Fig. 79. Illustration of LD310 and the four-wire end of the sensor head.

A circuit was designed to generate and send out the analog signal showing the presence of water leakage, which is depicted in Fig. 80. With this improvement, the controller can now automatically send out analog signals as a record of the monitoring history. This analog signal is then input into one of the single end channels of the data transmitter V-Link, and will be able to travel wirelessly to the data aggregator. Once received and stored in the data aggregator, the record can be copied to the host computer and displayed there.

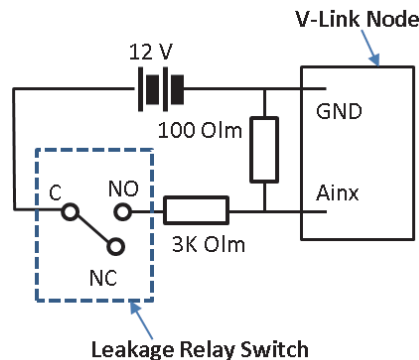


Fig. 80. Diagram of the water leakage detecting circuit to generate signal when water is present.

■ Data Transmitting System

To transmit the signals from the sensor head, a data transmitting system is needed. Here the data aggregator WSDA 1500 for the displacement sensor system is shared. The operation of this data aggregator includes several steps. First, the data aggregator has to be connected via an Ethernet cable to a host computer to start. The host computer can be a laptop with the driving programs (including Node commander, Live connect, and Data downloader) installed on it. The host computer has to be configured to have a local network IP address (IPv4) as 192.168.0.x. Here the digit x refers to an arbitrary integer other than 100, which is the default setting of the aggregator. The Subnet mask is chosen automatically as 255.255.255.0. The settings can be seen in Fig. 81. Then the data aggregator can be reached via the web explorer on the host computer, when the address <http://192.168.0.100> is input.

Bridge Waterproofing Details Phase II

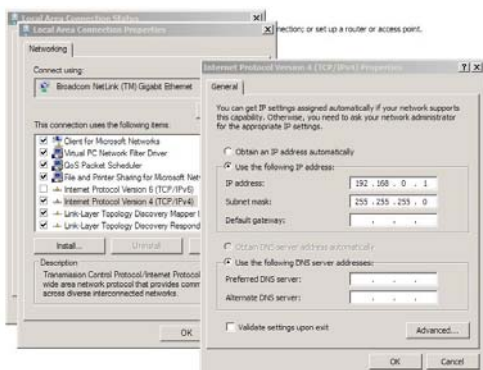


Fig. 81. Local network IP address setting (IPV4)



Fig. 82. Login page of the WSDA control panel.

Once the connection is established and the IP address is visited, the page shown in Fig. 82 will appear on the host computer. The default username and password for login are both “wsda”. Since all the settings in this data aggregator have been already adjusted to meet the requirements of this project, no further setting is needed. Then, to start the data aggregator, the driving program Live Connect has to be run on the host computer. The aggregator appears on the host computer as a base station, with its IP address being 192.168.0.100. More details can be found in the WSDA 1500 manual (LORD Product User Manual).

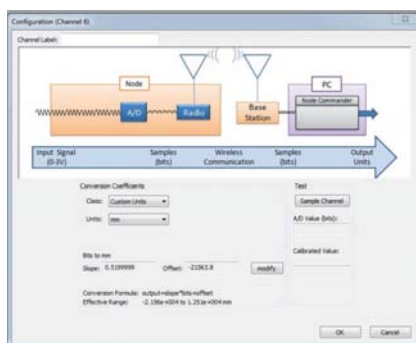


Fig. 83: Setting the Conversion of the A/D value to displacement in the node configuration option.

Following the procedure of setting up the node (V-Link), the node commander can be run on the host computer. The node can be found by inputting its serial number, which is 52371 (LORD User Manual). After that, the configuration of the nodes displays on the host computer. Based on the configuration, one may choose the channels to be used in this sensing system. In this project, for the displacement sensor (LVDT), the digit values translated from the analog signal (A/D value (bits)) are converted to the displacement values with unit mm after the conversion formula is obtained based on calibration and then input into the option of Bits to mm; see Fig. 83. For the water leakage detection, because the values of A/D signals different from zero will tell the presence of water at the sensor head, it is not necessary to further interpret the A/D values

Bridge Waterproofing Details Phase II

■ Power Supply for The System

In this project the independent power supply of the whole system needs to be considered due to the requirement of outdoor application. Among the possible options, rechargeable battery is selected due to its advantages in cost and installation. Based on requirement of this project, the rechargeable battery must be capable of working more than one month before it is recharged.

In this sensing system, the components needing power supply are the displacement sensor head, controller LD310 together with a signal generating circuit, data transmitter V-Link and the data aggregator WSDA 1500. When the whole system is installed on the bridge, the data aggregator is placed at a safe place far away from the bridge to avoid accidental damage. As a result, it should have an independent power supply. The V-Link data transmitter is designed to share the power supply of the water leakage detecting system, while the displacement sensor head has an independent battery since it is always placed at a distance far away from the sensor head for water leakage. Therefore, three rechargeable YIX30L batteries (Fig. 84) from YUASA Battery Inc were selected for this system to build the power supply. Each battery has a capacity up to 30 AH. Thus, they can last more than one month, and allow the engineers to do the maintenance every month and at the same time to collect the data from the data aggregator.



Fig. 84: YIX30L Battery selected for the power supply.

■ Test and Integration

After the integration of different components in the sensing system, the displacement monitoring and water leakage detection were tested separately. In Fig. 85, a displacement signal, which represented the real movement captured by the LVDT, was wirelessly transmitted and stored in the data storage by the displacement monitoring system. The displacement monitoring component in the integrated system is shown in Fig. 86, which consists of a LVDT sensor head, power supply, a circuit board, and the wires connecting to the data aggregator.

Similarly, the water detection component in the integrated system is shown in Fig. 87, which is comprised of the sensor head, controller, circuit board, power supply and wires connecting to the data aggregator. To examine the functionality this system, the sensor head was tested at three different conditions, which are common for outdoor applications.

Bridge Waterproofing Details Phase II

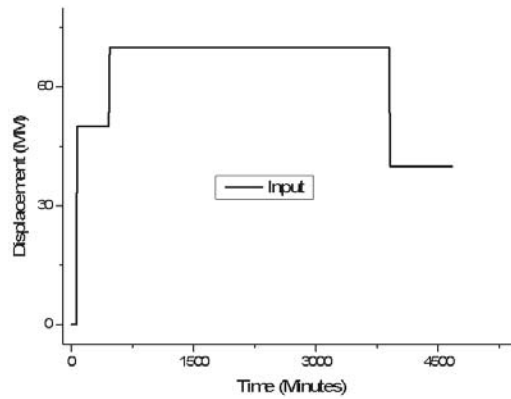


Fig. 85. The displacement signal captured by the system.

First, the sensor head was placed to contact with water. This condition is to mimic the water leakage during rain. In this test, water leakage was supposed to happen 70 minutes after the system was powered on. Second, the sensor head was placed in a room with the relative humidity close to 100%. The objective of this test is to check if any false detection will be made by the system in humid conditions. In this test, the curing room of structural lab at PITT was used. The last test was conducted outdoors when it was snowing. The three tests were designed to totally run three and a half days to test the robustness of the battery supply as well as the reliability of the wireless data transmitting system.

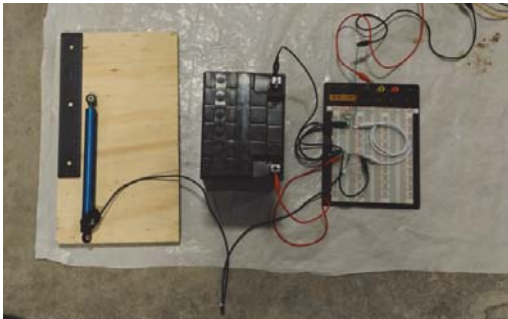


Fig. 86. The displacement monitoring system.

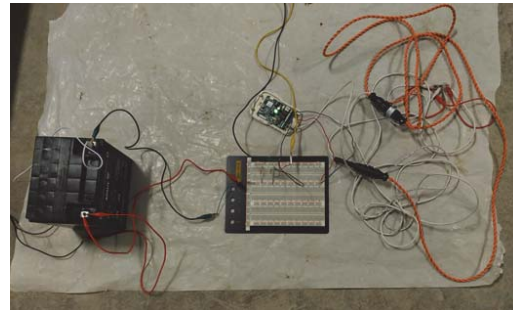


Fig. 87. The water leakage detection system.

All the data were collected offline in the form of excel tables, and can be copied to the host computer via the software Data Downloader when needed. As shown in the data collected, the displacement and water leakage history during the test can be retrieved. In Fig. 88, the exact time and the corresponding displacement data point are shown in the excel table, which were retrieved from the data storage. In the default setting, UTC time is used, and it can be converted to local time in the setting. To change the time format for easy reading, one may use the format cell option shown in Fig. 89.

The retrieved displacement data are plotted in Fig. 90. By comparing the signal captured by the LVDT sensor in Fig. 85 with the data retrieved from the data storage, a good agreement is achieved. The relative error is less than 5%. This means that the displacement monitoring

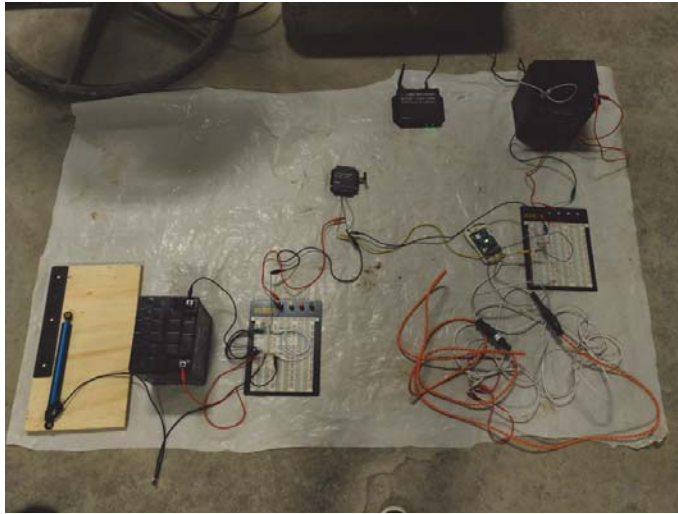


Fig. 92: The integrated sensing system.

■ Optical Fiber Sensor Head

In the preliminary report of this project, optical fiber sensor head was also listed as an option for water leakage detection system. To use the optical header for water leakage detection, the sensor head must be treated to fabricate grating on the fiber, which causes the change of wavelength or intensity when water leakage happens. To fabricate grating on the fiber, the cladding layer of the cable has to be removed and the core of the cable has to be etched with a hydrofluoric (HF) solution. During the etching process, it was found that the use of heavily corrosive HF solution required for good training and great attention. Any operation mistake may cause severe damage to a human body. Since the sensor head is designed to monitor a certain range of beam/abutment adjunction, a number of etching operations are required when the grating is fabricated. Thus, it imposes a heavy burden on cost, labor and time. Furthermore, it was also found that a significant financial input is needed to protect the sophisticated components of the optical fiber system when it is used outdoors. For example, the laser diode controller and laser diode must be protected from vibration and cold weather. In light of these obstacles, the fiber optical sensor system was discarded and the focus was placed on the electric sensor head, which is more economical and easier in manufacturing and installation.

■ Protection

Since the sensing system will be installed outdoors, protection is needed to prevent damages induced by wild animals and environmental conditions (e.g., moisture). To protect the circuit board, controller, transmitter/receiver combo and batteries, steel boxes were used (Fig. 93a). The parts in the boxes were further protected by polyurethane foam (Fig. 93b). To protect the circuit board from moisture, the acrylic conformal coating were procured; see Fig. 93c. To resist the hostile outdoor conditions, vehicle wires (Fig. 93d) were used to connect the parts through the small holes on the boxes. To avoid the contact with the water on the ground, the boxes are raised with the plastic seats; see Fig. 93a,b.

Bridge Waterproofing Details Phase II

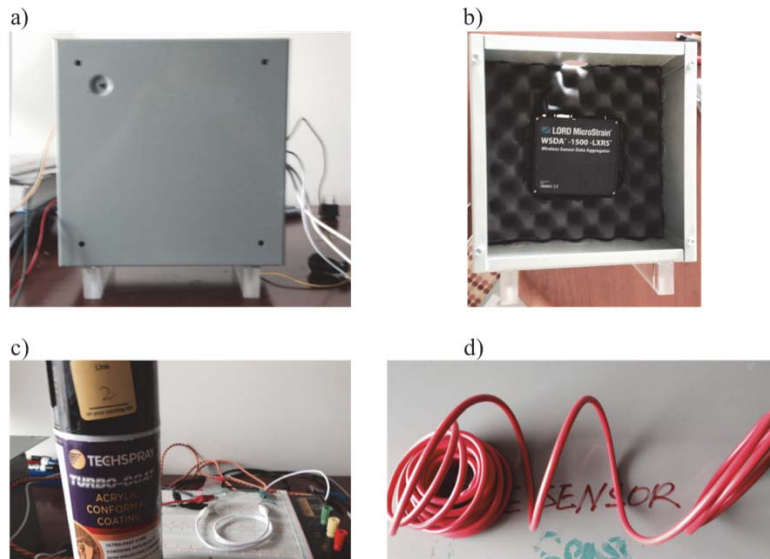


Fig. 93. a) Steel box for parts; b) polyurethane foam inside the box to protect the parts; c) spray to protect the circuit board; and d) outdoor electric wire.

■ Summary

In this investigation, a sensing system detecting water leakage was designed and constructed. The system is featured with an electric sensor head and a signal controller improved by a signal generating circuit. The accuracy and robustness of this system was tested at different conditions, which mimic the possible weather variation of outdoor environment.

The water leakage system was integrated with the displacement monitoring system developed in Task 2 by sharing a wireless signal transmitting/receiving combo. Powered by the rechargeable batteries, this data receiver is capable of capturing and storing the data inside its inner disk. In the tests carried out, the integrated system simultaneously captured and stored the signals transmitted from the LVDT sensor head and SeaHawk sensor head.

4. Summary

In this work task, the designs and implementation maps to improve the header materials and develop an integrated sensing system were assessed experimentally. The test results show that:

- *Header Materials:* five types of tests were conducted to characterize the material resistance to compression, impact, abrasion, chemical attack and frost respectively. The test results show that the addition of steel wires improves the resistance of elastomeric concrete to these physical and chemical attacks. As a consequence of this comprehensive improvement, its resistance to rutting, which was found to be a concern in a previous investigation, will be substantially enhanced. This suggests that the steel wire-reinforced elastomeric concrete would provide a strong and more durable header material for the block-outs. Due to the stickiness of elastomeric concrete, proper casting process may need to be developed in practice when steel wires are used as reinforcement.

Bridge Waterproofing Details Phase II

- *Integrated Sensing System:* a system capable of detecting water leakage was developed. This system is featured with an electric sensor head, which is able to detect water leakage along its length. Thus, it is suitable for the application in the beam/abutment adjunctions, where the water leakage is neither uniform, nor concentrated at a point. The accuracy and robustness of this system was tested under different conditions, which the system may be exposed to during service. This system was integrated with the displacement monitoring system and the power supply and wireless data transmitting/receiving were tested. To protect the important components from accidental damage during installation and service, protective device using steel wire cloth and electric enclosure were designed.



Chapter 4
Executable Implementation

1. Implementation Roadmap

■ Enhanced Abutment/Beam Adjunction Design

Design I (Fig. 94):

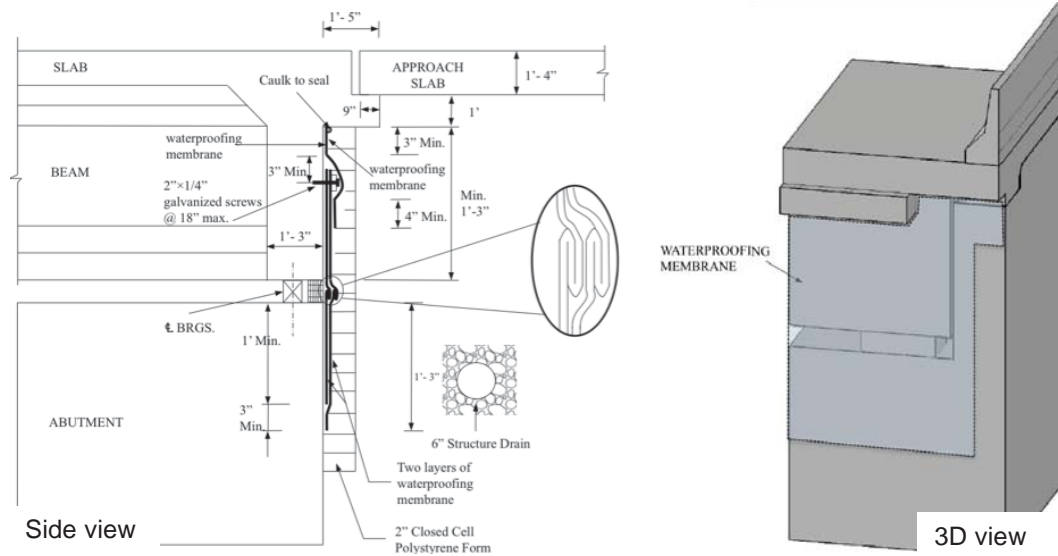


Fig. 94. Design I for abutment/beam adjunction.

The advantages of this design include:

1. An extension slab is used to move the expansion joint away from the abutment;
2. The paving notch is eliminated;
3. The geometry of the adjunction is greatly simplified;
4. In addition to the gap at beam seat, the gaps between the abutment and cheekwalls can be fully covered by waterproofing membrane;
5. The flat surface benefits the installation of waterproofing membrane;
6. Its application scope can cover the typical beams, span lengths and skew angles in the current practice.

Bridge Waterproofing Details Phase II

Design II (Fig. 95):

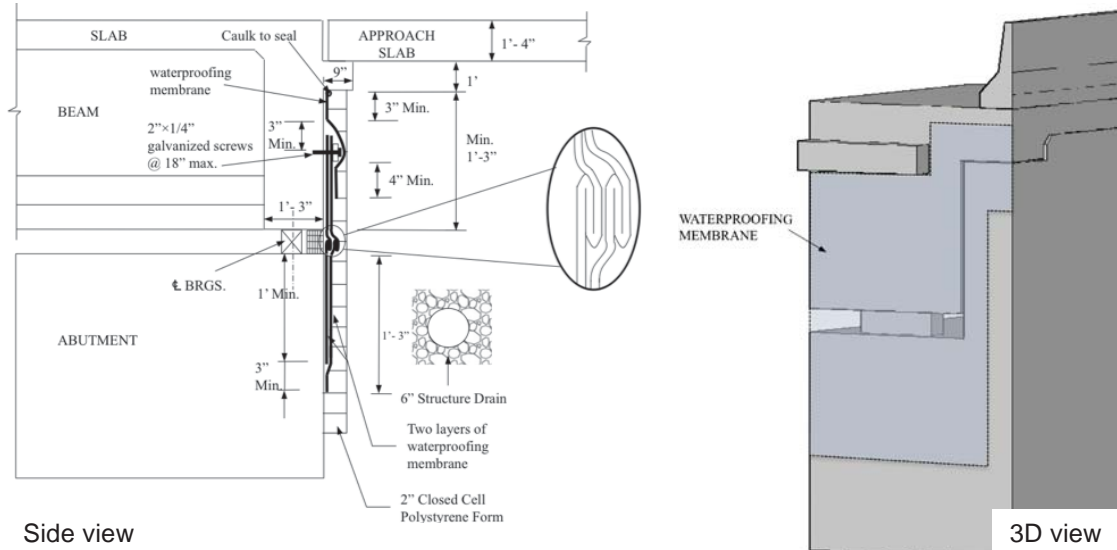


Fig. 95. Design II for abutment/beam adjunction.

The advantages of this design include:

1. Tensile stress in the lip support is lower than that in the extension slab of Design I;
2. Paving notch is eliminated;
3. The geometry of the adjunction is greatly simplified;
4. The open gaps at beam seat and between the abutment and cheekwalls can be fully covered by waterproofing membrane;
5. The flat surface benefits the installation of waterproofing membrane;
6. Its application scope can cover the typical beams, span lengths and skew angles in the current practice.

Bridge Waterproofing Details Phase II

Design III (Fig. 96):

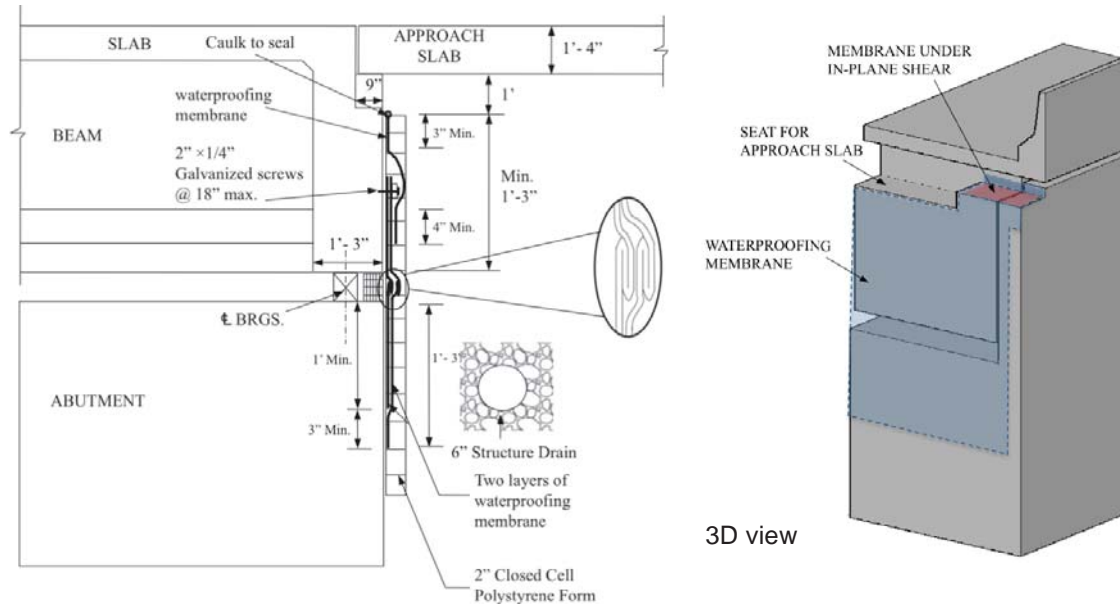


Fig. 96. Illustration of Design III for the enhanced abutment.

The advantages of this design include:

1. The simple structural form of the step-like seat leads to simple structural design;
2. All the gaps between the abutment, abutment stem and cheekwalls can be covered by the waterproofing membrane;
3. The flat surface benefits the installation of waterproofing membrane;
4. Its application scope can cover the typical beams, span lengths and skew angles in the current practice.

Among these three designs, Design I has the highest waterproofing capacity and Design III has the lowest. However, the structural form of Design III is the simplest among these three. Therefore, the selection of the abutment/beam adjunction design should take this effect into account in bridge construction.

Bridge Waterproofing Details Phase II

■ Use of Crystalline Waterstops

Table 16. Implementation roadmaps of Krystol and Xypex waterstops

	Krystol waterstop	Xypex waterstop
Preparation	<ol style="list-style-type: none"> 1. Prepare the slurry with a volume ratio of Krystol slurry powder to water being 3:1; 2. After mixing, stir for 1 minute to achieve a uniform slurry; 3. Prepare the grout with a ratio of Krystol grout powder to water being 4:1; 4. After mixing, stir for 1 minute to achieve a uniform paste-like product 	<ol style="list-style-type: none"> 1. Prepare the slurry treatment with a volume ratio of Xypex concentrate powder to water being 2:1; 2. After mixing, stir for 1 minute to achieve a uniform slurry; 3. Prepare the dry-pack with a ratio of concentrate powder to water being 4:1; 4. After mixing, stir for 1 minute to achieve a uniform paste-like product; 5. Prepare the Plug N pack with a ratio of pack powder to water being 3:1; 6. After mixing, stir for 1 minute to achieve a uniform paste-like product;
Installation	<ol style="list-style-type: none"> 1. Clean the concrete surface with clean water and then make the concrete surface-dry; 2. Use a brush to pave the slurry on the concrete surface to form a uniform layer about 0.04 in. thick; 3. Cure this layer for 12 to 24 hours before the casting of the next part of the joint; 4. 24 hours after the next casting, clean the pre-formed groove and then make it surface-dry; 5. Pave the groove with the slurry; 6. Wait for at least 10 minutes, then fill the groove with the grout; 7. Then use the slurry to make the surface flat; 8. Cure the treatment with light mist or wet burlap for 24 hours. 	<ol style="list-style-type: none"> 1. Clean the concrete surface with clean water and then make the concrete surface-dry; 2. Use a brush to pave the slurry on the concrete surface to form a uniform layer about 0.04 in. thick; 3. Cure this layer for 48 hours before the casting of the next part of the joint; 4. 24 hours after the next casting, clean the pre-formed groove and then make it surface-dry; 5. Pave the groove with the slurry; 6. Wait for at least 10 minutes, fill the groove with the dry-pack, and then use the Plug N pack to make the surface flat; 7. Cure the treatment with light mist or wet burlap for 24 hours.

Note that due to the inherent working mechanisms of crystalline waterstops, curing time is needed for them. This may demand for careful construction management to avoid prolonging the total construction time.



■ Mitigation of The Delamination of Waterproofing Membrane

The construction of an overlap is recommended to mitigate the risk of the delamination of waterproofing membrane. The main advantage of this overlap is that it accommodates the relative movement between the concrete parts without causing any peeling stress in the waterproof membrane. The key steps of its implementation roadmap include:

- Prepare fiberglass powder or dry fine sand;
- Based on the expected relative movement and gap size, determine the size of cover to be removed from the waterproofing membrane;
- With the aid of proper tools (e.g., a sharp blade and a straightedge), remove the cover of waterproofing membrane to expose its adhesive surface;
- Uniformly spread the fiberglass powder or dry fine sand on the exposed surface until it is no longer sticky;
- Peel off the rest of the cover of the membrane and start the installation as recommended in the current practice;
- Examine the bond quality between the membrane and concrete before adding the polystyrene foam layer to protect the membrane;
- Fold the overlap and then install the polystyrene foam layer to support it.

■ Sensing System

To monitor the joint displacement and detect water leakage, the fabricated sensing system (Fig. 97) consists of the following components:

1. A LVDT displacement sensor head (e.g., LDI 119-150-A20A from OMEGA Engineering)
2. A electric cable sensor head for water leakage detection (e.g., the SeaHawk sensor cable from RLE Technology)
3. A circuit board containing two conditioning circuits, one for the LVDT and the other for the cable sensor
4. A controller (e.g., LD310 from RLE Technology), which converts the water leakage detected by the sensor head to analog signals and sends them to the circuit
5. A wireless signal transmitter and receiver combo (e.g., V-link/WSDA from LORD Sensing)
6. Power supplies for sensor heads and wireless combo (e.g., YIX30L batteries)

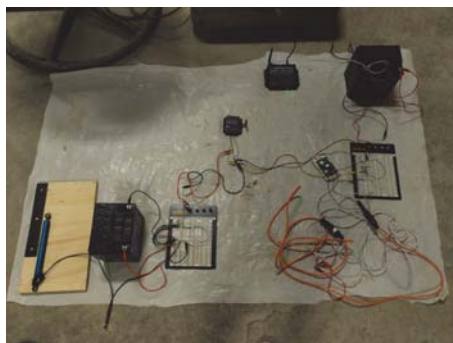


Fig. 97: The integrated sensing system fabricated.

Bridge Waterproofing Details Phase II

To protect the sensing system during its outdoor use, all the key components are encased in steel boxes (Fig. 98a); in the box the parts are protected by polyurethane foam (Fig. 98b); acrylic conformal spray is sprayed on the circuit board to protect it from moisture (Fig. 98c); and vehicle wires (Fig. 98d) are used to connect all the components through the small holes on the boxes. To prevent the contact with the water on the ground, plastic seats are added on the boxes (Fig. 5a,b). Since the holes for the pass of wires are small and blocked with the polyurethane foam, there is no need to guard them with steel fence.

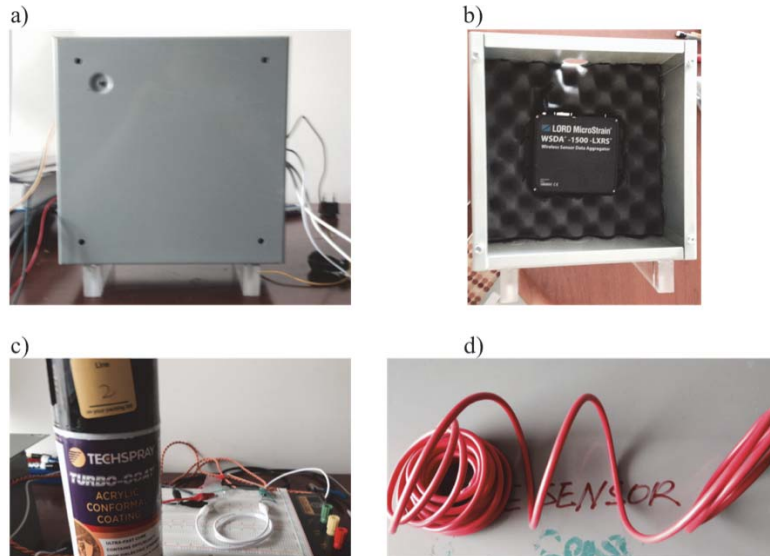


Fig. 98. a) Steel box for parts; b) polyurethane foam inside the box to protect the parts; c) spray to protect the circuit board; and d) outdoor electric wire.

■ Header Materials

Elastomeric concrete reinforced with steel wires is recommended to improve the performance of block-outs. Its implementation roadmap is described as follows:

- Use steel wires (of diameters not greater than 1/8 in.) to fabricate steel wire frames
- Place the steel wire frames in the molds based on the designed layout;
- Mix the elastomeric concrete as recommended by the supplier;
- Pour the elastomeric concrete into the molds;
- Wait until the elastomeric concrete is hardened.

Since elastomeric concrete is sticky, attention should be paid to ensure its flowability during casting to avoid segregation. It is recommended that the spacing between the steel wire frames and the spacing between the steel wires in each frame should be at least 3 times as large as the maximum aggregate size of the elastomeric concrete.

2. Adjustment in Construction

In this investigation, the implementation roadmaps are made based on the numerical analyses and experimental tests. The size scales and environmental conditions are different from the real

Bridge Waterproofing Details Phase II

applications in construction. Thus, certain adjustment may be needed in construction, which includes:

1. Structural design. In the enhanced designs for abutment/beam adjunction, an extension slab exists in Design I and a lip support exists in Design II. Although numerical investigation shows that these structural changes will not lead to high tensile stress, standard design following AASHTO code is needed for bridges of different spans and skew angles to determine the reinforcement ratio and placement layout. Considering that these structural regions are in the disturbed regions, the strut-and-tie method may be explored to conduct the standard structural design for the extension slab and lip support.
2. Construction management. Different from the conventional polymer-based waterstops, the implementation of crystalline waterstops requires curing. Therefore, adjustment may be needed to incorporate the implementation of crystalline waterstops into the construction management so as to avoid the increase of construction time. Besides construction scheduling, material and construction specifications would need to be developed based on an actual field placement.
3. Placement of steel wire. The block-out size is much larger than the specimens used in the experimental test. Thus, the placement of steel wire in elastomeric concrete may be more challenging in worksite than in the lab. Adjustment may be needed to improve the efficiency and construction friendliness of steel wire placement in the real construction.

Besides, adjustment on the installation and maintenance of the sensing system is also of great importance for improving its serviceability.



Bridge Waterproofing Details Phase II

References

- AASHTO LRFD Bridge Design Specifications, Customary U.S. Units (6th Edition). (2012). Washington: American Association of State Highway and Transportation Officials (AASHTO).
- Application Instructions Construction Joints and Details, 4.11 & 4.12. (2016). Kryton International Inc.
- ASTM C39/C39M-16b Standard Test Method for Compressive Strength of Cylindrical Concrete Specimens, ASTM International, West Conshohocken, PA, 2016, https://doi.org/10.1520/C0039_C0039M-16B.
- ASTM C192/C192M-16a Standard Practice for Making and Curing Concrete Test Specimens in the Laboratory, ASTM International, West Conshohocken, PA, 2016, https://doi.org/10.1520/C0192_C0192M-16A.
- ASTM A370-16 Standard Test Methods and Definitions for Mechanical Testing of Steel Products, ASTM International, West Conshohocken, PA, 2016, <https://doi.org/10.1520/A0370-16>.
- ASTM C666/C666M-15 Standard Test Method for Resistance of Concrete to Rapid Freezing and Thawing, ASTM International, West Conshohocken, PA, 2015, https://doi.org/10.1520/C0666_C0666M-15.
- ASTM C672/C672M-03 Standard Test Method for Scaling Resistance of Concrete Surfaces Exposed to Deicing Chemicals (Withdrawn 2012), ASTM International, West Conshohocken, PA, 2003, https://doi.org/10.1520/C0672_C0672M-03.
- ASTM C944/C944M-12 Standard Test Method for Abrasion Resistance of Concrete or Mortar Surfaces by the Rotating-Cutter Method, ASTM International, West Conshohocken, PA, 2012, https://doi.org/10.1520/C0944_C0944M-12.
- Casas, J. R., & Cruz, P. J. (2003). Fiber optic sensors for bridge monitoring. *Journal of Bridge Engineering*, 8(6),362-373.
- Crescini, D., Flammini, A., Marioli, D., & Taroni, A. (1998). Application of an FFT-based algorithm to signal processing of LVDT position sensors. *Instrumentation and Measurement, IEEE Transactions*, 47(5), 1119-1123.
- Distlehorst, J., & Wojakowski, J. (2005). Evaluation of Elastomeric Concrete in Bridge Expansion Joint Header Repair Applications (No. FHWA-KS-05-1).
- Fleming B.C., Beynnon B. D., Renstrom P. A., Johnson R. J., Nichols C. E., Peura G. D., & Uh B. S., (1999). The Strain Behavior of the Anterior Cruciate Ligament During Stair Climbing: an In Vivo Study, *Arthroscopy*, 15, No. 2, pp. 185-191.
- Gopalaratnam, V.S., Shah, S.P. and John, R. (1984). A modified instrumented Charpy impact test for cement-based composites. *Experimental Mechanics* (24)102–111.



Bridge Waterproofing Details Phase II

- Hollis J. M., Pearsall A. W. 4th, & Niciforos P. G., (2000). Change in Meniscal Strain With Anterior Cruciate Ligament Injury and After Reconstruction. *Am. J. Sports Med.*, 28, No. 5, pp. 700-704.
- Keck, R. H. (2001). Improving concrete durability with cementitious materials. *Concrete International*, 23(9), 47-51.
- LORD User Manual, V-Link-LXRS*. (2015). LORD MicroStrain Sensing System.
- LORD Product User Manual, WSDA-1500-LXRS*. (2015). LORD MicroStrain Sensing System.
- Mather, B. (2004). Crystal Growth in Entrained-Air Voids. *ACI Special Publication*, 223.
- Merzbacher, C. I., A. D. Kersey, & E. J. Friebele. (1996). Fiber optic sensors in concrete structures: a review. *Smart materials and structures*, 5(2), 196.
- Mohammad, L. N., Puppala, A. J., & Alavilli, P. (1994). Influence of testing procedure and LVDT location on resilient modulus of soils. *Transportation Research Record*, (1462).
- Saxena, S. C., & Seksena, S. L. (1989). A self-compensated smart LVDT transducer. *Instrumentation and Measurement, IEEE Transactions*, 38(3), 748-753.
- Sprouts, S., Huang, L., & Amey, S. L. (1994). Evaluating performance of cementitious waterproofing systems for concrete. *Concrete International*, 7, 38-41.
- Tariq, H., Takamori, A., Vetrano, F., Wang, C., Bertolini, A., Calamai, G., ... & Stanga, R. (2002). The linear variable differential transformer (LVDT) position sensor for gravitational wave interferometer low-frequency controls. *Nuclear Instruments and Methods in Physics Research Section A: Accelerators, Spectrometers, Detectors and Associated Equipment*, 489(1), 570-576.
- Tinnea, J., Li, L., Hartt, W. H., Sagues, A. A., Pianca, F., & Chandler, B. (2006). Corrosion in Bridges and Highways. *ASM International*, 559-597.
- Xypex Concentrate Product Data. (2004). Xypex Chemical Corporation.
- Wright T. W., Glowczewskie F. Jr., Cowin D., & Wheeler D. L., (2001). Ulnar Nerve Excursion and Strain at the Elbow and Wrist Associated with upper extremity motion. *J. Hand Surg.*, 26, No. 4, pp. 655-662.
- Zhang, shiping, Deng, Min, & Tang, Mingshu. (2008). Advance in Research on Damagement of Concrete Due to Freeze-thaw Cycles. *Journal of Materials Science & Engineering*, 26(6), 990 -994.

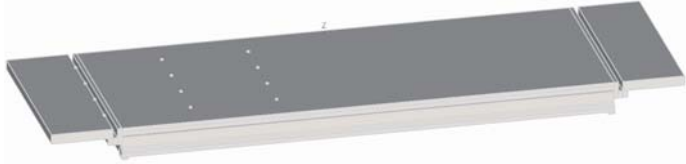
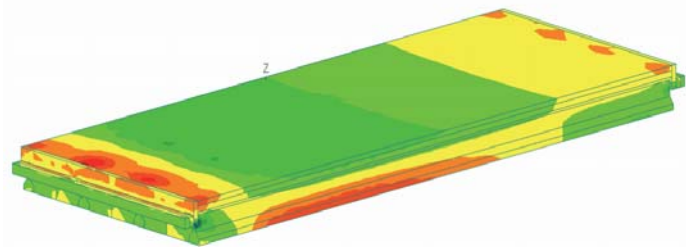
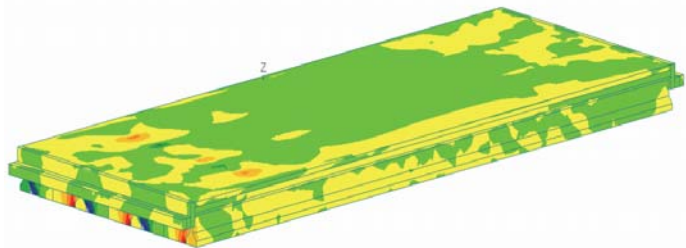
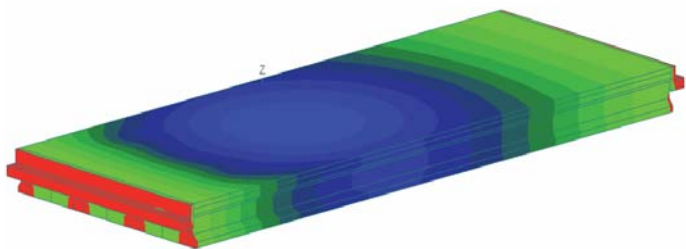


Bridge Waterproofing Details Phase II

Appendix


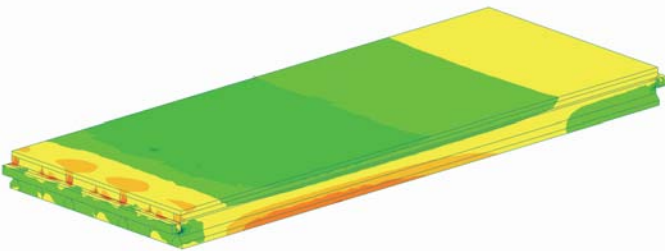
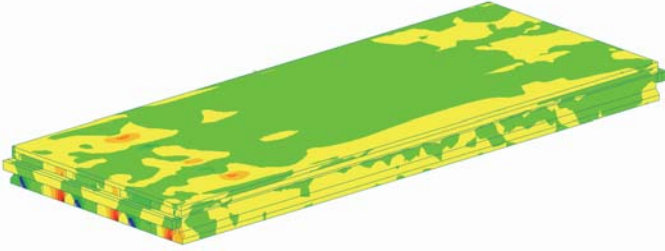
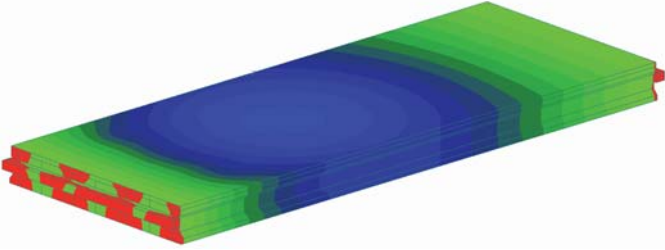
1. Tables:

Table A1: Case 1 using Design I

Computer model	
Normal stress	
Shear stress	
Deflection	
<p>Span: 80 ft; Width: 30 ft; Skewed angle: 0°; Lanes: 2; Number of girders: 4 Maximum tensile stress: 0.05 ksi Maximum compressive stress: 0.10 ksi Maximum shear stress: 0.009 ksi Vertical deflection over length of extended slab: <1/1000</p>	

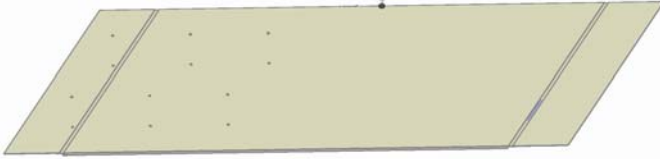
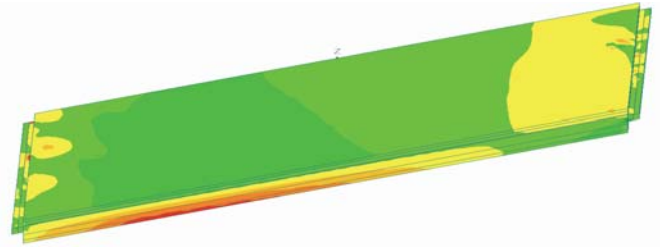
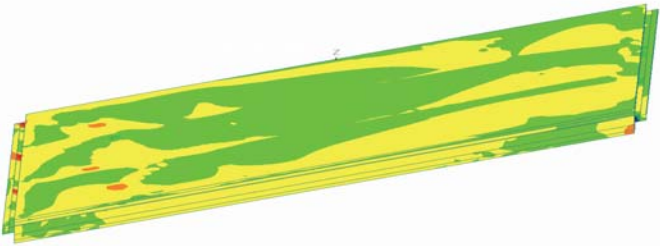
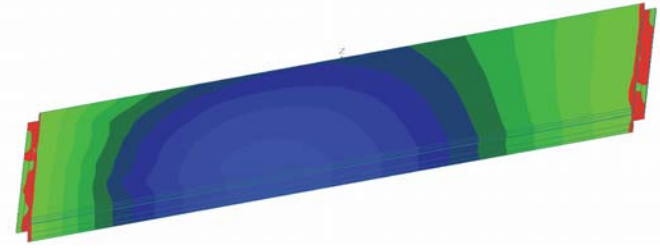
Bridge Waterproofing Details Phase II

Table A2: Case 1 using Design II

Computer model	
Normal stress	
Shear stress	
Deflection	
<p>Span: 80 ft; Width: 30 ft; Skewed angle: 0°; Lanes: 2; Number of girders: 4 Maximum tensile stress: 0.10 ksi Maximum compressive stress: 0.10 ksi Maximum shear stress: 0.012 ksi Vertical deflection over length of lip-shaped support: <1/1000</p>	

Bridge Waterproofing Details Phase II

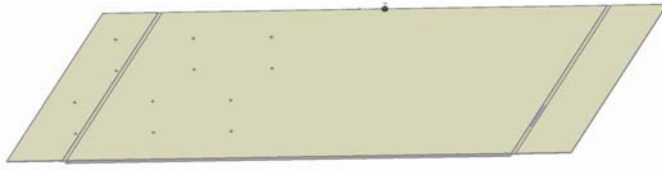
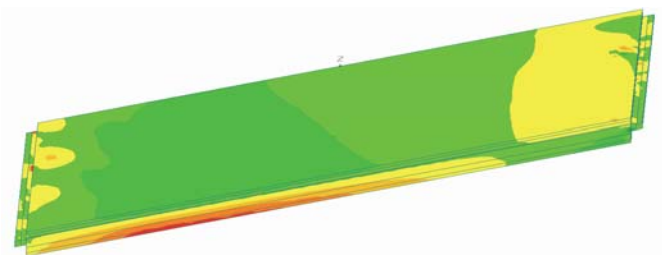
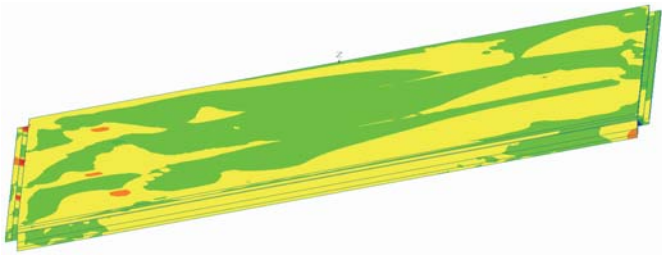
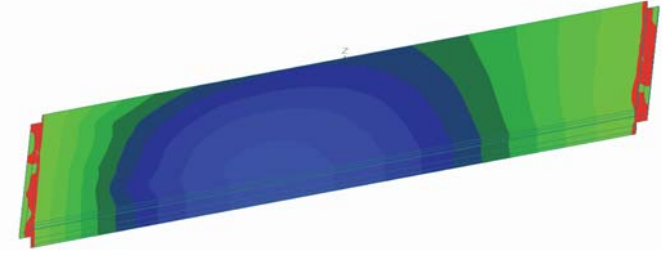
Table A3: Case 3 using Design I

Computer model	
Normal stress	
Shear stress	
Deflection	
<p>Span: 80 ft; Width: 30 ft; Skewed angle: 30°; Lanes: 2; Number of girders: 4 Maximum tensile stress: 0.09 ksi Maximum compressive stress: 0.09 ksi Maximum shear stress: 0.014 ksi Vertical deflection over length of extended slab: <1/1000</p>	




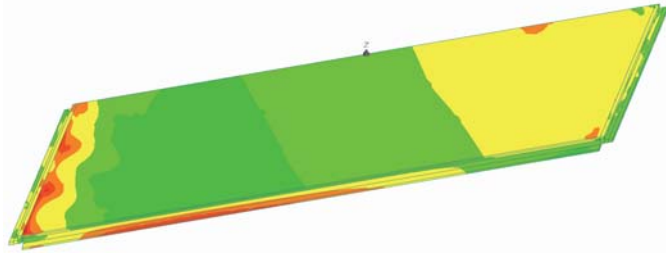
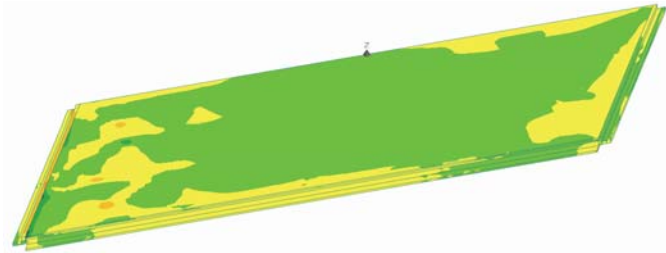
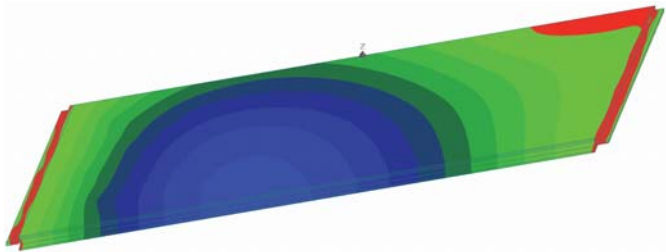
Bridge Waterproofing Details Phase II

Table A4: Case 3 using Design II

Computer model	
Normal stress	
Shear stress	
Deflection	
<p>Span: 80 ft; Width: 30 ft; Skewed angle: 30°; Lanes: 2; Number of girders: 4 Maximum tensile stress: 0.09 ksi Maximum compressive stress: 0.09 ksi Maximum shear stress: 0.014 ksi Vertical deflection over length of lip-shaped support: <1/1000</p>	

Bridge Waterproofing Details Phase II

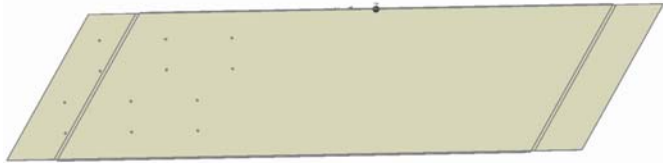
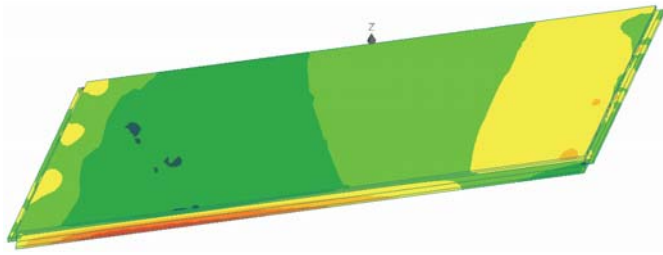
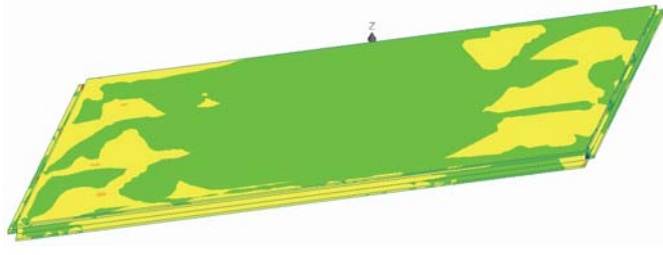
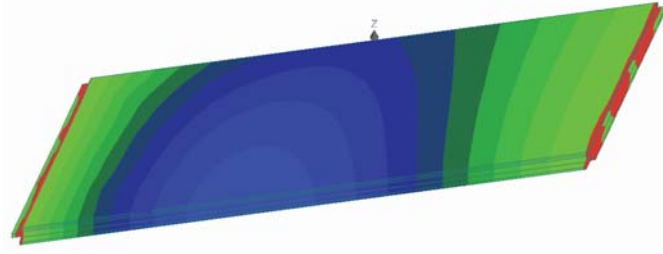
Table A5: Case 4 using Design I

Computer model	
Normal stress	
Shear stress	
Deflection	
<p>Span: 100 ft; Width: 30 ft; Skewed angle: 30°; Lanes: 2; Number of girders: 4 Maximum tensile stress: 0.07 ksi Maximum compressive stress: 0.13 ksi Maximum shear stress: 0.018 ksi Vertical deflection over length of extended slab: <1/1000</p>	



Bridge Waterproofing Details Phase II

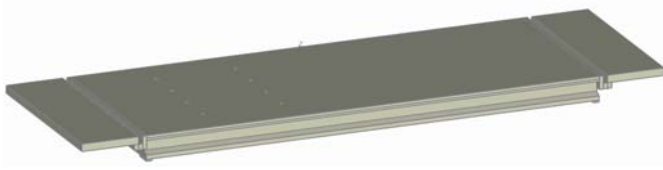
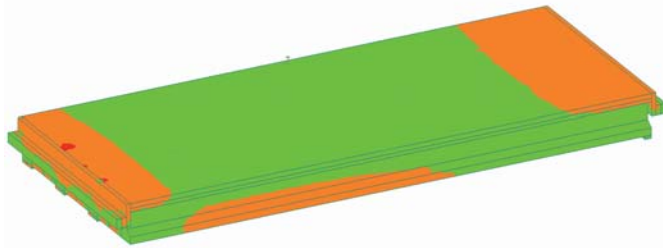
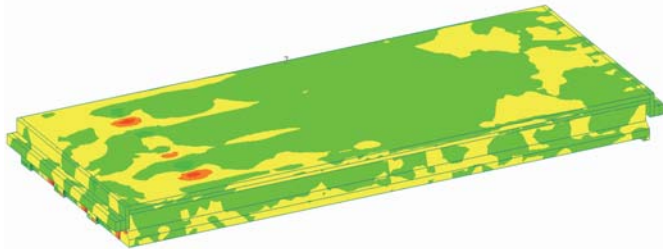
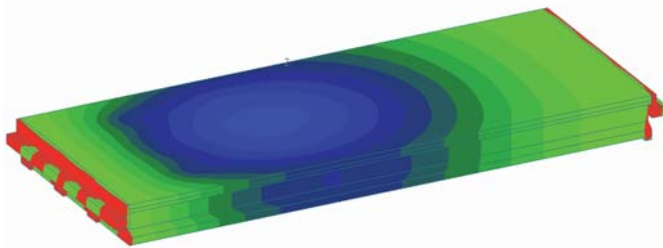
Table A6: Case 4 using Design II

Computer model	
Normal stress	
Shear stress	
Deflection	
<p>Span: 100 ft; Width: 30 ft; Skewed angle: 30°; Lanes: 2; Number of girders: 4 Maximum tensile stress: 0.08 ksi Maximum compressive stress: 0.08 ksi Maximum shear stress: 0.016 ksi Vertical deflection over length of lip-shaped support: <math><1/1000</math></p>	



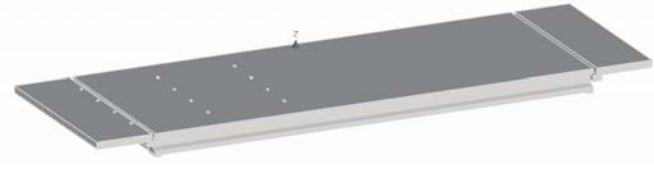
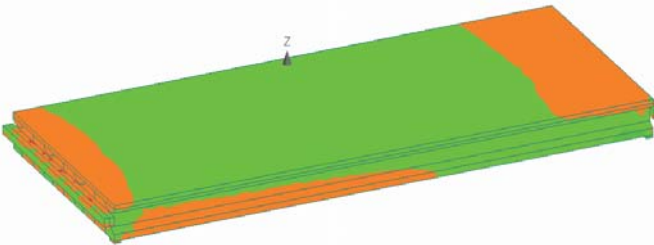
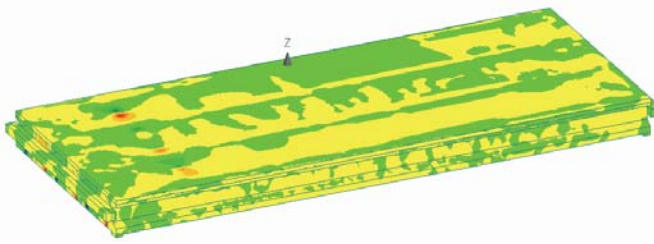
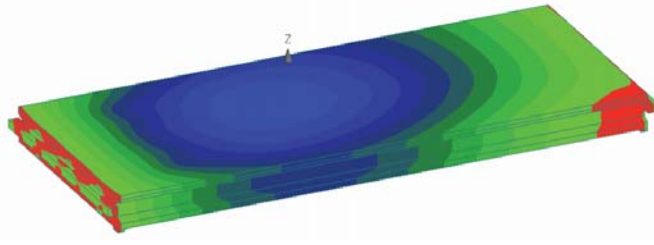
Bridge Waterproofing Details Phase II

Table A7: Case 5 using Design I

Computer model	
Normal stress	
Shear stress	
Deflection	
<p>Span: 80 ft; Width: 30 ft; Skewed angle: 0°; Lanes: 2; Number of girders: 4 Maximum tensile stress: 0.05 ksi Maximum compressive stress: 0.10 ksi Maximum shear stress: 0.011 ksi Vertical deflection over length of extended slab: <1/1000</p>	


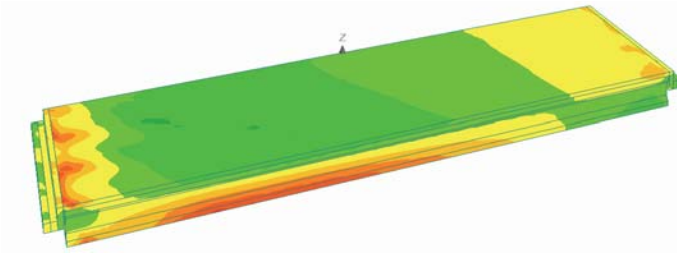
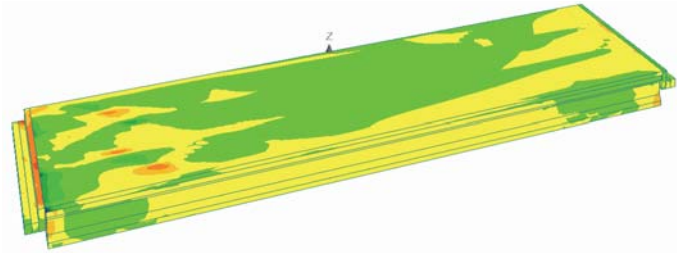
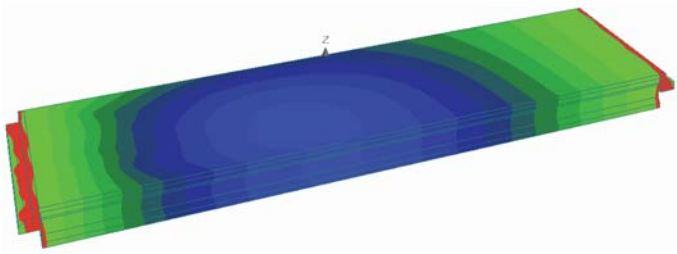
Bridge Waterproofing Details Phase II

Table A8: Case 5 using Design II

Computer model	
Normal stress	
Shear stress	
Deflection	
<p>Span: 80 ft; Width: 30 ft; Skewed angle: 0°; Lanes: 2; Number of girders: 4 Maximum tensile stress: 0.10 ksi Maximum compressive stress: 0.10 ksi Maximum shear stress: 0.015 ksi Vertical deflection over length of lip-shaped support: <math><1/1000</math></p>	

Bridge Waterproofing Details Phase II


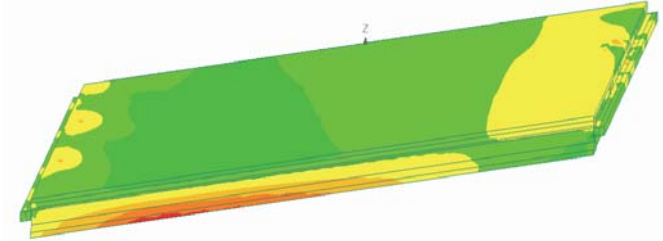
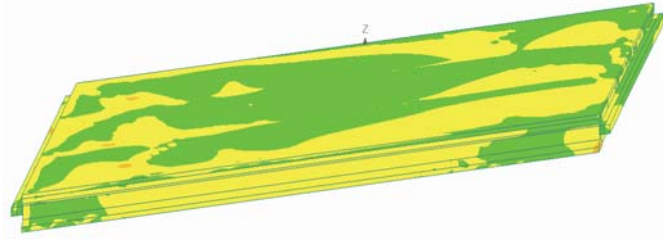
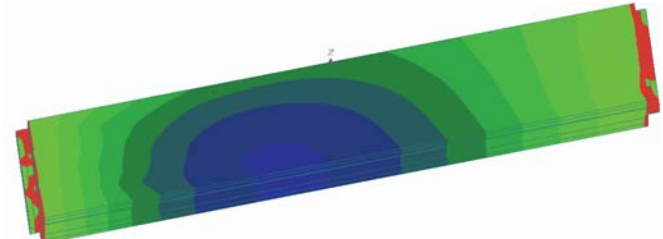
Table A9: Case 7 using Design I

Computer model	
Normal stress	
Shear stress	
Deflection	
<p>Span: 80 ft; Width: 30 ft; Skewed angle: 30°; Lanes: 2; Number of girders: 4 Maximum tensile stress: 0.04 ksi Maximum compressive stress: 0.07 ksi Maximum shear stress: 0.016 ksi Vertical deflection over length of extended slab: <math><1/1000</math></p>	



Bridge Waterproofing Details Phase II


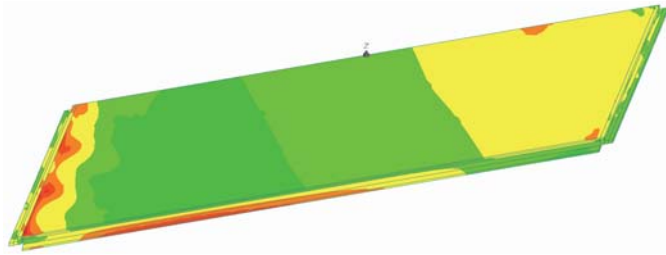
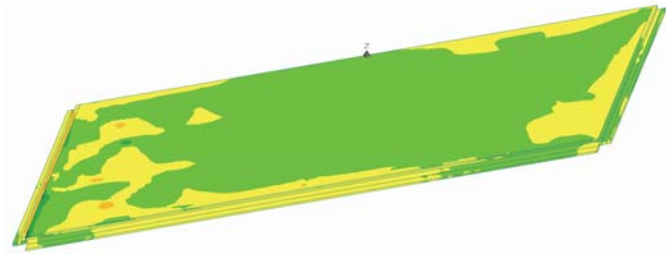
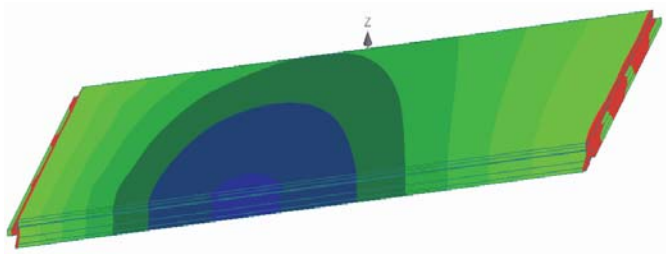
Table A10: Case 7 using Design II

Computer model	
Normal stress	
Shear stress	
Deflection	
<p>Span: 80 ft; Width: 30 ft; Skewed angle: 30°; Lanes: 2; Number of girders: 4 Maximum tensile stress: 0.09 ksi Maximum compressive stress: 0.09 ksi Maximum shear stress: 0.012 ksi Vertical deflection over length of lip-shaped support: <math><1/1000</math></p>	



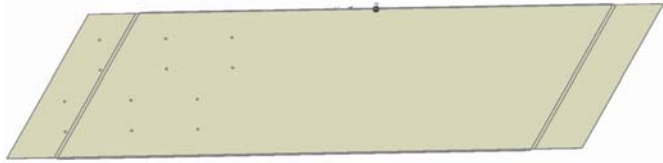
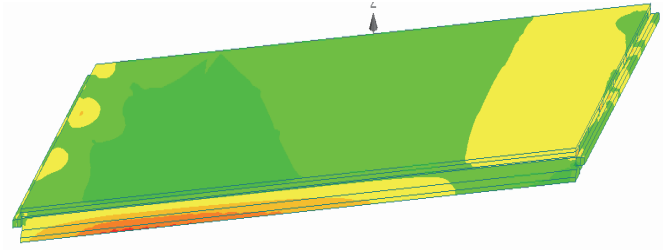
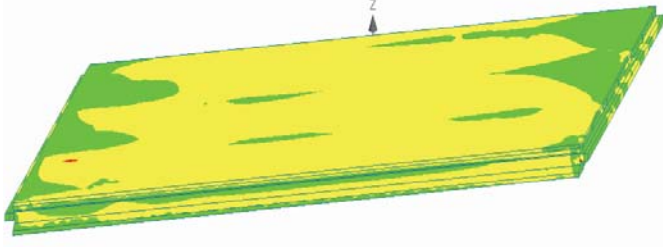
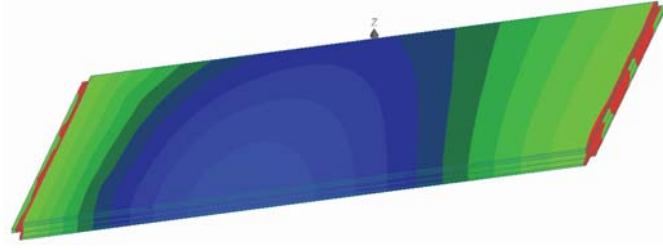
Bridge Waterproofing Details Phase II

Table A11: Case 8 using Design I

Computer model	
Normal stress	
Shear stress	
Deflection	
<p>Span: 100 ft; Width: 30 ft; Skewed angle: 30°; Lanes: 2; Number of girders: 4 Maximum tensile stress: 0.07 ksi Maximum compressive stress: 0.12 ksi Maximum shear stress: 0.012 ksi Vertical deflection over length of extended slab: <1/1000</p>	


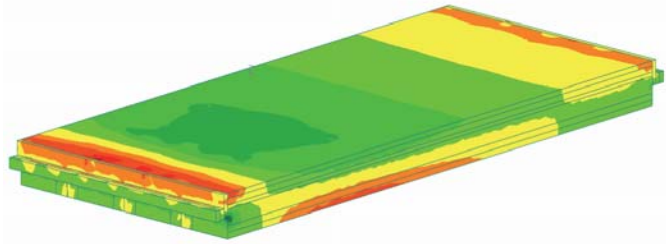
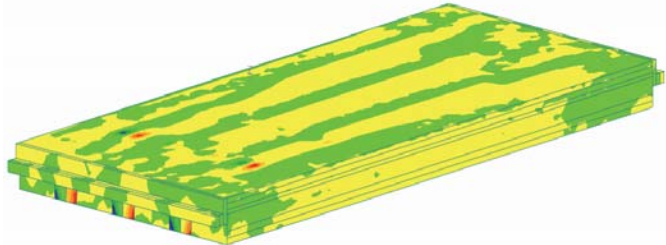
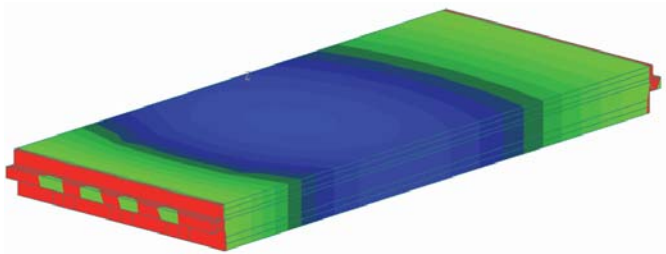
Bridge Waterproofing Details Phase II

Table A12: Case 8 using Design II

Computer model	
Normal stress	
Shear stress	
Deflection	
<p>Span: 10 ft; Width: 30 ft; Skewed angle: 30°; Lanes: 2; Number of girders: 4 Maximum tensile stress: 0.08 ksi Maximum compressive stress: 0.08 ksi Maximum shear stress: 0.015 ksi Vertical deflection over length of lip-shaped support: <math>< 1/1000</math></p>	

Bridge Waterproofing Details Phase II


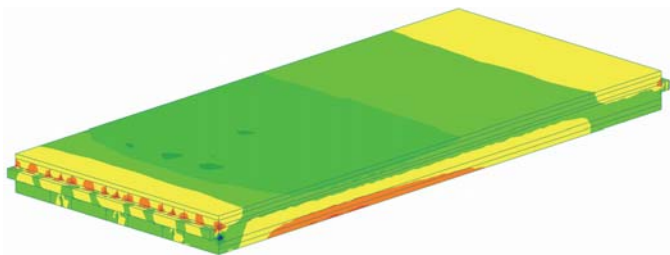
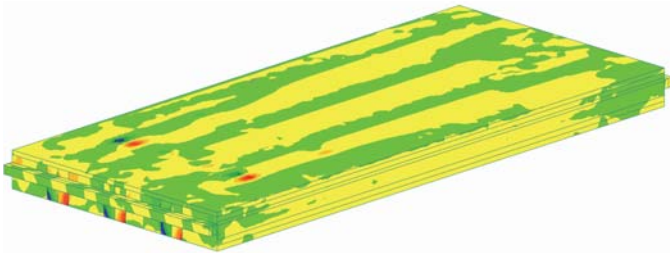
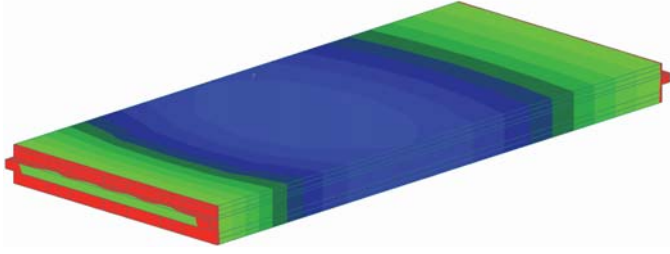
Table A13: Case 9 using Design I

Computer model	
Normal stress	
Shear stress	
Deflection	
<p>Span: 80 ft; Width: 30 ft; Skewed angle: 0°; Lanes: 2; Number of girders: 4 Maximum tensile stress: 0.05 ksi Maximum compressive stress: 0.11 ksi Maximum shear stress: 0.010 ksi Vertical deflection over length of extended slab: <1/1000</p>	



Bridge Waterproofing Details Phase II


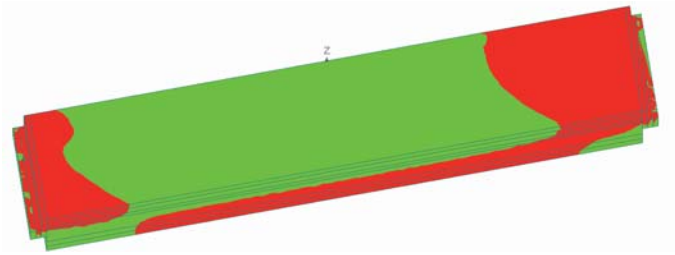
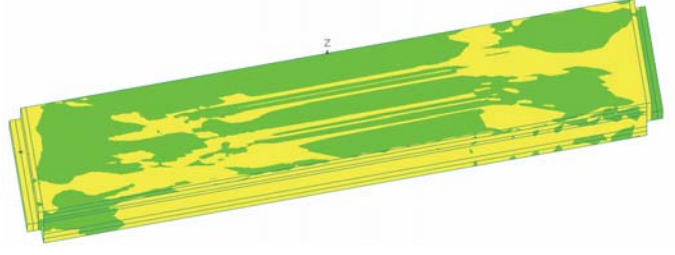
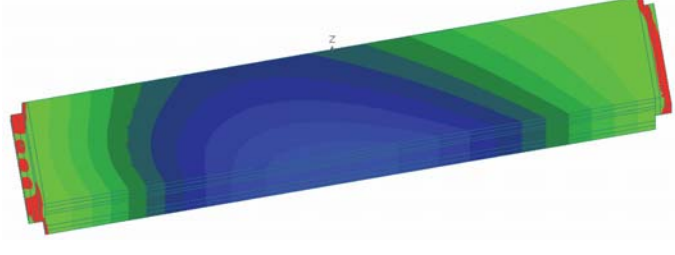
Table A14: Case 9 using Design II

Computer model	
Normal stress	
Shear stress	
Deflection	
<p>Span: 80 ft; Width: 30 ft; Skewed angle: 0°; Lanes: 2; Number of girders: 4 Maximum tensile stress: 0.09 ksi Maximum compressive stress: 0.09 ksi Maximum shear stress: 0.013 ksi Vertical deflection over length of lip-shaped support: <1/1000</p>	




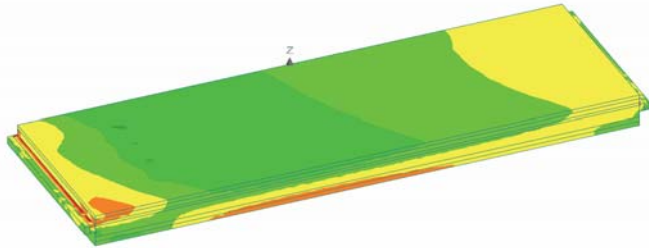
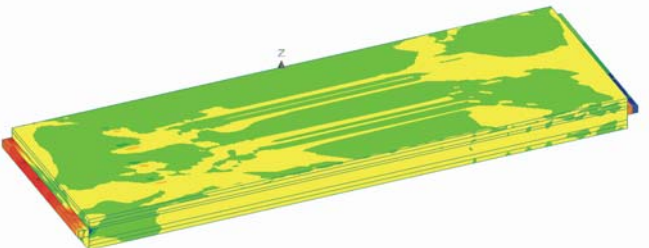
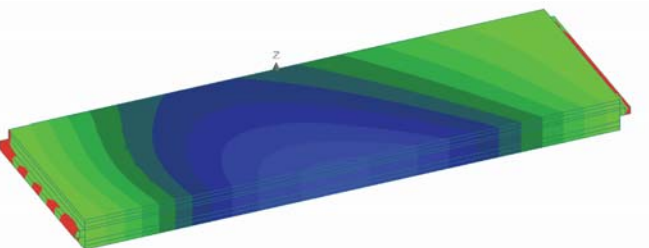
Bridge Waterproofing Details Phase II

Table A15: Case 11 using Design I

Computer model	
Normal stress	
Shear stress	
Deflection	
<p>Span: 80 ft; Width: 30 ft; Skewed angle: 30°; Lanes: 2; Number of girders: 4 Maximum tensile stress: 0.04 ksi Maximum compressive stress: 0.10 ksi Maximum shear stress: 0.016 ksi Vertical deflection over length of extended slab: <math><1/1000</math></p>	


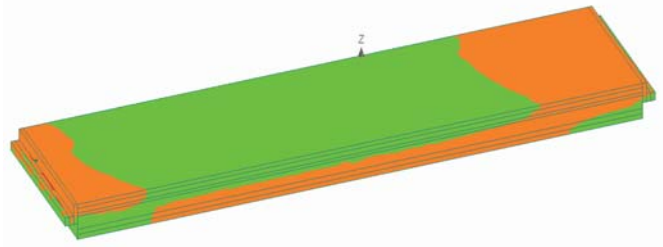
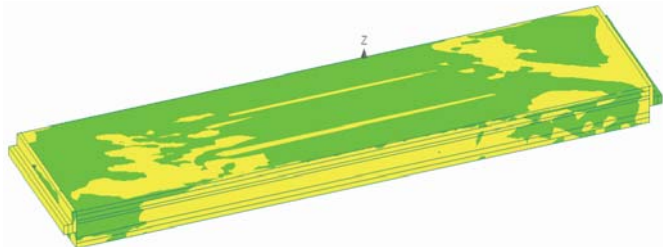
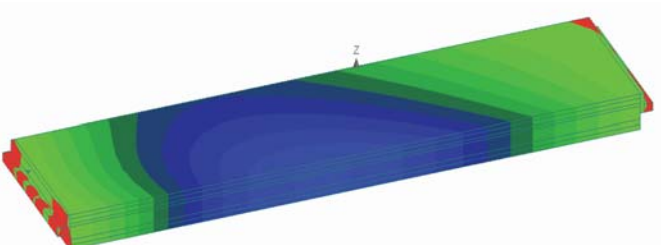
Bridge Waterproofing Details Phase II

Table A16: Case 11 using Design II

Computer model	
Normal stress	
Shear stress	
Deflection	
<p>Span: 80 ft; Width: 30 ft; Skewed angle: 30°; Lanes: 2; Number of girders: 4 Maximum tensile stress: 0.10 ksi Maximum compressive stress: 0.10 ksi Maximum shear stress: 0.014 ksi Vertical deflection over length of lip-shaped support: <math><1/1000</math></p>	


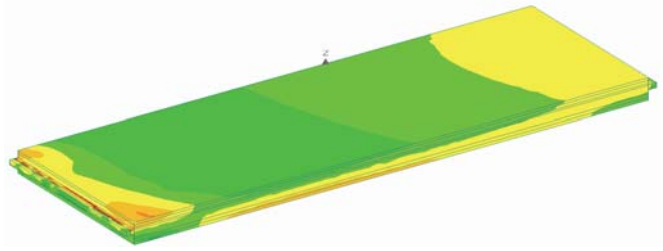
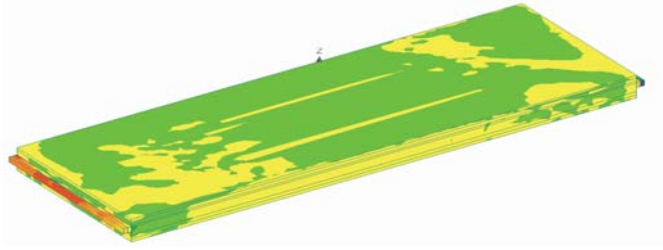
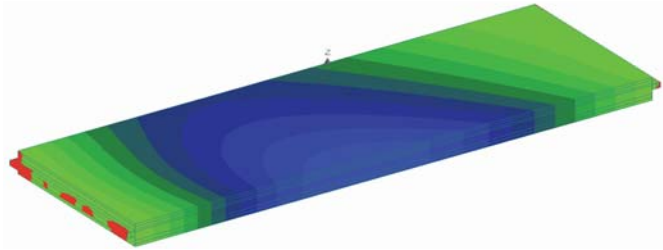
Bridge Waterproofing Details Phase II

Table A17: Case 12 using Design I

Computer model	
Normal stress	
Shear stress	
Deflection	
<p>Span: 100 ft; Width: 30 ft; Skewed angle: 30°; Lanes: 2; Number of girders: 4 Maximum tensile stress: 0.07 ksi Maximum compressive stress: 0.11 ksi Maximum shear stress: 0.02 ksi Vertical deflection over length of extended slab: <1/1000</p>	

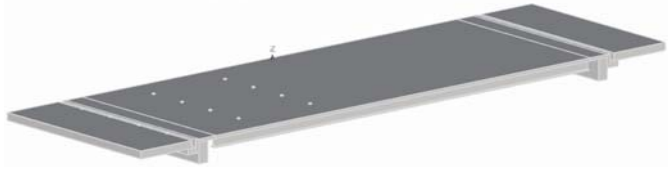
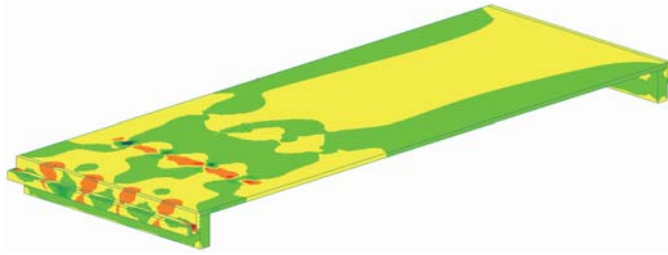
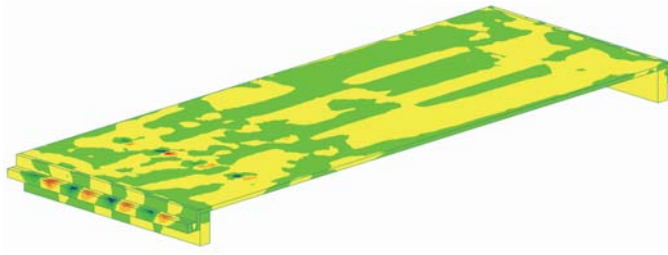
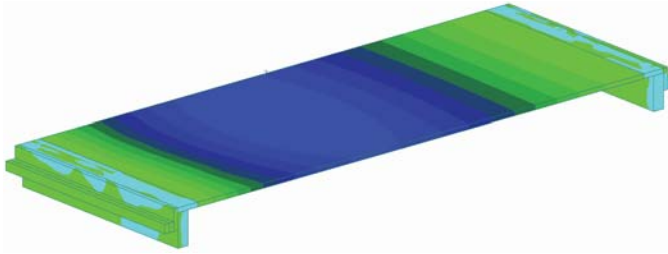
Bridge Waterproofing Details Phase II

Table A18: Case 12 using Design II

Computer model	
Normal stress	
Shear stress	
Deflection	
<p>Span: 100 ft; Width: 30 ft; Skewed angle: 30°; Lanes: 2; Number of girders: 4 Maximum tensile stress: 0.08 ksi Maximum compressive stress: 0.08 ksi Maximum shear stress: 0.01 ksi Vertical deflection over length of lip-shaped support: <math><1/1000</math></p>	

Bridge Waterproofing Details Phase II

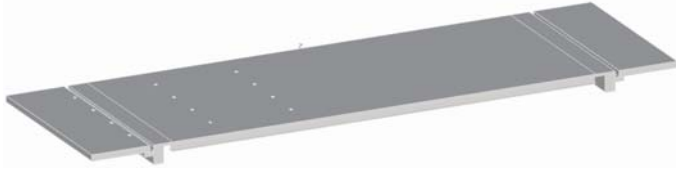
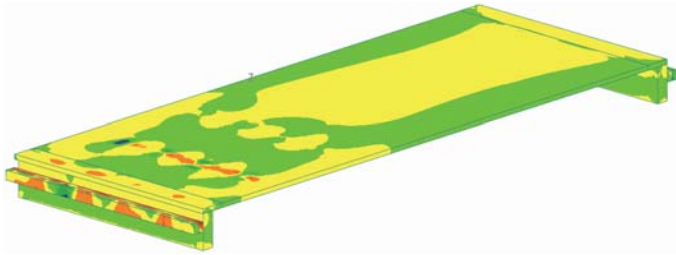
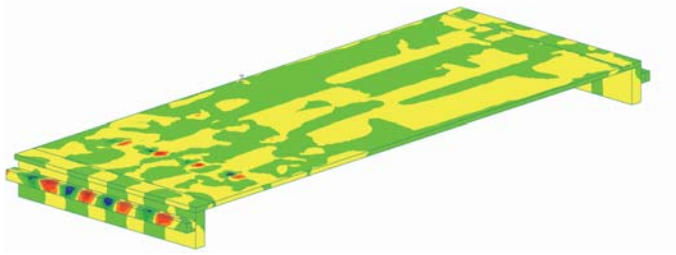
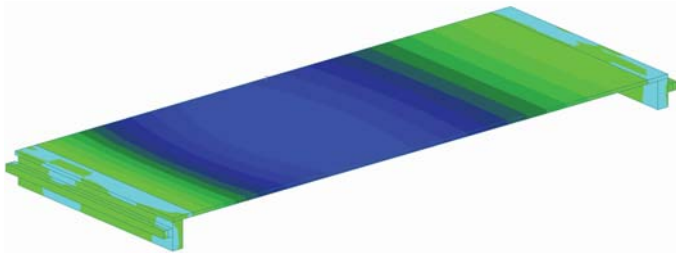
Table A19: Case 13 using Design I

Computer model	
Normal stress	
Shear stress	
Deflection	
<p>Span: 80 ft; Width: 30 ft; Skewed angle: 0°; Lanes: 2; Number of girders: 4 Maximum tensile stress: 0.05 ksi Maximum compressive stress: 0.09 ksi Maximum shear stress: 0.011 ksi Vertical deflection over length of extended slab: <math><1/1000</math></p>	




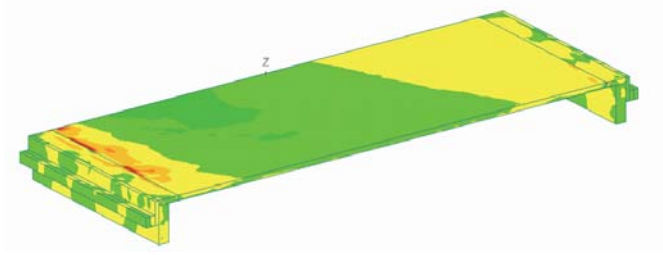
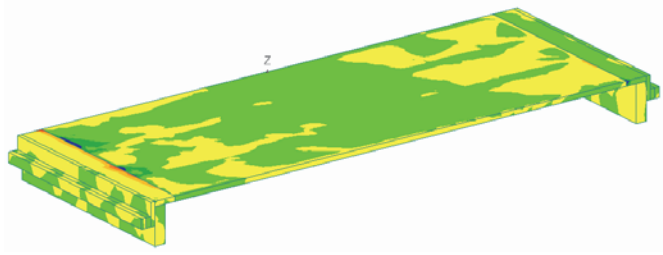
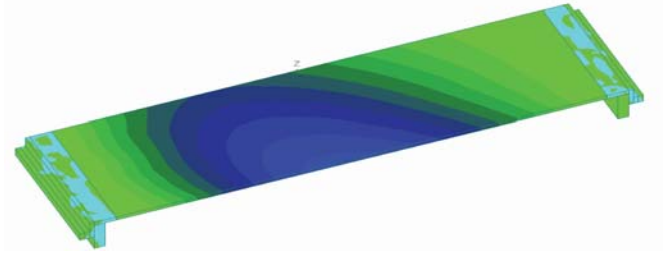
Bridge Waterproofing Details Phase II

Table A20: Case 13 using Design II

Computer model	
Normal stress	
Shear stress	
Deflection	
<p>Span: 80 ft; Width: 30 ft; Skewed angle: 0°; Lanes: 2; Number of girders: 4 Maximum tensile stress: 0.11 ksi Maximum compressive stress: 0.10 ksi Maximum shear stress: 0.013 ksi Vertical deflection over length of lip-shaped support: <1/1000</p>	

Bridge Waterproofing Details Phase II


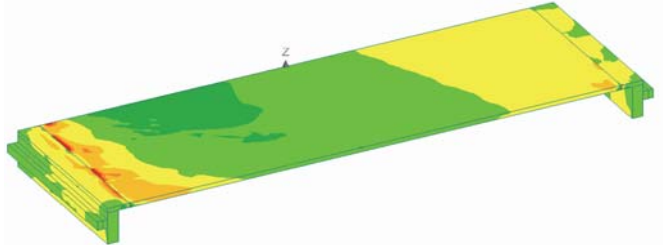
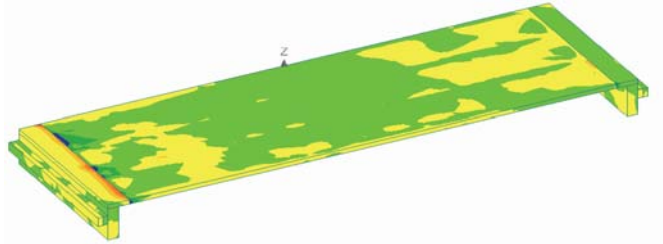
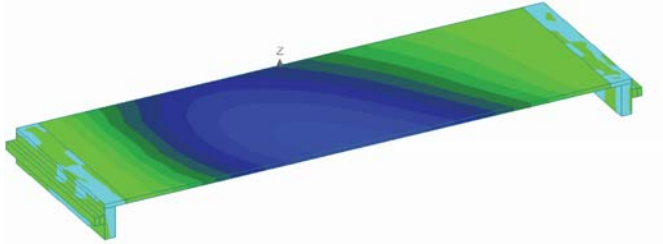
Table A21: Case 15 using Design I

Computer model	
Normal stress	
Shear stress	
Deflection	
<p>Span: 80 ft; Width: 30 ft; Skewed angle: 30°; Lanes: 2; Number of girders: 4 Maximum tensile stress: 0.05 ksi Maximum compressive stress: 0.09 ksi Maximum shear stress: 0.014 ksi Vertical deflection over length of extended slab: <math><1/1000</math></p>	



Bridge Waterproofing Details Phase II


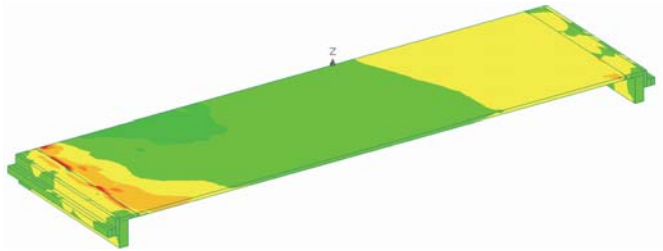
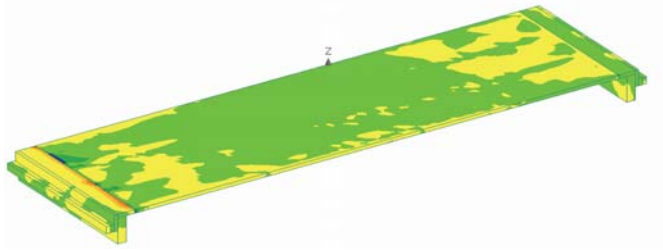
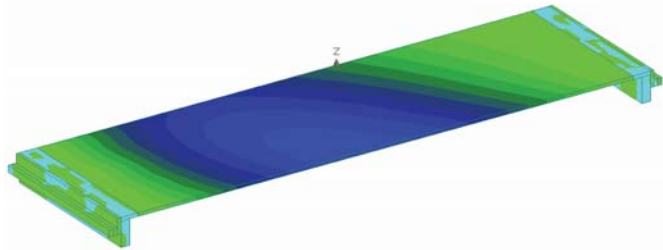
Table A22: Case 15 using Design II

Computer model	
Normal stress	
Shear stress	
Deflection	
<p>Span: 80 ft; Width: 30 ft; Skewed angle: 30°; Lanes: 2; Number of girders: 4 Maximum tensile stress: 0.09 ksi Maximum compressive stress: 0.09 ksi Maximum shear stress: 0.015 ksi Vertical deflection over length of lip-shaped support: <math><1/1000</math></p>	



Bridge Waterproofing Details Phase II


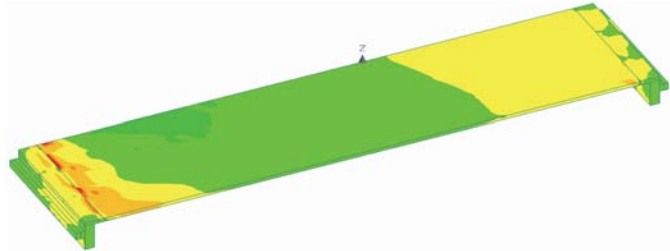
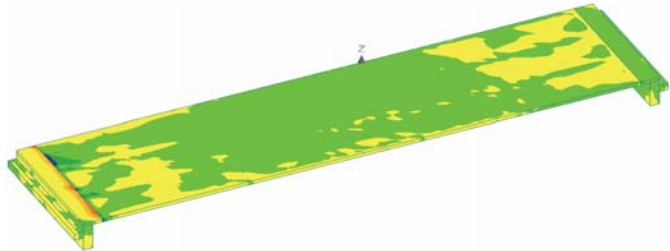
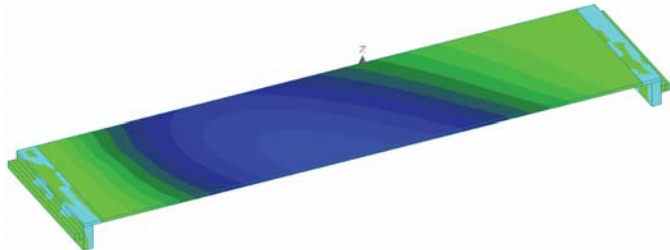
Table A23: Case 16 using Design I

Computer model	
Normal stress	
Shear stress	
Deflection	
<p>Span: 100 ft; Width: 30 ft; Skewed angle: 30°; Lanes: 2; Number of girders: 4 Maximum tensile stress: 0.07 ksi Maximum compressive stress: 0.13 ksi Maximum shear stress: 0.018 ksi Vertical deflection over length of extended slab: <math>< 1/1000</math></p>	



Bridge Waterproofing Details Phase II

Table A24: Case 16 using Design II

Computer model	
Normal stress	
Shear stress	
Deflection	
<p>Span: 100 ft; Width: 30 ft; Skewed angle: 30°; Lanes: 2; Number of girders: 4 Maximum tensile stress: 0.08 ksi Maximum compressive stress: 0.08 ksi Maximum shear stress: 0.016 ksi Vertical deflection over length of lip-shaped support: <math><1/1000</math></p>	

2. Figures:

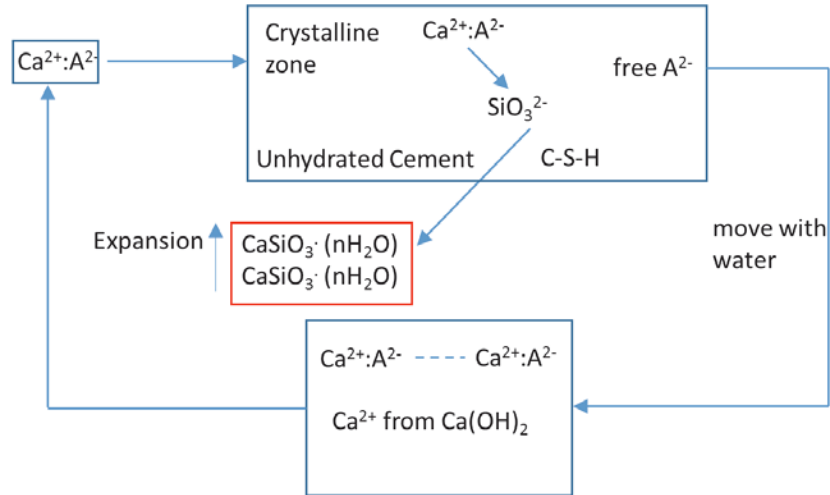


Fig. A1. Illustration of the complex precipitation reaction to produce the crystalline formation.

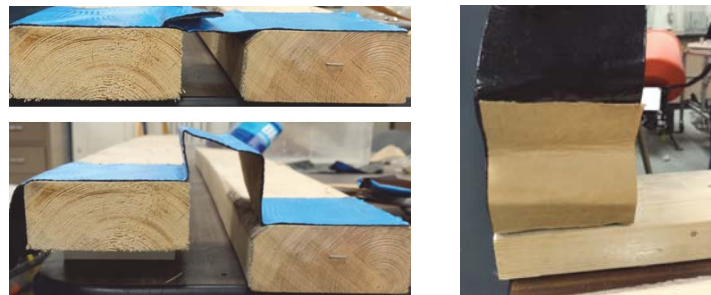


Fig. A2. Membrane treated with thin paper sheet.

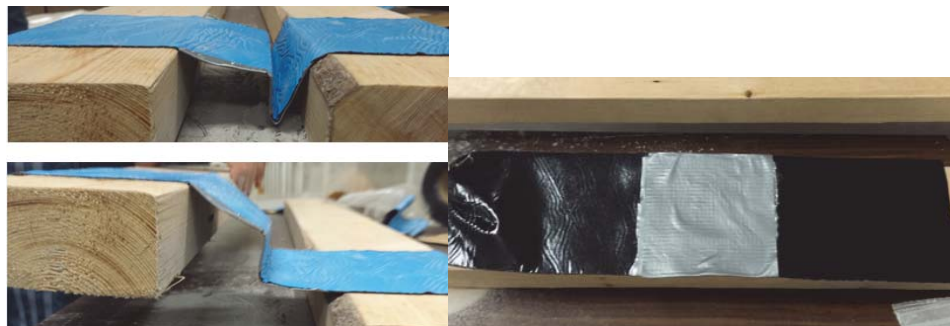


Fig. A3. Membrane treated with tape.

Bridge Waterproofing Details Phase II

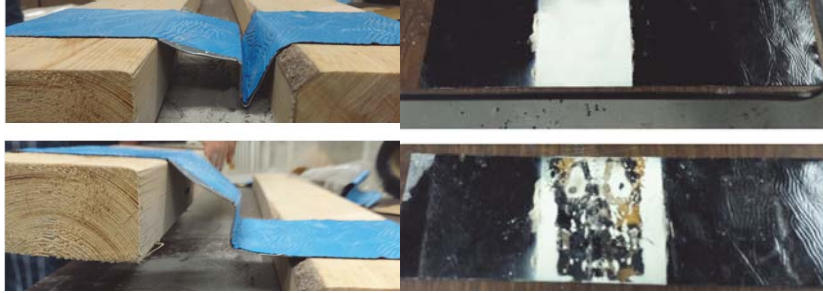


Fig. A4. Membrane treated with paint spray.

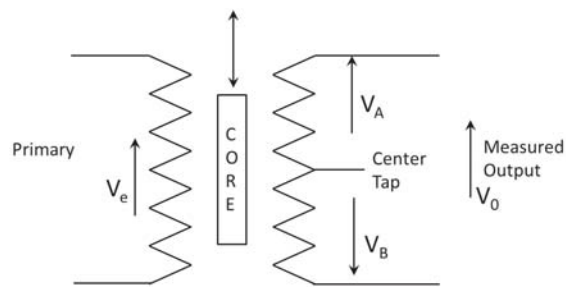


Fig. A5. Illustration of the basic mechanism of LVDT sensors.

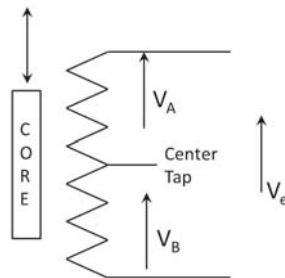


Fig. A6. Illustration of the mechanism of DVRT sensors.

Bridge Waterproofing Details Phase II

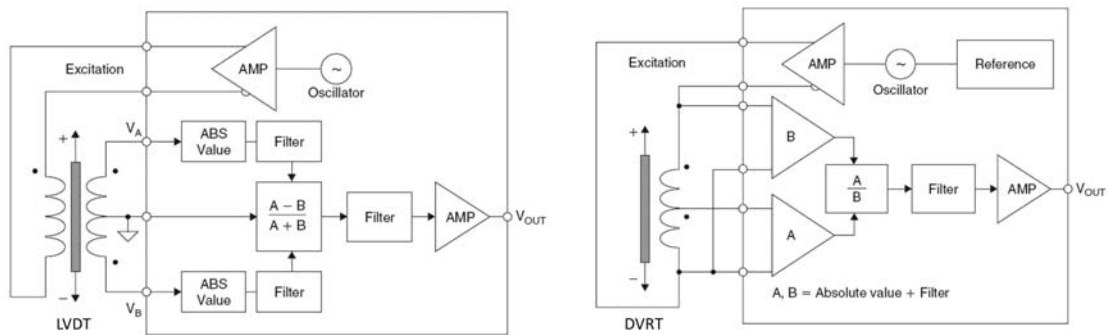


Fig. A7. Diagrams of the signal conditioning circuits for a) LVDT sensors and b) DVRT sensors.

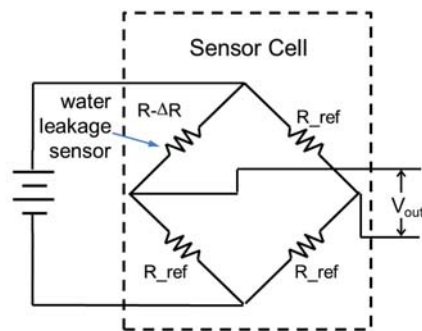
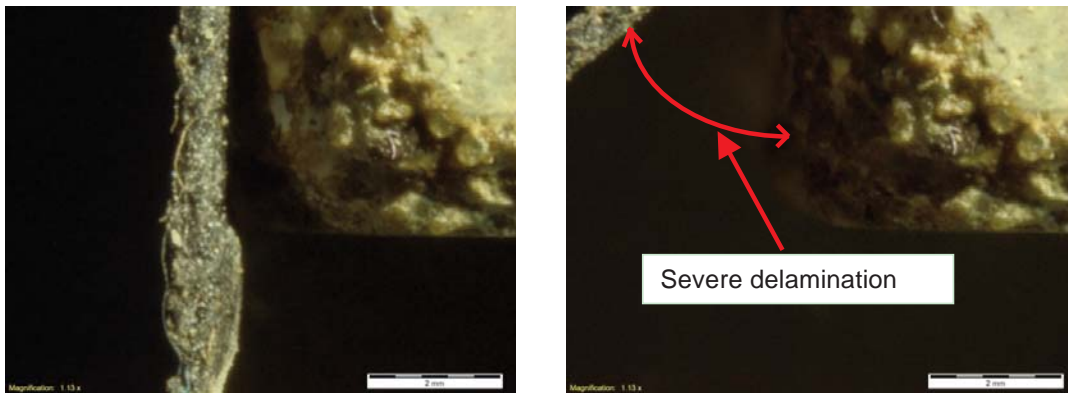


Fig. A8. Diagram of the signal conditioning circuit for electric water leakage sensor.



b)

Fig. A9. Delamination shown in the optical microscopy system: a) no delamination; and b) significant delamination.

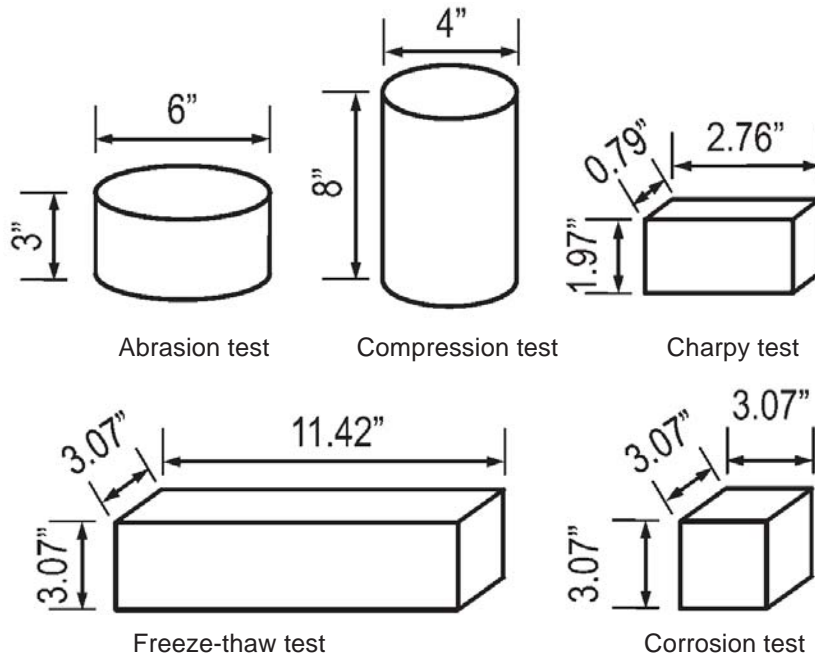


Fig. A10. Dimensions (in inch) of specimens used in the tests

a)



b)

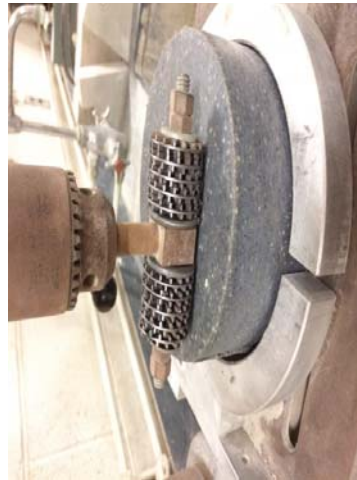


Fig. A11. The setup of abrasion test: a) the abrasion device (drill press), and b) the rotating cutter head and its contact with the specimen surface.

Bridge Waterproofing Details Phase II



Fig. A12. Abraded surfaces of the elastomeric concrete specimens without 0.5% reinforcement.



Fig. A13. Abraded surfaces of the elastomeric concrete specimens without 1% reinforcement.